공학박사 학위논문

Fabrication of Electrochromic Device Using Nano-particle Deposition System and Its Response Time Modeling for Large-area(1m^2 Class) Application

나노입자 적층시스템을 이용한 전기변색소자의 제작 및 대면적(1m^{2}급) 전기변색유리의 변색시간 모델링

2018년 2월

서울대학교 대학원

기계항공공학부

박 성 익

Fabrication of Electrochromic Device Using Nano-particle Deposition System and Its Response Time Modeling for Large-area(1m^2 Class) Application

나노입자 적층시스템을 이용한 전기변색소자의 제작 및 대면적(1m^{2}급) 전기변색유리의 변색시간 모델링

지도교수 안 성 훈

이 논문을 공학박사 학위논문으로 제출함
2017년 10월

서울대학교 대학원
기계항공공학부
박 성 익

박성익의 공학박사 학위논문을 인준함
2017년 11월

위 원 장 : _____ (인)

부위원장 : _____ (인)

위 원 : _____ (인)

위 원 : _____ (인)

위 원 : _____ (인)

Abstract

Fabrication of Electrochromic Device Using Nano-particle Deposition System and Its Response Time Modeling for Large-area(1m^2 Class) Application

Sung-Ik Park
School of Mechanical and Aerospace Engineering
The Graduate School
Seoul National University

Electrochromism refers to a color change under an externally applied voltage. Increasing interest in this phenomenon has led to new manufacturing processes for electrochromic devices (ECDs). Herein, major processes are introduced and compared in terms of their process parameters. The six representative fabrication processes discussed in this paper are electrodeposition, sol-gel, spray pyrolysis, chemical vapor deposition (CVD), thermal evaporation deposition and sputtering. Commercialization of ECDs requires a consideration of environmental issues, cost, performance and scale of manufacture. Therefore, in this study, we fabricated ECDs using a novel nanoparticle deposition system (NPDS), a seventh fabrication process. It is a low-cost eco-friendly process. The possibility of commercialization of the NPDS is discussed.

Deposition of tungsten oxide (WO_3) thin films on fluorine-doped tin oxide (FTO) and indium tin oxide (ITO) substrates was conducted using the NPDS. This is a deposition approach based on low-vacuum air-spraying at room temperature. The structure of the WO_3 films was characterized using X-ray diffraction, and the surface morphology was investigated using scanning electron microscopy and atomic force microscopy. The electrochemical properties of the films were

examined using cyclic voltammetry and chronocoulometry. The ECD was fabricated using the deposited WO_3 film, a counter electrode and an electrolyte. When a predetermined voltage (3 V) was applied, the color of the prepared WO_3 films changed from transparent yellow to dark blue, demonstrating electrochromism. The WO_3 film exhibited an optical contrast of up to 50% at a wavelength of 800 nm.

After confirming the feasibility of using the NPDS for fabricating ECDs, we constructed a large-area NPDS and used it to produce large-area electrochromic windows (ECWs). The conventional response-time model showed a large difference from the actual value with increasing ECW active area. To overcome this problem, a new electrochromic response-time model based on the transient response of a resistance–capacitor (RC) direct-current (DC) circuit was developed. This model provided an estimation of the coloration time of ECWs as a function of the size of the active area. Five samples of different sizes were prepared: 10×10 mm^2, 50×50 mm^2, 300×300 mm^2, 500×500 mm^2 and 1×1 m^2. We then measured the current and transmittance variation of the fabricated ECWs during coloration. The response time was defined in terms of the current difference. The response model defined the RC value as proportional to the length of one side of the active area of the ECW. The estimates derived using the response model were in good agreement with measured data for relatively large ECWs.

A plasma process was introduced into a conventional NPDS to improve the contrast of the ECDs. Plasma is the fourth material state in which gas molecules are ionized; it is used for electrically or chemically modifying object surfaces. Plasma treatment of WO_3 particles decreased the contact angle of the WO_3-deposited surface. This meant that the contact area between the WO_3-deposited surface and the electrolyte had increased. Moreover, the WO_3 surface crystal structure became more amorphous. These effects improved the contrast from 50 to 65.9%.

Keywords: Electrochromic device, Nano-particle deposition system, Response time model, Large-area electrochromic window, Plasma treatment

Student Number: 2013-30196

Contents

List of Tables

List of Figures

Chapter 1. Introduction

1.1 Overview

Recently, new functional devices have been developed through advanced technologies, especially nanotechnology. The size of devices or parts influence material/system behaviors, such as mechanical, electrical, chemical, and optical properties. Fabrication of electrochromic devices (ECDs) provide a good example for use of these new technologies. Electrochromism is a phenomenon of changing color under an externally applied voltages. It was first reported in academia that color change is generally reversible according to the direction of voltages applied in the 1960s. An electrochromic material is functionalized when materials are deposited on a nanoscale on to the surface of substrates; due to electrochemical reactions (oxidation/reduction) in systems. The optical characteristics are changed reversibly. The importance of electrochromic technology is increasing because it is related to green technology [1].

Applications of electrochromic technology are various, such as optical shutters in airplanes, rear view mirrors and sunroofs in automobile, sunglasses, displays. Electrochromic windows in buildings is for reduction of energy loss and effective use of energy. Also, the active control of window transmittance from incoming light provides emotional or esthetic effects.

In the United States, about 41% of primary energy is used for buildings energy and about 60% of building energy is used for heating/cooling/lighting [2]. If electrochromic windows are used in buildings to help control the internal temperature, huge amounts of energy could be saved. For this reason, many researchers have focused on smart windows as an application of electrochromic

technology. Various fabrication methods related to smart windows have been studied, such as chemical vapor deposition (CVD), sputtering, and sol-gel processes. Many factors affect cost of system fabrication; usually, the deposition cost of electrochromic materials and transparent electrodes are dominant. Because the deposition process typically requires high temperatures, it leads to high process costs. Additionally, various limitations caused by the necessary high temperature and vacuum still exist in fabricating ECDs. In this chapter, various methods and materials to fabricate ECDs are listed and their characteristics are discussed to show advantages and disadvantages of each process.

1.2 Principles of electrochromic devices (ECDs)

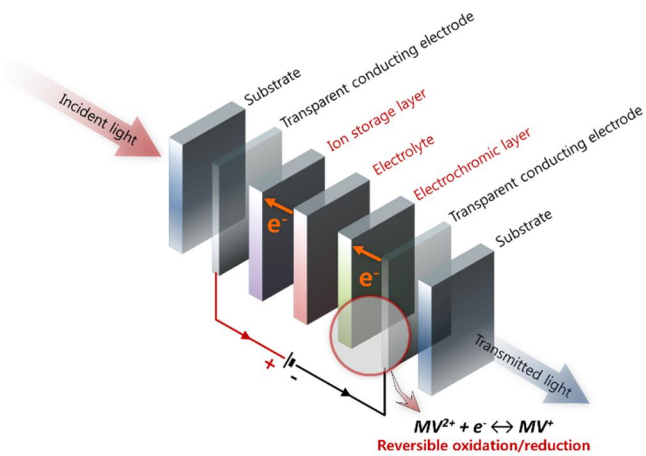

Figure 1.1 Schematic diagram of an electrochromic device

ECDs consist of an electrochromic layer, an electrolyte (Li^+, H^+), an ion storage layer, and a transparent conducting electrode (Figure 1.1). When a voltage is applied, the electrolyte move into the electrochromic layer resulting in color change. However, the layer become transparent again when the voltage is reversely applied. The color

changes can be explained in two different ways according to Schirmer's work using WO_3 in the 1980s [3].

There are two different electrochromic mechanisms of WO_3 films depending on the phase. The mechanism of color change in amorphous tungsten oxide (WO_3) films was proposed by Schirmer [3], whereby the optical change occurs with small polaron transitions between two nonequivalent sites of tungsten (W^{5+} and W^{6+}); the inserted electrons are localized in W^{5+} sites and polarize their surrounding lattice to form small polarons. In contrast, the basic mechanism of color change in crystalline WO_3 films was explained by Drude theory, with behavior similar to that of a heavily doped semiconductor with ionized impurities [4]. When ions and electrons are inserted into the crystalline WO_3 films, the electrons go into extended states in the band structure of WO_3 – with scattering by impurities resulting in high reflectance in the infrared [5, 6] – rather than entering into localized states, as in amorphous tungsten. The major difference in the mechanisms of color change between amorphous and crystalline WO_3 films is electron localization or delocalization [7].

1.3 Current fabrication trends of ECDs

As mentioned in the introduction section, the most important aspects of the ECD are the electrochromic materials and the deposition of the ion storage material onto a transparent electrode, which can range from hundreds of nanometers to tens of micrometers in size. Recently, deposition technology has been improved because most electrical devices and semiconductors are fabricated through deposition processes. Also, various different deposition processes can be applied to the manufacture of ECDs.

Because various deposition processes are used for fabrication of ECDs,

researchers are continuously developing new methodologies. The processes can be categorized into three classes, based on the status of the materials followed by a detailed classification (Figure 1.2). Generally, the environment depends on the deposition technology or basic status of the precursor. If the processes are based on solutions, the main parameter will be temperature rather than vacuum. However, the vacuum is dominant in the vapor-based processes.

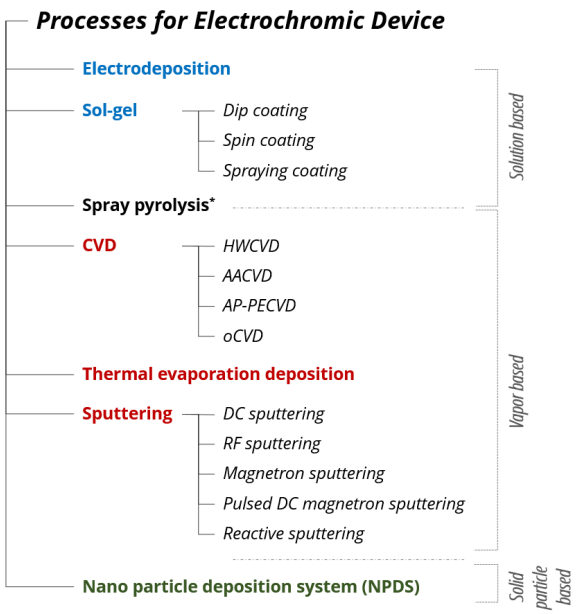

** Spray pyrolysis is in between solution and vapor base*

Figure 1.2 Fabrication methods for electrochromic devices

The electrodeposition and sol-gel processes, which include dip coating, spin coating, and spraying, are well-known solution-based processes. CVD, thermal evaporation, and sputtering are processes based on vapors. These vapor-based processes can be classified in various ways, such as hot-wire CVD (HWCVD),

aerosol-assisted CVD (AACVD), atmospheric pressure-plasma enhanced CVD (AP-PECVD), oxidative CVD (oCVD), direct current (DC) sputtering, radio-frequency (RF) sputtering, magnetron sputtering, pulsed DC magnetron sputtering, and reactive sputtering, according to their materials and process parameters. Spray pyrolysis can be classified between solution and vapor processes because a solution is sprayed but it is deposited as a vapor. Recently, direct material deposition has been tried at room temperature.

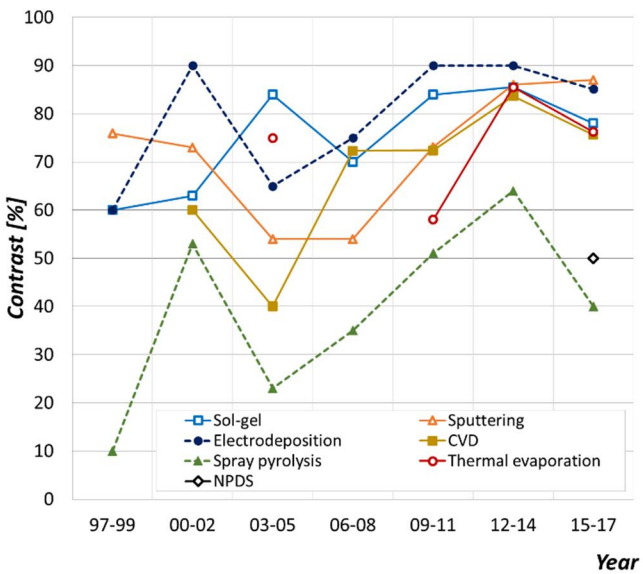

Figure 1.3 The contrast trend of ECDs made by various process

From the outset of ECD fabrication, most of the processes mentioned in Figure 1.2 have been tried. Figure 1.3 shows a contrast trend of ECDs made by each process according to time. The contrast of ECD is an important factor to evaluate the quality of ECD. Since 1995, sol-gel, sputtering, electrodeposition, and CVD have been the major processes used to deposit materials on to substrates. However, there is no dominant process for fabricating ECDs; each process has advantages and limitations.

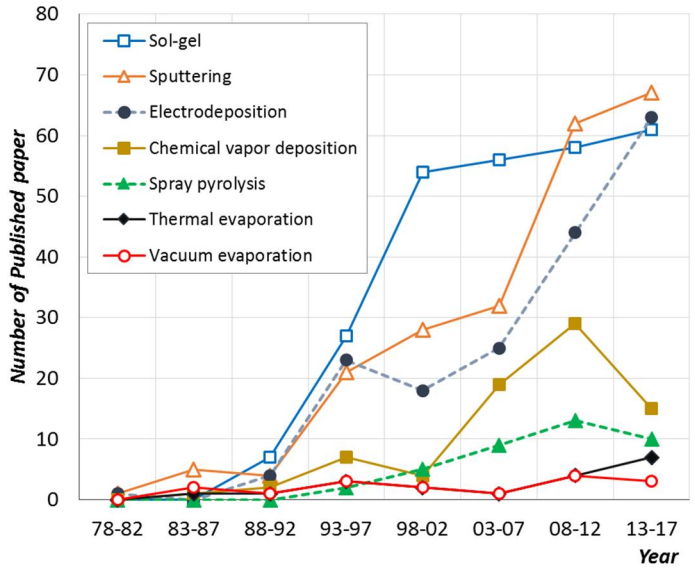

Figure 1.4 Fabrication methods trend of electrochromic devices

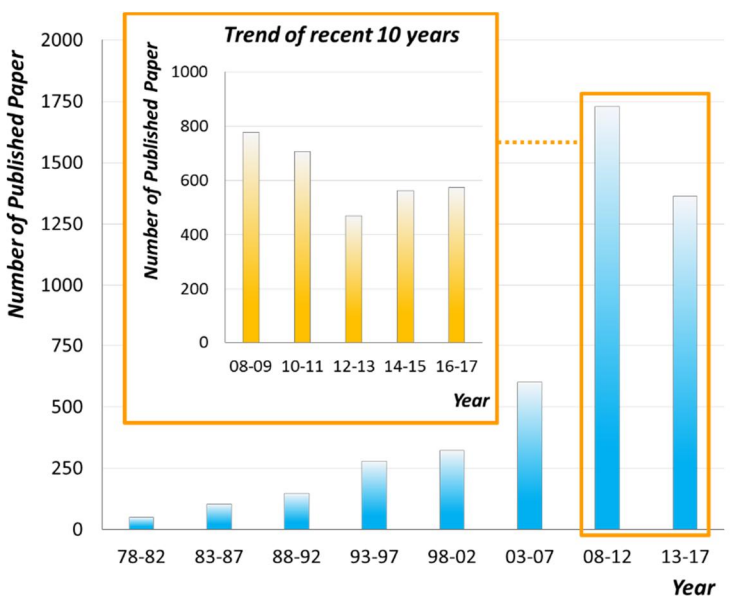

Figure 1.5 Trend to publish articles on electrochromic devices

Since the electrochromic effect was discovered, the fabrication technology of ECDs has been significantly studied (Figure 1.4). Since 2004, over 100 articles related to ECD have been published each year, with the most (458) being published in 2009 (Figure 1.5). At present, over 200 papers are still published annually, although the number is decreasing. Research on the efficiency and performance of ECDs according to unit size (i.e., a few centimeters) has reached a mature stage. The next step in this research will be to address technological issues related to specific applications. This paper will discuss with the concepts, materials, process parameters, advantages, and limitations of each process.

1.4 Fabrication methods of ECDs

1.4.1 Electrodeposition

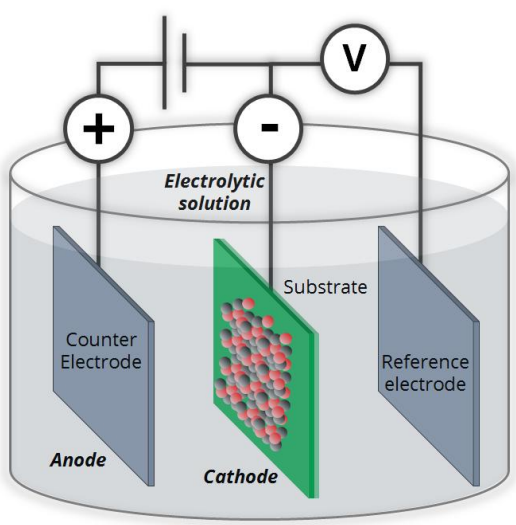

Figure 1.6 Scheme of electrochemical deposition technique

Electrodeposition, or electrochemical deposition, is an economical, fast, and versatile method for producing metal or metal oxide coatings on conductive substrates and does not require high vacuum facilities or high temperature conditions. As shown in Figure 1.6, a three-electrode configuration is typically employed, and the conductive substrate is used as the working electrode while the counter electrode is typically platinum. The applied potential is given with respect to that of the reference electrode, typically Ag, Ag/Cl, or a saturated calomel electrode (SCE), because of the stability of its potential [8-10].

For electrochromic applications, the working electrode should be transparent, such as indium tin oxide (ITO) glass or fluorine-doped tin oxide (FTO) glass. The principle of electrochemical deposition is well known. Metal ions or precursors in an electrolytic solution can move to the working electrode (or cathode) due to an electrical potential, and deposition of metal, as in equation 1.1, or metal oxide takes place at the cathode with a reduction reaction after hydroxide formation, as in equations 1.2 and 1.3.

$$M^{+} + e^{-} \rightarrow M \quad (1.1)$$

$$M^{+} + OH^{-} \rightarrow M\text{-}OH \quad (1.2)$$

$$\text{-M-OH} + \text{HO-M-} \rightarrow \text{-M-O-M-} + H_2O \quad (1.3)$$

For electrochromic applications, metals (Ag and Au) and metal oxide depositions, such as TiO_2, NiO, WO_3, ZnO, Co_3O_4, and V_2O_3, are used mainly with

electrochemical deposition [9-47]. With electrochemical deposition, hydroxide formation, or precursors such as $TiO(OH)_2$, $Ni(OH)_2$, $W_2O_{11}^{2-}$, $Co(OH)_2$, $Zn(OH)_2$ and so on, can be formed in the working electrode. For example, one of typical metal oxides for electrochromic applications is WO_3, and the electrodeposition of WO_3 can be performed with peroxotungstic acid (one of the precursors) made by the dissolution of tungsten metal in concentrated hydrogen peroxide. Also, a drying or annealing process can change hydroxides or precursors into metal oxides. The process temperature of electrochemical deposition is typically room temperature, and the process time is quite short, from several seconds to 1 h. However, electrolytic solution preparation and additional post-processes, such as washing, drying, and annealing, require a relatively longer time (up to 48 h) and higher temperature (up to 500°C) [13, 33].

Electrochemical deposition has many advantages. Precise control of the thickness and morphology of the nanostructure is possible by changing the electrochemical parameters with high deposition rates. The equipment is inexpensive due to its process conditions, such as requiring no vacuum and occurring at low reaction temperatures. In addition, unique film structures, such as nanoplate arrays and ordered porous structures, can be realized readily using seed materials or microscale polystyrene spheres [9, 18, 41]. Also, composite materials with two different metal oxides, or metal-doped metal oxides such as V_2O_5-TiO_2, Cu-doped NiO, and Mo-doped V_2O_5, have been deposited with this process to improve electrochromic performance [19, 34, 35]. Multi-layer deposition with other deposition processes is also possible. NiO/PPy, PANI/SiO_2, Prussian Blue/ATO, Prussian Blue/TiO_2, WO_3/TiO_2, PEDOT:PSS/WO_3, PEDOT/WO_3, WO_3-Copolymer, WO_3/PPy and other multi-layer depositions have been reported [25, 26, 31, 32, 39, 47-50].

For polymer deposition, the same cell used for electrochemical deposition can be used, but the mechanism of film formation is different from that of electrochemical deposition. Electro-polymerization can be used for polymerization of monomers dissolved in a solvent, but the deposition electrode should be the anode for oxidation. The process time is very short and deposition can be done typically at room temperature. A patterned structure with polystyrene spheres and multi-layer deposition have been reported [47-49, 51-54].

Electrochemical deposition and electro-polymerization are possible with the same cell, and these processes are fast and convenient. Large-area depositions, such as 100 × 100 cm^2, have been reported [30]. However, the material preparation and post processes require long process times, relatively high temperatures, and toxic chemicals.

1.4.2 Sol-gel processes

A colloidal oxide can be synthesized through a polycondensation process from acidification of an aqueous salt or hydrolysis of an organometallic compound [55, 56] (Figure 1.7). Interest in sol-gel processes for electrochromic layers has increased over the last 10 years [57]. They have been used widely for the synthesis of inorganic compounds based on chemical reactions in solution at low temperatures. The main advantage of this reaction is the transition from a liquid into a solid [58]. Moreover, sol-gel processes are versatile and allow easy control of the microstructure and composition at relatively low temperatures with simple and low-cost equipment [56]. There are various types of deposition method based on sol-gel process, such as dipping, spin-coating, and spraying (Figure 1.8).

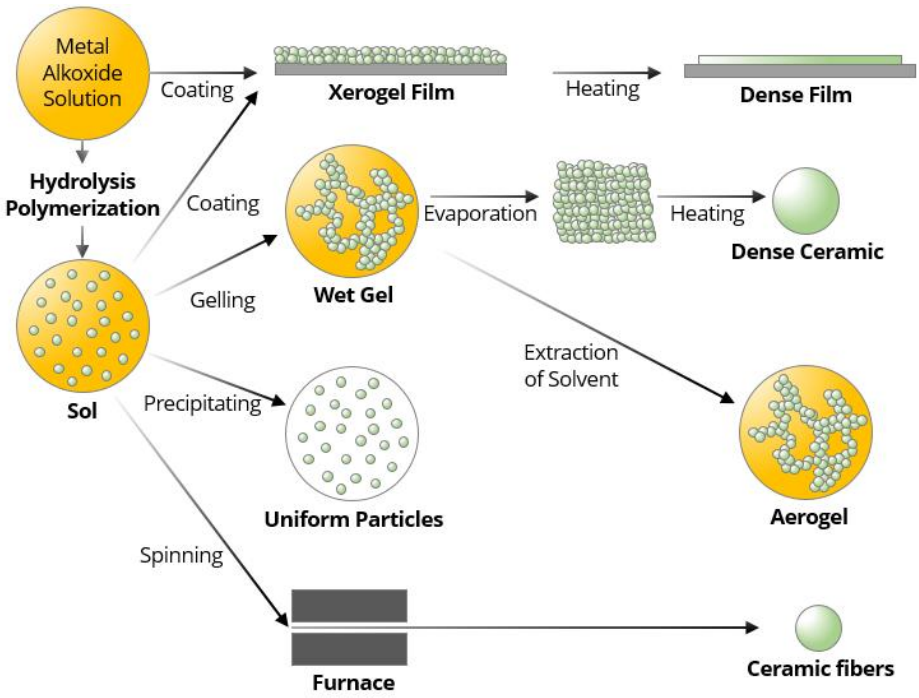

Figure 1.7 Simplified chart of sol-gel process

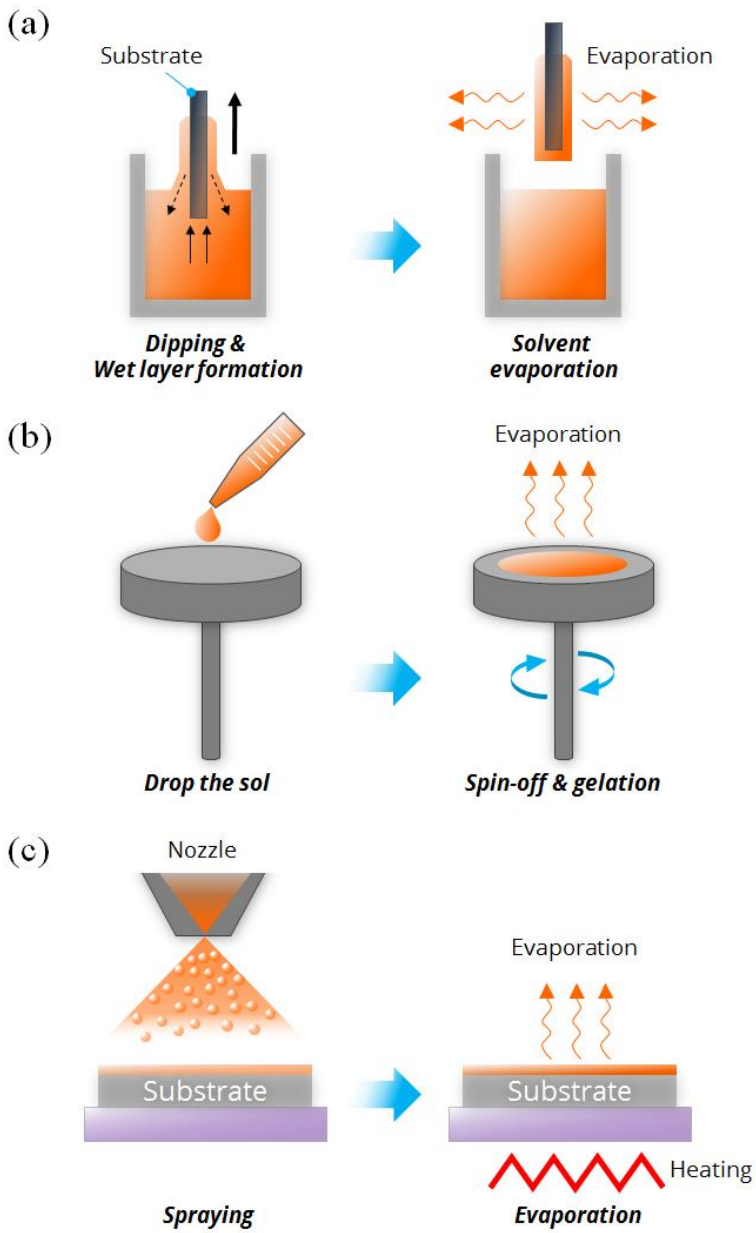

Figure 1.8 Different kinds of sol-gel process: (a) Dip coating, (b) Spin coating, and (c) Spray coating

Sol-gel processes have been used not only to synthesize powders and coat thin-films but also to modify the surfaces of electrodes. Moreover, one of the most important aspects of sol-gel processes is that prior to gelation, the fluid sol or solution are ideal for preparing thin films using dipping, spinning, or spraying processes. Microstructures, whether dense or porous, can be controlled easily through the precursors and there is no limitation on the shape, size, or kinds of substrate [59-61]. Disadvantages of sol-gel processes include the cost of the raw materials (especially alkoxide precursors), shrinkage of films during drying and sintering, and the fact that they are time consuming. One well-known application of a sol-gel process is thin-film coating, which benefits from most of the advantages of sol-gel processes while avoiding the disadvantages [60, 62]. Sol-gel processes are used widely in various applications needing thin-film coating, such as solid oxide fuel cells, dye-sensitized solar cells (DSSCs), electrochromic cells, and ferroelectric and thermoelectric materials [63].

Specially, for the electrochromic applications using sol-gel process, Judeinstein and Livage in 1988, reported that the first all sol-gel EC-device laminated a device consisting of a counter electrode, a WO_3 electrochromic layer and a TiO_2 and gel ionic conductor. [64] Then Özer et al. [65] fabricated an EC-device using a sol-gel process, which is composed of TiO_2 layer as an electrochromic and a Li^+-doped polymeric electrolyte. An transmittance change of this device was measured to be 40% (80–40%) but the response time was slower (50 s) than that of WO_3-based EC-devices fabricated by sol-gel process. Moreover, EC-device consisting of a WO_3 layer, a CeO_2–TiO_2 counter electrode and a gel electrolyte was described by Macêdo et al. [66]; the transmittance change was from 60 to 20% during the first cycle and a response time of several seconds. Additionally, the use of a hard silica-

polyethyleneglycol ormolyte as electrolyte was also reported but the transmission change in the visible light was poor (78–48%) [67]. Bell et al. [68, 69] fabricated EC-devices using multiple dip-coating of Ti-doped WO_3 films as an electrochromic layer and Ti-doped V_2O_5 films as a counter electrode, both deposited on FTO- or ITO-coated glass and a polyether polyurethane copolymer containing a lithium salt. The optical transmittance at 550 nm changed from a low value (44%) in the bleached state, 20% in the colored state. Orel's group have also been developed EC-devices fabricated by sol-gel process of WO_3 or Nb_2O_5 based electrochromic layer using different counter electrodes such as SnO_2(Mo,Sb) and LiCo-oxide, Nb/Fe-oxide, $CeVO_4$, Ce/V, V/Ti/Ce and V/Ti-oxide [70, 71].

Various wet chemistry methods have been developed to deposit and synthesize electrochromic coating layers. Spin-coating, dip-coating, and spray processes are used for depositing over large areas, based on a sol-gel process. With this method, precursors can be transformed into oxide materials by hydrolysis and condensation reactions.

There are two methods that are in use currently; the method used depends on the molecular precursors, such as metal alkoxides in organic solvents and metal salts in aqueous solutions [72]. First, the sol-gel synthesis of metal oxides is based on the polycondensation of metal alkoxides, $M(OR)_z$, in which R is usually an alkyl group ($R = CH_3$, C_2H_5, ...) and z is the oxidation state of the metal ion, M^{z+}. The chemistry of metal alkoxides has been studied extensively for over 30 years [73].

Most alkoxides (e.g., M = W, V, Nb, Ti) used for electrochromic materials are now commercially available and the sol-gel chemistry involves two steps:

(i) hydrolysis for the formation of reactive M-OH groups

$$M\text{-}OR + H_2O \rightarrow M\text{-}OH + ROH \quad (1.4)$$

(ii) condensation leading to the formation of bridging oxygen

$$M\text{-}OH + RO\text{-}M \rightarrow M\text{-}O\text{-}M + ROH \quad (1.5)$$

or

$$M\text{-}OH + HO\text{-}M \rightarrow M\text{-}O\text{-}M + H_2O \quad (1.6)$$

Metal alkoxides are not miscible with water and have to be dissolved in a solvent. The electronegativity of the metal atom and its ability to increase its coordination number "N" affect the chemical reactivity of metal alkoxides for hydrolysis.

The other method, which involves transition metal alkoxides in alcoholic solutions, offers several advantages as precursors for electrochromic layers, including wetting properties and allowing multi-component films to be synthesized readily by mixing alkoxides in the solvent. However, they are expensive and highly reactive. Thus, aqueous precursors are more appropriate for industrial applications. Much research is being conducted on the sol-gel synthesis of electrochromic layers using transition metal salts.

Two different mechanisms have been suggested for the condensation, as follows:

(i) Olation with the formation of an "ol" bridge and the departure of one molecule of water.

$$\text{-M-OH} + \text{H}_2\text{O-M-} \rightarrow \text{-M-OH-M-} + \text{H}_2\text{O} \qquad (1.7)$$

(ii) Oxolation involving the condensation of two OH groups to form one water molecule, which is then removed giving rise to an "oxo" bridge.

$$\text{-M-OH} + \text{HO-M-} \rightarrow \text{-M-O-M-} + \text{H}_2\text{O} \qquad (1.8)$$

Olation reactions primarily occur with cations of low oxidation state ($z < 4$) in aquo-hydroxo precursors. In contrast, oxolation has been observed with cations of higher oxidation states ($z > 4$).

For a given cation, many different molecular species can be found in aqueous solutions, depending on the experimental conditions. These have been reported in several books and reviews [74].

As mentioned before, sol-gel processes have been used and developed to synthesize and deposit electrochromic layers using various kinds of precursors.

For the formation of sol-gel coatings, there are chemical bonding between the film and the substrate, as is the case for metal, ceramic and glass substrates. The adhesion of the oxide coating film to the oxide substrates is achieved by formation of chemical and metallic ions in the film and substrate. For metal substrates, the bond is formed through a thin oxide layer. It has been shown that the formation of chemical bonds at

high temperatures may be easier when many -OH groups is present at the contacting surfaces of the film and the substrate. It was found in the formation of films was changed by processing temperature. Moreover, if high viscosity of the coating solution was used, the film is very thick in coating process, consisting of application of the film and heating to high temperature, the film totally peels off the substrate. In contrast, when the film is thinner due to the use of lower viscosity solutions, the film has good adhesion with the substrate after the coating process, however the cracks are formed. It was observed that cracks are accompanied by peeling of local areas of the film and the film scatters light due to the occurrence of air spaces between the film and substrate. [75, 76] Hence, to form a high quality of films via sol-gel process, optimum coating thickness and processing temperature should be concerned. Moreover, coating films fabricated by sol-gel process show the preferred orientation, resulting in amorphous or crystalline phase. It seems that the choice of substrate gives the orientation of coating layer [77]. Sol-gel coating films of oxides often show a porous microstructure due to the volatile of solvent during the drying and annealing process. Organic-inorganic composite materials consisting of inorganic bonding such as W-O, Ti-O and Ni-O combined with organic polymers give a mechanically and chemically stable coatings.

In this section, the various materials used for producing electrochromic layers via sol-gel processes will be introduced.

Tungsten oxide (WO_3) has a transparency or yellowish color in the bleached state. In contrast, if ions such as H^+ and Li^+ are inserted, the WO_3 color changes to deep blue. This material is one of the most studied as a cathodic coloration material, and has a large coloration efficiency (CE). To synthesize WO_3, four different sol-gel processes have been developed for the sol preparation. They are described in detail

elsewhere [78, 79] and only a brief summary is given below.

First, a thick coating layer of sodium tungstate, produced through acidification, can be obtained with this method, but the sol stability is too low. A second method is hydrolysis of alkoxides, which is the conventional sol-gel route for many kind of oxides; however, this method is expensive and not suitable for industrial applications. Vroon et al. reported large area coatings using a hydrolysis method [80]. Third, a reaction between tungsten chloride and oxychloride with alcohol is a cost-effective method with high stability of sols (i.e., stable over several months). The coating layer is more uniform than those prepared by the colloidal route. Using this process, thin films have been dip-coated on flexible ITO/polyethylene terephthalate (PET) substrates and heat-treated at 80°C to form a coating layer with a stoichiometry of $WO_3 \cdot 18\ H_2O$. However, the transmittance change was too low and the ITO coating layer was rapidly degraded due to the acidity of the solution [81]. Ultimately, use of peroxypolytungstic acid, which uses hydrogen peroxide with an organic acid, such as acetic or propionic acid, under low temperature conditions (-10 to 12°C), is the best way to synthesize stable aqueous solutions of W(VI) precursors. W-peroxy acids can be obtained easily through the reaction of tungsten or tungsten carbide powder.

Niobium oxide (Nb_2O_5) is another interesting material for electrochromic layers and counter electrodes in ECDs. The first attempt to fabricate a Nb_2O_5 coating layer via a sol-gel process using a mixture of $NbCl_5$ was reported in 1991. However, the long-term stability of the ECD was low and the device was easily degraded within a few cycles. Moreover, other precursors such as niobium ethoxide ($Nb(OEt)_5$) or pentabutoxide of niobium ($Nb(OBun)_5$) have been reported for the formation of a NbO_2 electrochromic layer. Nb_2O_5 has cathodic coloration properties, like WO_3, with Li^+ insertion depending on the annealing temperature of the films. An amorphous

Nb_2O_5 coating layer, formed below 450°C, has a brown color, while that of the crystalline material, annealed at 560°C, is dark blue [72].

MoO_3 coating layers have been deposited using many kinds of precursor, such as alkoxides, chlorides, chloroalkoxides, and molybdic acid, via sol-gel processes. Although the electrochromic properties of MoO_3 itself are poorer than those of WO_3 and Nb_2O_5, coating layers formed with compounds and other elements (MoO_3:W [82], MoO_3:V [83] and MoO_3:Ce [84]) exhibit good electrochromic properties.

Nickel oxide (NiO) is well-known anodic coloration materials and has been studied widely using sol-gel processes. NiO films have been synthesized using various precursors, such as nickel diacetate tetrahydrate, nickel(II) acetylacetonate, nickel diacetate tetrahydrate, and nickel diacetate dimethylaminoethanol (DMAE). However, the use of DMAE as a solvent is not suitable for industrial applications due to its low flash point (39°C).

TiO_2 is another electrochromic materials that has been widely studied, however, it shows low electrochromic performance. Its properties are strongly affected by its preparation and structure, amorphous or crystalline (anatase or rutile). TiO_2 coatings were prepared initially from the classical alkoxy route [64, 85] as well as by other methods [86-88].

1.4.3 Spray pyrolysis

The basic principle of the spray pyrolysis technique is pyrolytic decomposition of salts that consist of deposition target material (Figure 1.9). Every sprayed droplet undergoes pyrolytic decomposition and forms a product of a single crystallite or cluster of crystallites when the droplet contacts the surface of the hot substrate. By-products and solvents evaporate during the process. The hot substrate provides

thermal energy to the droplets and thermal decomposition occurs because of this. After thermal decomposition, recombination of the constituent elements progresses, followed by sintering and crystallization of the clusters of crystallites, and eventually a film of the target material forms. The technique has been used for the deposition of dense and porous films on a variety of substrates like glass, ceramics, and metals. Multilayered films can also easily be prepared using this technique. Various metal oxides, such as V_2O_5, V_2O_5-MoO_3, WO_3, WO_3-Nb_2O_5, NiO, LiNiO, and CeO_2-ZrO_2 have been prepared using the spray pyrolysis technique [89-92]

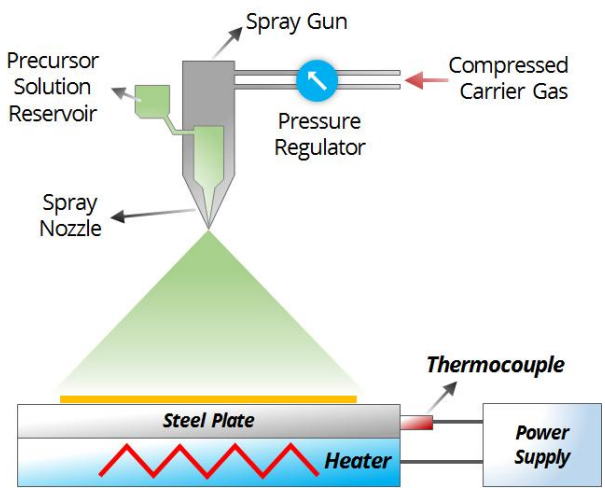

Figure 1.9 Scheme of spray pyrolysis technique

Spray pyrolysis is a simple and relatively cost-effective processing method, being a non-vacuum technique for preparing films of any composition. This technique produces large-area and high-quality-adherent films of uniform thickness. It does not require high-quality substrates or chemicals. Spray pyrolysis has been used for several decades in the glass industry and in solar cell production. Film properties can

be easily controlled over a wide range of conditions by changing the spray parameters, such as the substrate temperature, air flow pressure, and precursor solution molarity [93, 94]. A major advantage of this technique is that it operates under moderate temperatures (100–500°C) and produces films even on poor quality substrates. It offers an easy way to dope films with any elements in any proportion by adding them in some form to the spray solution [95, 96]. Recently, many researches have enhanced electrochromic properties by doping materials to conventional electrochromic materials. The mixed V_2O_5 – WO_3 film showed good coloration efficiency (49 cm^2/C) [90]. Sb doped WO_3 film showed faster response time (Tc = 2.72 s, Tb = 3.17 s) [97]. Lithium Doped NiO film showed 41.2 cm^2/C while 31.0 cm^2/C of the undoped film [95]. It also can make multi-layer films by varying the composition of the spray during the process. However, this technique also has disadvantages, such as non-uniformity of films with larger grain sizes due to uncontrollable spray droplet size, wastage of solution, and low deposition rate. Spray pyrolysis does not require high quality substrates or high vacuum conditions. These characteristics have enabled its use for industrial applications because the scale of product coated can easily be increased. Large-area NiO thin films prepared by this technique have been reported [98] and further development of large films with other metal oxides is in progress.

1.4.4 Chemical vapor deposition (CVD)

CVD is a widely used processing technology to produce thin films. CVD of films involves the chemical reaction of gaseous reactants on or near a heated substrate surface (Figure 1.10). CVD is able to produce high-purity bulk materials, powders, and composite materials.

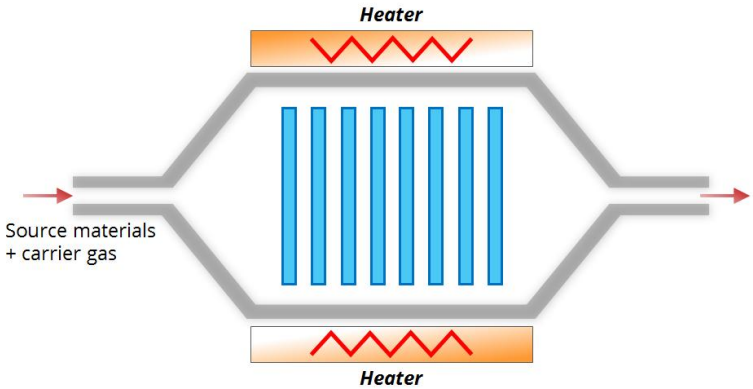

Figure 1.10 Thermal chemical vapor deposition

Typically, CVD involves the flow of volatile precursors into a chamber containing a heated substrate to be deposited. The precursors react or decompose on the substrate surface that is to be coated as a thin film form. It is followed by exhausting by-products out of the chamber along with unreacted precursors. For the deposition of thin films, CVD has several advantages. CVD films are conformal and the film thickness on the sidewalls of features is comparable to thickness on the top. This means that films can be applied to elaborately shaped pieces, including the inner and outer features, and that high-aspect ratio holes and other features can be filled completely. Second, CVD provides films with very high purity. Impurities can be removed from volatile precursors using distillation methods. Finally, CVD does not require as high a vacuum as physical vapor deposition (PVD) processes and can provide relatively high deposition rates. CVD also has disadvantages. Volatile precursors are required at near-room temperatures. However, some of the precursors are highly toxic ($Ni(CO)_4$), explosive (B_2H_6), or corrosive ($SiCl_4$). The by-products of CVD reactions can be hazardous (CO, H_2, or HF). The kinds of substrates may be limited due to the elevated temperature of deposition, which causes stresses and

mechanical instabilities of the deposited films.

CVD has various reactor and process types. Substrate and coating materials, morphology, film thickness and uniformity, precursors, and cost determine the process or reactor. There are various enhanced CVD processes that use plasma, ions, photons, lasers, hot filaments, or combustion reactions for higher deposition rates or lower deposition temperatures. Here, we discuss representative types of CVD: low-pressure CVD (LPCVD), HWCVD, plasma-enhanced CVD (PECVD), AACVD, and atmospheric pressure plasma jet (APPJ).

LPCVD is based on a hot-wall reactor. The chamber is surrounded by a furnace. In the chamber, the parts are loaded into the system, which is heated to the desired temperature. The reactive precursors are then introduced. This system operates at high temperatures and the coating materials are limited by the materials used in constructing the furnace. These systems are able to process large substrates, and have stable substrate temperatures, resulting in uniform coating thicknesses. CVD of hydrocarbon gases on metal surfaces allows scaling of polycrystalline graphene films to large sizes that can be transferred onto arbitrary substrates [99-101]. However, the walls inside the system become heavily coated. Frequent cleaning is required, resulting in higher thermal loads and energy usage.

HWCVD is an elegant, low-pressure deposition technique for both inorganic and organic films and is based on decomposition of precursor sources at a heated metallic surface. It uses a hot filament to chemically decompose the source gases. The filament and substrate temperatures are independently controlled, allowing colder temperatures for better adsorption rates at the substrate and higher temperatures. It is necessary for decomposition of precursors to free radicals at the filament. Recently, HWCVD was used for the high-density production of crystalline WO_3 nanoparticles

[102-105]. Because HWCVD is an economical and commercially usable technique, the nanoparticles derived from the deposition are used to improve device performance (e.g., ECDs) while maintaining low manufacturing costs. Crystalline WO_3 nanoparticles were synthesized by this HWCVD and subsequently used to form electrochromic thin films using ultrasonic spray deposition. Particle morphology was tuned using the HWCVD synthesis parameters, including filament temperature, substrate temperature, and oxygen partial pressure[104].

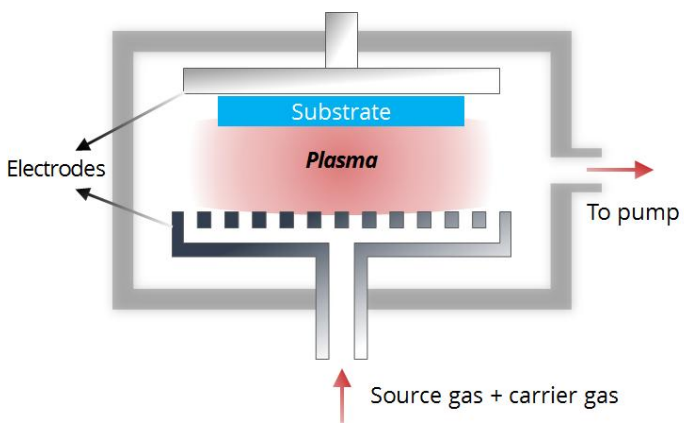

Figure 1.11 Plasma chemical vapor deposition

In the PECVD process, plasma is added to the deposition chamber with reactive gases to produce the desired solid surface on a substrate (Figure 1.11). Plasma is a partially ionized gas with a high free electron content (about 50%). In cold plasmas, the electrons have a much higher temperature than the neutral particles and ions. Thus, cold plasmas can use the energy of the electrons by changing the pressure. This allows a PECVD system to operate at low temperatures (100–400°C). PECVD has high deposition rates that results in a low cost of film deposition. Electrochromic WO_xC_y films were deposited on flexible PET/ITO substrates by a 23°C PECVD

process with a precursor (tungsten carbonyl, $W(CO)_6$), and air [106]. Flexible electrochromic organomolybdenum oxide (MoO_xC_y) films were synthesized using a precursor of molybdenum carbonyl vapor [107].

AACVD involves the atomization of a precursor solution into submicrometer-sized aerosol droplets. The droplets are moved into a heating zone, where the solvent is rapidly evaporated. The chemical precursors decompose or react near or on a heated substrate to produce thin films [108]. The AACVD method has several advantages [109-113]. It has a variety of available precursors, and generates an aerosol to simplify the delivery and vaporization of precursors. It can synthesize multi-component products with precise stoichiometric control. Moreover, it provides high deposition rates, low cost, and can be executed under various environmental conditions (e.g., at low pressure or in an open atmosphere). These characteristics of AACVD enable fabrication of large ECDs. Electrochromic nickel (II) oxide (NiO) thin film was produced by this method with precursor solution (nickel (II) acetylacetonate in toluene)[114].

AP-PECVD, which uses 'atmospheric-pressure non-equilibrium discharges' (e.g., corona, spark, dielectric barrier and atmospheric-pressure glow discharge), has recently attracted interest due to its low cost, high processing speed, and simple system that does not require a vacuum [115]. AP-PECVD has been used to deposit thin films, such as SiO_x [116], SiN_x [117], TiO_x [118], Al [119], AlO_x [120], ZnO_x [121], SnO_x [122], InO_x [123], a diamond-like coating [124], fluorocarbons [125], and hydrocarbons [126]. Electrochromic WO_xC_y films were created previously on flexible PET/ITO substrates by AP-PECVD with an APPJ [127]. A precursor $W(CO)_6$, carried by argon gas, was used. Electrochromic NiO_xC_y films have also been synthesized by this process with a precursor NO vapor [128], in addition to

flexible organo-tungsten-molybdenum oxide ($WMo_xO_yC_z$) films [129, 130] and flexible organic-inorganic hybrid composite $WTa_xO_yC_z$ films [131].

There are also derivatives of the CVD technology. Electrochromic TiO_2 thin films were produced by metal-organic CVD [132]. It has been reported that CVD methods produce homogeneous and thin layers of polymers at the nanoscale on the surface of substrates. Film formation on the surface of fabric is achieved without any change in the polymeric structure of the substrate in different polymerization situations. CVD of poly(3-methylthiophene) and poly(3-hexylthiophene) as conducting polymers on the surface of polyester fabrics has been described [133]. Oxidative CVD (oCVD) is a unique liquid-free synthesis method to enable continuous polymerization and thin-film deposition of polythiophene (PTh) [134]. The technique relies on the transport of both monomer and initiator in the vapor phase to the substrate, thus benefitting from being able to control the reactant concentrations at the growth surface, offering tenability and continuous growth conditions during synthesis. Recently, oCVD has been successfully used for the formation of poly(3,4-ethylenedioxythiophene) (PEDOT) and PEDOT copolymers [135-137]. CVD techniques have been used for the production of optical coatings (e.g., low-E coatings) for large-scale applications. Also, variants, such as HWCVD, AACVD, AP-PECVD, and oCVD continue to be developed.

1.4.5 Thermal evaporation deposition

Thermal evaporation involves heating a solid material inside a high-vacuum chamber, taking it to a temperature that produces some vapor cloud inside the vacuum (Figure 1.12). This evaporated material constitutes a vapor stream, which traverses the chamber and hits the substrate, sticking to it as a coating or film. This

technique is one of the most commonly used to produce WO_3 thin films. Besides WO_3, MoO_3 and NiO can also be used for thin film deposition by thermal evaporation deposition [138, 139].

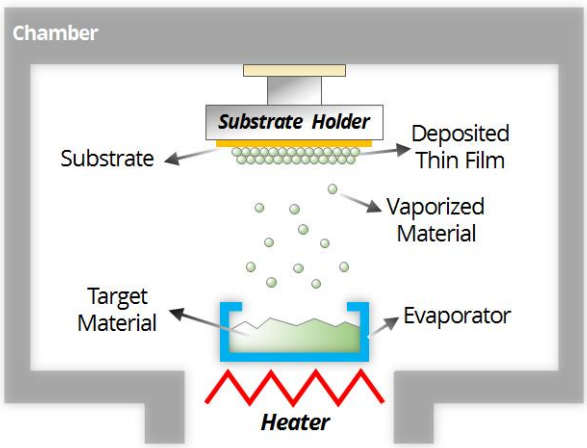

Figure 1.12 Scheme of thermal evaporation deposition

Thermal evaporation deposition has the advantages of being able to deposit thin film with low contamination at a controlled deposition rate. Moreover, larger charges (source materials) can be loaded per deposition run. However, it requires large and costly RF power supplies, step coverage is poor and control of film composition is more difficult than with sputtering.

Main process parameter for this deposition method is substrate temperature. By changing substrate temperature, thermal evaporation deposition method controls film properties such as porosity, adhesion, surface roughness, and crystallinity. WO_3 Films deposited at low substrate temperature showed better optical density (0.74) and transmittance modulation (ΔT = 61.8% at 550 nm wavelength) due to its amorphous structure, high porosity, and smooth surface roughness [140]. But, film adhesion was

weak at low substrate temperature. Chiu et al enhanced adhesion even at low substrate temperature by ion beam-assisted deposition (IAD) [141].

There have been several studies on large-sized film deposition by thermal evaporation deposition, and 15 × 15 cm^2 film deposition of WO_3 has been reported [27]. In e-beam evaporation, the effective source size can be made larger by rastering the beam, improving the thickness uniformity and coverage of the substrate. Thus, thermal evaporation deposition has the potential to produce large-size thin films.

1.4.6 Sputtering

Sputtering was first observed in a DC gas discharge tube by Grove in 1852 and he discovered the cathode surface of discharge tube was sputtered by energetic ions in the gas discharge, and cathode materials were deposited on the inner wall of the discharge tube. Today, sputtering deposition is a widely used technique to deposit thin films for ECDs. Sputtering deposition is one of the PVD methods for thin film deposition. The source material, called the 'target,' is ejected on to the 'substrate,' such as silicon wafer, ITO-coated glass, or FTO, during the deposition process of ion or atom bombardment. Ions with high energy impact the target to erode the surface of the source material via energy transfer; then, the particles of the source material are impacted energetically on to the substrate.

With the advantage of high energy atoms, the method can easily sputter even materials with high melting points. The sputtered films have good uniformity and the same composition as the source material. Sputtering deposition typically has better reproducibility and adhesion than other deposition processes. Additionally, it allows low vacuum pressure and low temperature conditions during the thin-film deposition.

Sputtering deposition is a commonly used technique for electrochromic materials,

and various materials can be deposited, such as metals, non-metals, alloys, oxides, and nitrides. WO_3 is a well-known cathodic EC material, with its high CE and proven cycle of more than 10^5 times [142]. Some oxide materials, such as nickel oxide, titanium dioxide, iridium oxide, tungsten-titanium oxide, and aluminum oxide, can be deposited by sputtering systems. In addition, sputtering deposition of gold, aluminum, and palladium has been reported in the recent literature [143-146].

DC and RF sputtering systems are the basic techniques for thin-film deposition. However, to improve the sputter rates and/or vacuum environment, specially designed sputtering systems have been developed, such as magnetron sputtering, reactive sputtering, pulsed sputtering, ion beam-assisted sputtering, high-power impulse magnetron sputtering, and gas flow sputtering.

Although there are many types of sputtering deposition systems to deposit thin films, we are interested in the systems used in ECDs and, in this report, we focus on the sputtering systems that have been used most widely in recent research and industrial coatings.

1.4.6.1 Direct current (DC) and radio-frequency (RF) sputtering

DC and RF sputtering deposition are the most standard deposition systems for EC materials. DC sputtering uses DC power and can be used for only metal targets; it is almost ineffective to deposit on insulators. To avoid this problem, RF sputtering was developed, using an AC power source at a high frequency. RF sputtering can not only deposit on metals, but also on semiconductors and insulators. Typically, a frequency of 13.56 MHz is used in industrially coatings, but there are also some other frequencies, such as 27.12 MHz and 40.68 MHz. A schematic of a DC/RF sputtering system is shown in Figure 1.13.

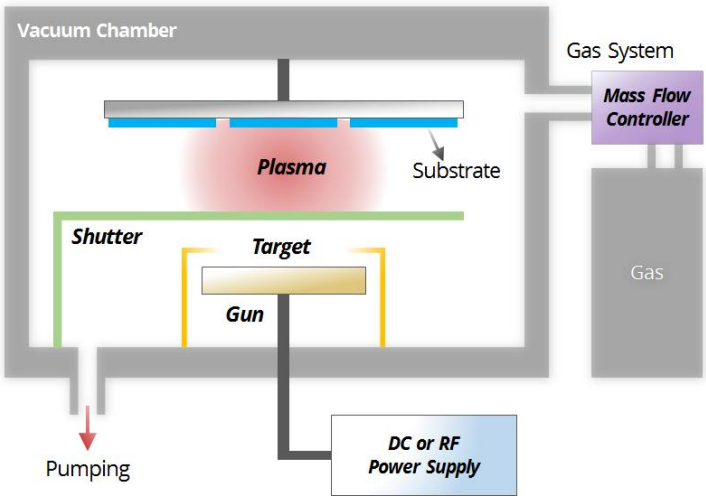

Figure 1.13 The schematic DC/RF sputtering system

Wang et al. [147] prepared a metallic tungsten film on ITO-coated glass by RF sputtering at a vacuum pressure of 2.6×10^{-4} Pa and a 300°C deposition temperature. Gomes et al. [148] deposited an indium zinc oxide (IZO) film from an In_2O_3:ZnO (87:13 wt.%) alloy target by RF and DC sputtering with a vacuum pressure of 0.133×10^{-4} Pa at room temperature. Park et al. [149] fabricated WO_3 thin films on ITO-coated glass using a RF sputtering deposition system with only argon gas from a WO_3 target; the thickness of the thin film was 70–100 nm.

1.4.6.2 Magnetron sputtering

The basic sputtering system has been used to successfully deposit many materials including EC materials. However, the process has limitations, such as low sputtering rates, low ionization of inert gases, such as argon, in the plasma, and a high temperature requirement. The magnetron sputtering process was developed to overcome these limitations by using magnetic fields.

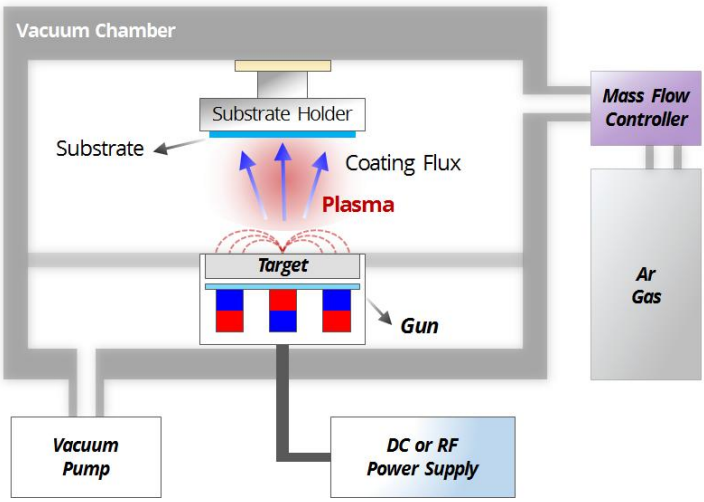

Figure 1.14 The schematic of magnetron sputtering system

Magnetron sputtering uses magnetrons behind the cathode to trap electrons near the cathode to keep the plasma close to the surface of the target. This can substantially increase the ionization efficiency and also increases the bombardment of ions of the target. This results in a higher deposition rate at the substrate. In addition, it also means magnetron sputtering allows the plasma to be maintained at a lower pressure (< 0.1 Pa). Figure 1.14 shows the fundamental process of a magnetron sputtering system.

The magnetron sputtering power source can be both DC and RF, and almost any metallic target materials and oxide can be deposited. Consequently, magnetron sputtering for EC materials has made a significant impact and is widely used in both research and industry. Many cases can be found over the last decade that used a magnetron sputtering system, with WO_3 thin films prepared onto FTO or ITO glasses using a magnetron sputtering process at room temperature [146, 150-157] with a large range of thicknesses, from 0.7 to 1,120 nm. Wang et al. [147] measured WO_3

thin films at a temperature of 700°C. Kang et al. [158] deposited TiO_2 onto FTO glass with chamber pressure of 0.667 Pa and Lansåker et al. [159] prepared TiO_2/Au/TiO_2 multilayer thin films using a DC magnetron sputtering process; both were fabricated at room temperature. Lin et al. [160, 161] deposited Li_2O, NiO, and Ni-Zr alloy using RF magnetron sputtering. Choi et al. deposited another widely used EC material, nickel oxide, and WO_3 by an RF magnetron sputtering process onto ITO/PET glass. Kubo et al. [142] studied the electrochromic properties of Li_xNi_yO thin films, including Li_2NiO_2, $LiNiO_2$, and $LiNi_2O_x$ at a temperature of 150°C. Gillaspie et al. [160] deposited nickel oxide-based nanocomposite films from ceramic targets composed of lithium, nickel, and WO_3 using RF magnetron sputtering with a mixed gas ratio of Ar:O_2 = 1:1. Rodrigues et al. [162] deposited IZO on glass substrate using a ceramic oxide target of ZnO/In_2O_3. Lim et al. [150] investigated the thin film performance of vanadium oxide and vanadium-titanium oxides using co-sputtering of V_2O_5 and TiO_2 targets by changing the Ti and V atomic ratio. Jee et al. [163] evaluated a LiPON-WO_3 (LPWON) composite thin film used as a solid electrolyte in solid state EC devices. Chen et al. [164] fabricated Li^+ ion-conducting Li-Al-Ti-P-O thin film on ITO-glass at temperatures from 25°C to 400°C. Tajima et al. [165] deposited multilayer thin films of Ta_2O_5, Al, Pd, and Mg_4Ni onto WO_3/ITO/glass using a DC magnetron sputtering method. Park et al. [149] prepared CdS and CdTe thin films. Iridium oxide thin films were prepared on FTO-coated substrate using Ir metal in an O_2 or H_2O atmosphere by Ito et al. [166]. Chu et al. [167] studied the effects of substrate temperature by depositing Nb_2O_5:MoO_3 (90:10) thin films on ultrasonically cleaned microscopic glass and FTO-coated glass substrate and Coskun et al. [168] deposited Nb_2O_5 thin films on glass using RF magnetron sputtering.

Although the magnetron sputtering process is one of the most widely used methods, it still has some disadvantages, such as slow deposition speed and lower plasma density than arc technology.

1.4.6.3 Pulsed DC magnetron sputtering

During the thin film deposition process, two problems faced researchers using DC power for thin deposition. First, it was difficult to deposit oxide materials with a DC power sputtering system; the second problem concerned the expense of the RF power supply. To solve these problems, pulsed DC magnetron sputtering deposition is one of latest techniques for thin film depositions, which is being used in many industrial and research applications, especially in ECDs. Positive DC voltage pulses are applied at frequencies in the range of 20–350 kHz [169]. The duration of reverse pulses depends on the discharge of the target surface dielectric. Basically, the negative voltage is reversed to a magnitude equivalent to 10% of the average positive voltage. When the duration and number of positive voltage pulses are sufficient to produce an electron current, it can discharge the ions on the target, and when the voltage turns to negative, there is a repelling effect on the incoming ions. This keeps the sputtering process working and oxide materials that cannot be deposited with DC sputtering can instead be deposited with a pulsed DC magnetron sputtering process.

Chen et al. [170, 171] reported an EC material of WO_3 that was deposited by pulsed DC magnetron sputtering at 70 kHz from WO_3 target material; the ratio of O_2/Ar was from 0.2 to 1.0 during the deposition. Also, Co_xSiO_z thin films were prepared from a Si-Co mixture target by Gil-Rostra et al.[172], and the pulsed voltage was from 250–400 V at a frequency of 80 kHz. Without changing the DC power to RF power, it is possible to deposit oxide compounds with pulsed DC

sputtering and the deposition rate is better than with RF sputtering, but the quality of deposition is not as high as with RF sputtering deposition.

1.4.6.4 Reactive sputtering

Reactive sputtering is a sputtering deposition process based on a chemical reaction between target material and a gas or mixture of gases introduced into a vacuum chamber. Today, reactive sputtering deposition is a well-known technique and is used widely for both research and industrial coating deposition.

Oxide and nitride films are the most common thin films for EC devices using reactive sputtering methods. Basically, oxygen and/or nitrogen mixed with an inert gas, such as argon, can be used as the reactive material during reactive sputtering deposition for EC devices. In addition, reactive sputtering deposition can be used with any sputtering method: e.g., DC/RF magnetron sputtering and pulsed DC sputtering. However, DC reactive sputtering is much more convenient than RF sputtering for metallic targets due to the expense of the RF power supply and low deposition rates. One advantage of reactive sputtering is that a functional gradient deposition can be measured by controlling the introduced reactive gas and inert gas pressure. That is, film stoichiometry, an important parameter for optimizing the properties of thin films, can be controlled. Also, the reactive sputtering deposition process can occur at room temperature.

For EC devices, reactive sputtering deposition is usually combined with magnetron sputtering to improve the deposition rate and functionality. Reactive sputtering is widely used for preparing WO_{3-x} films on ITO-coated glass substrates. It occurs at room temperature and the important parameter is the Ar/O_2 ratio to control the composition of the oxide [107, 173-180]. Tajima et al. [143-145, 175, 181]

deposited one of the most common EC materials, Ta_2O_5, on ITO-coated glass with the mass flow ratio of $Ar/O_2 = 7$ using a Ta target material. Deposition of nickel oxide thin films was reported by Valyukh et al. [173], Wen et al. [172], and Song et al. [182]. Avendaño et al. [183] fabricated EC Ni oxide-based thin films by reactive DC magnetron sputtering from Ni and $NiV_{0.08}$ with different ratios of Ar, O_2, and H_2 gases. ZnO:Al (ZAO) films were deposited on soda lime glass using a self-made reactive magnetron sputtering system by Wang et al. [184]. Wen et al. [185] prepared Ir oxide thin films by reactive DC magnetron sputtering onto ITO and carbon plates. The film thickness was between 30 and 700 nm. A reactive DC magnetron co-sputtering method was used to deposit nickel-WO_3 from nickel and tungsten metals by Green et al. [186]. Multilayers of ITO/NiO_x/$LiTaO_3$/WO_3/ITO were deposited on a flexible PET/ITO substrate by Liu et al. [187].

A reactive RF magnetron co-sputtering process was used to deposit $IrTaO_x$ thin films with a thickness of 180 nm on an ITO substrate by Yun et al. [188]. Abe et al. [189] fabricated NiOOH thin films with H_2O gas using reactive RF magnetron sputtering, showing a higher transferred charge density and optical density change compared with NiO thin films prepared in an O_2 atmosphere.

WO_3 was deposited onto FTO substrates by reactive pulsed (20 kHz) DC sputtering from a metallic tungsten target by Sun et al. [190]. Gil-Rostra et al. [191] and Garcia-Garcia et al. [178] reported $W_xSi_yO_z$ thin films using a reactive pulsed DC magnetron sputtering system with the frequency of 80 kHz onto silicon, soda lime glass, and an ITO substrate from a tungsten target at room temperature. If the partial pressure of the reactive gas is too high, a thin layer of dielectric can build up on the surface of target material, which can decrease the deposition rates.

1.4.7 Nanoparticle deposition system (NPDS)

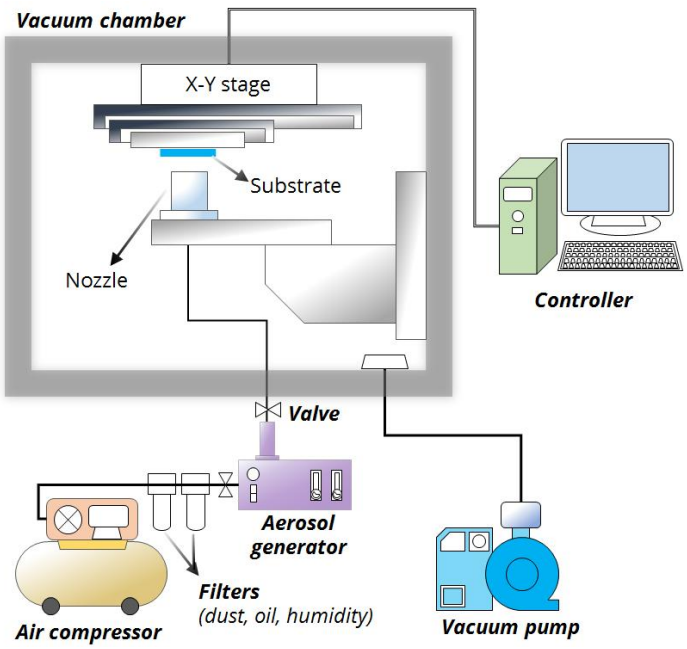

Figure 1.15 A solid particle based system to fabricate ECD (NPDS)

In 2008, an air-spray deposition system operating at room temperature and low-vacuum conditions, the NPDS, was reported by Chun et al. [192, 193]. NPDS was developed for the deposition of nano/micro-class metal and ceramic particles under dry conditions. Available substrates include ceramics, metals, polymers, and papers. No precursor or post-processes are required, so it is considered a relatively simple and low-cost method of film deposition. The application areas of NPDS have been expanded recently from DSSCs to ECDs [194, 195].

Figure 1.15 shows a schematic diagram of NPDS. NPDS consists of an air compressor, a fluidized-bed aerosol generator, a subsonic slit nozzle, a vacuum chamber, a vacuum pump, and a stage system for moving a substrate or nozzle.

NPDS included a number of commercial components, except the nozzle and vacuum chamber. However, the key to the technique is the design of the nozzle and control of the aerosol flux. The deposition chamber is maintained at a base pressure of 10 kPa by the rotary vacuum pump and compressed air is supplied with target particles at 0.3 MPa by the air compressor. WO_3 powder ($\leq$ 20 μm) was used as an electrochromic material and FTO-coated glass and ITO-coated glass were used as substrates. During the deposition process, the powder particles fragment into smaller particles and adhere to the substrate. The WO_3 film-coated FTO glass exhibited electrochromic contrast of 50% at 800 nm. This showed that NPDS is another alternative solution for inorganic electrochromic material deposition, although this has not yet been verified sufficiently by researchers in this area.

1.5 Summary of processes

Recent technological advances have resulted in the development of various ECDs. In this article, processes to fabricate ECD were introduced and discussed relative to electrochromic materials. In contrast to semiconductors (crystallized structure, high surface quality), ECD requires an amorphous structure with a porous surface. For these reasons, different processes required development. Seven representative processes to fabricate ECDs were summarized and discussed in this chapter.

- Electrodeposition: Electrochemical deposition is an economical and versatile process for producing various electrochromic layers without the need for a high vacuum or high temperatures. Large deposition areas are also possible. However, material preparation and post-processes, such as drying and annealing, require long process times, relatively high temperatures, and toxic chemicals.

- Sol-gel: The sol-gel process is an efficient method to prepare the electrochromic layer based on various coating techniques, such as dip-, spin-, and spraying coating. However, breakthroughs are still required to overcome some disadvantages, such as weak bonding, difficulty in controlling porosity, and mismatch of cracks from thermal expansion with the substrate.

- Spray pyrolysis: Spray pyrolysis is cost effective and can be sued to produce large-area thin films at atmospheric pressure. However, it has the disadvantages of a slow deposition rate and wastage of solution.

- CVD: CVD techniques have been used in the production of optical coatings for large-scale applications. CVD confers the benefits of deposition conformity, high purity films, and high deposition rate, although it requires volatile precursors. Thus, various enhanced CVD processes, such as HWCVD, AACVD, AP-PECVD, and oCVD, have been developed.

- Thermal evaporation deposition: A thin film with low contamination can be produced while controlling film deposition rates by thermal evaporation deposition. However, this technology is expensive.

- Sputtering: The sputtering deposition technique is one of the most widely used technologies for preparing thin films. To improve the deposition rate using the basic sputtering process, magnetron and pulsed magnetron sputtering processes were developed. Deposition at room temperature is one of the most important advantages

of the sputtering deposition process.

- NPDS: NPDS uses room temperature and low vacuum conditions to deposit a dry solid particle aerosol on a substrate. This is a relatively simple and low-cost process. However, performance and durability have not yet been verified sufficiently by other researchers in this area.

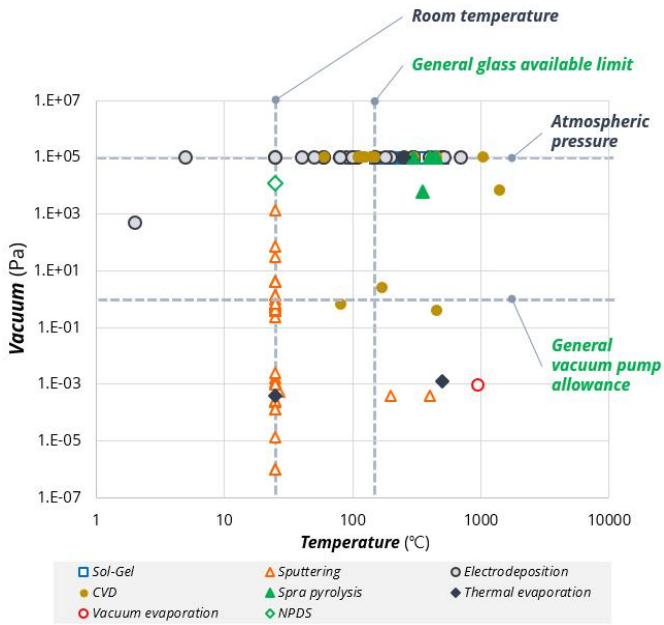

Figure 1.16 Process temperature and vacuum of each representative process

The most important factors in determining the cost of the process are the process temperature and vacuum conditions. Figure 1.16 shows the process temperature and vacuum of each representative process. The limit temperature in Figure 1.16 is the temperature when a general glass substrate is used. The limit reference for a vacuum is decided according to the capacity of a rotary vacuum pump. Most

electrodeposition and sol-gel processes are conducted under atmospheric pressure regardless of process temperature. CVD can be performed in any region and the maximum process temperature can reach over 1,000°C. Sputtering is usually conducted at room temperature but some processes require high vacuum and temperatures. The recently introduced NPDS is a direct deposition method at room temperature under low vacuum conditions. Because commercialization is a big issue, there is a continuing need for new deposition processes that are environmentally friendly, low cost, and provide enhanced deposition options.

1.6 Process information tables

Table 1.1 Electrochemical deposition for electrochromic devices

Material	Structure	Process time	Area (cm^2)	Post process	Ref.
Ag	Ag nanoplate array	10 hr	1 × 2	Drying at 40 °C	[9]
	Ag nano-particles	0~20 sec	1 × 1		[10]
Au	Au nono-particles		1 × 5	WO_3 deposition, annealing 100°C for 2 hr	[11]
Co_3O_4	Co_3O_4	300 sec	1.5 × 1.5	Drying at 85°C, annealing at 200~300°C for 1 hr	[12]
	Co_3O_4	300 sec	2.5 × 2.5	Cleaning for 2 days, annealing 200~300°C for 1 hr	[13]
	Co_3O_4	100 sec	1 × 1	Washing, drying at 80°C	[14]
MoO_3	MoO_3		0.7	Washing, drying, annealing at 350°C for 2 hr	[15]
$Ni(OH)_2$	$Ni(OH)_2$			Annealing for 1 hr at 250°C in air.	[16]
NiO	NiO	30~50 min			[17]
	NiO with PS template	300 sec	2 × 2	PS removing 24 hr in toluene, drying at 85°C, annealing 300°C for 1.5 hr	[18]
	Cu-doped NiO	15 min	1 × 3		[19]
	NiO	30 min		Annealing at 300°C for 1.5hr	[20]
	NiO	30~200 sec	1.2 × 5.0		[21]
	NiO	10/30/60 sec	3 × 2.5	Oxidizing at 300°C for 2 hr	[22]
	NiO		3 × 2.5	Rinsing	[23]
	NiO	20/40 min		Annealing at 400°C for 1 hr	[24]
	NiO on PPy		1 × 1		[25]
Poly-aniline (PANI)	PANI		2 × 2	Rinsing with HCl, drying with N_2	[19]
	PANI				[20]
	PANI	15~120 min	1 × 2.5	Washing with DI water, drying	[21]
Polyoxometalates (POMs)	POMs-P2W18 or P2W17			Rinsing, drying, 150°C for 30 min	[22]
Prussian blue	Prussian Blue	30 min	100 × 100		[23]
	Prussian Blue on ATO		2.5 × 2.5		[24]
	Prussian Blue on TiO_2	240 sec	4.0 × 2.0		[25]
SiO_2	silica(SiO_2) on PANI		2 × 2		[26]
TiO_2	TiO_2	300~1200 sec	1 × 1	Drying, annealing 350~500°C for 3 hr	[33]
V_2O_5	V_2O_5:TiO_2 (7:3)		2.5 × 2.5	Drying, firing at 120°C	[34]
	Mo doped V_2O_5	20/200 sec		Drying, heat treatment at 120°C for 24 hr	[35]
	V_2O_5		50 × 50	Baking 110°C for 10 hr	[36]
	V_2O_5 on NiO		2 × 4	Drying at 80°C for 12 hr	[37]
WO_3	WO_3	30 min	100 × 100		[30]
	WO_3	7 min	2.5 × 3.5		[38]
	WO_3 on TiO2		1 × 1	Drying in N_2 gas	[39]
	WO_3-MoO_3	5 min	1 × 1	Washing, drying in air at 80°C.	[40]
	WO_3 with PS template		2 × 3	PS removing for 24 hr in toluene, washing, drying	[41]
	WO_3-TiO_2	200~600 sec	2 × 2		[42]
	WO_3			TaN sputtering, annealing at 200°C under a vacuum	[43]
	WO_3			Washing for 2 hr, drying for 24 hr, annealing at 100°C for 2 hr	[44]
	WO_3				[45]
	WO_3 on Ag	20 min	1 × 5		[46]
	WO_3	500 sec	2		[47]
	PEDOT:PSS/WO_3	350 sec	2		[47]
	PEDOT/WO_3	6 hr	2 × 1.5		[48]
	WO3-copolymer	30 min	2 × 0.9	Rinsing with DI water, drying in air at room temperature for 24 hr	[49]
	WO_3/PPy	15 min	3 × 1	Annealing at 400°C for 3 hr	[50]
ZnO	ZnO		3 × 2	Cathodic polarization	[51]

Table 1.2 Electro-polymerization for electrochromic devices

Material	Structure	Process time	Area (cm^2)	Post process	Ref.
poly(3,4-ethylenedioxythiophene) (PEDOT)	PEDOT and poly(3-methylthiophene)(PMeT)		1 × 2	Removing residue monomers	[52]
	PEDOT with PS template		3 × 3	PS removing for 12 hr in toluene	[53]
	PEDOT:PSS	50 sec	2		[47]
	PEDOT	1 hr	2 × 1.5		[48]
Phenylbenzidine	Phenylbenzidine	10 min	1 × 2	Washing with ethanol	[54]
Copolymer	Copolymer		2 × 0.9	Rinsing with DI water, drying in air at room temperature for 24 hr	[49]

Table 1.3 Sol-gel process for electrochromic devices

Material	Structure	Process time	Area (cm^2)	Post process	Ref.
WO_3	WO_3	1~2 hr	1 × 1	Drying at 60°C for 2 min, thermal annealing at 100~450°C	[196]
	WO_3	2 hr		Drying at 120°C for 1 min, calcination at room temperature, 300/400°C	[197]
	WO_3	1 hr	1 × 2	Drying at 120°C thermal annealing at 200°C	[198]
	WO_3	1 hr		Drying at 100°C for 10 min, thermal treatment at 100~500°C	[199]
	WO_3	1~20 hr		Drying at room temperature for 10 min, thermal treatment at 100~450 °C	[200]
	WO_3 gold nano particle composite	2 hr	1 × 5	Drying at room temperature for 12 min, thermal treatment at 100°C	[201]
	Porous WO_3	1 hr	1 × 3	Drying at 48°C for 48 hr, thermal treatment at 150°C	[202]
	Porous WO_3	2 hr		Drying at room temperature for 1 hr, calcination at 300°C	[203]
	Nano Porous WO_3	2 hr		Drying at room temperature for 24 hr, two step annealing at 190°C and 300~400°C	[204]
	Mesoporous WO_3	1 hr		Drying with heated air, calcination at 300°C	[205]
	Mesoporous WO_3	1 hr	2.3 × 1.9	Calcination at 300°C	[206]
	WO_3 / $ZnWO_4$ Bilayer	2 hr		Calcination at 500°C	[207]
NiO	NiO	5 min		Drying at 250~450°C for 1 hr, annealing at 250°C	[208]
	B doped NiO	2 hr		Calcination at 350°C	[209]
	NiO	15 min	2 × 1	Drying at 200°C, annealing at 400~460°C	[210]
	NiO	1 hr		Drying at room temperature for 5 min, oxidation at 350°C for 5 min and annealing at 400°C	[211]
	NiO-TiO_2 Composite	30 min	5 × 3	Thermal treatment at 300/500°C	[212]
V_2O_5	Mo-doped V_2O_5	24 hr		Drying at room temperature, thermal treatment at 120°C	[213]
	V_2O_5	20 min		Thermal treatment at 150°C	[214]
MoO_3	MoO_3 multi-layered	1 hr		Drying at room temperature for 5 min, oxidation at 200~350°C	[215]
Copper manganese oxide	CMO	0.5~2 hr		Drying at 160°C for 20 min, calcination at 300~450°C	[216]

Table 1.4 Spray pyrolysis for electrochromic devices

Materials	Structure	Area (cm^2)	Process temperature	Ref.
WO_3	V_2O_5 mixed		Substrate 400°C	[90]
	Nb_2O_5 mixed		Substrate 450°C	[91]
	High porous, high surface roughness	2.5 × 2.5	Annealing 350°C for 6hr	[93]
	Sb-doped	2 × 1	Substrate 400°C	[97]
V_2O_5	V_2O_5		Substrate 450°C	[94]
NiO	Smooth morphology	10 × 4	Substrate 330~420°C	[98]
	Lithium-doped NiO film	2 × 2	Substrate 350°C	[95]
CeO_2	ZrO_2 mixed	7 × 3.5	Substrate 400°C	[92]
MoO_3	Amorphous	7 × 2.5	Substrate 350°C	[96]

Table 1.5 Chemical vapor deposition for electrochromic devices

Material	Structure	Process time	Area (cm^2)	Post process	Ref.
W	WO_3	1 hr	7.5 × 1.2	Heated for drying	[217]
	WO_3/Gold nanoparticles				[218]
	WO_xC_y				[219]
	WO_3 nanoparticles			Annealed in air for 2 hr at 300°C.	[104]
	WOx	15 min		Thermal annealing at 150°C	[220]
	Hexagonal WO_3 (h-WO_3)	5 min		Annealed for 1 hr at 150°C	[221]
NiO	NiO				[17]
	NiO/polyaniline (PANI)				[222]
	Nanoporous NiO			300°C in air for 90 min	[223]
	Highly porous NiO	1.5 hr	4 × 5	Annealed at different temperatures (300/400/500°C) in air for 1.5 hr	[224]
	NiO_xC_y		3 × 4		[128]
	NiO	30 min	3 × 0.7		[114]
MoO_3	MoO_3			Annealed at 673K in an O_2 atmosphere (99.99%) for 1 hr	[225]
TiO_2	TiO_2	50 min	21 × 30		[226]
	TiO_2	30 min			[132]
Prussian blue	Prussian blue				[227]
$Mo_xO_yC_z$	MoO_xC_y				[228]
	MoO_yC_z & $WMo_xO_yC_z$		3 × 3		[129]
	$WMo_xO_yC_z$		3 × 3		[130]
$WTa_xO_yC_z$	$WTa_xO_yC_z$		3 × 3		[131]

Table 1.6 Thermal evaporation deposition for electrochromic devices

Material	Structure	Process time	Area (cm^2)	Process temperature	Ref.
WO_3	Polycrystalline		15 × 15		[27]
	Amorphous	> 2 hr		Annealing at 200°C for 2 hr	[141]
	Amorphous		3 × 3.5	Deposition at RT~240°C	[140]
NiO	Polycrystalline	2 hr		Deposition at RT	[138]
MoO_3	Polycrystalline			Deposition at RT/100/200°C, annealing at 200/300°C	[139]

Table 1.7 Sputtering process for electrochromic devices (I)

Material	Structure	Film thickness (nm)	Process time	Area (cm^2)	Post process	Ref.
W	WO_3	385.9				[157]
	WO_{3-z}		3 hr			[93]
	WO_3	140, 135, 135, 120, 121		1 × 2		[175]
	N-doped WO_3					[158]
	WO_3	400, 500		3 × 3		[159]
	WO_3	100				[135]
	WO_3	430~460		5 × 5		[139]
	WO_3		20~50 min			[131]
	WO_3	325, 330, 318, 326,311			Annealing at 450°C for 3hr	[160]
	WO_3 and Mo doped WO_3		120 min			[140]
	WO_3	330		5 × 5		[170]
	WO_{3-x}		30 min	2.5 × 2.5		[163]
	WO_3		25 min			[172]
	WO_3	380		2 × 2		[164]
Si and W	$W_xSi_yO_z$					[192]
W and Ni	Ni-W oxide	200				[161]
W, W(95wt%)+Ti(5wt%), W(90wt%)+Ti(10wt%)	WO_3 and W-Ti-oxide	300		5 × 5		[177]
WO_3	WO_3			3 × 3		[152]
	WO_3	301/315/333	60 min			[170]
	WO_3	151/195/482	30/45/60 min			[153]
	WO_3			3 × 3		[154]
	WO_3	70~110				[171]
	WO_3	300		5 × 5		[150]

Table 1.8 Sputtering process for electrochromic devices (II)

Material	Structure	Film thickness (nm)	Process time	Area (cm^2)	Post process	Ref.
Ta, Al, Pd, Mg-Ni	Ta_2O_5, Al, Pd, Mg_4Ni			3 × 3		[143] [144] [145] [165] [181]
TiO_2	TiO_2	400	60 min			[158]
	TiO_2					[159]
$Li_2O/NiO/WO_3$	$Li_{1.2}NiW_{0.1}O_x$	300				[160]
Li_2NiO_2, $LiNiO_2$, and $LiNi_2O_x$	Li_xNi_yO			1 × 5		[142]
LATP	$Li_{1.3}Al_{0.3}Ti_{1.7}(PO_4)_3$ (LATP)	275	60 min			[164]
$LiPO_4$ and WO_3 (2 wt%) (LPWO)	LPWON	700				[163]
$LiTaO_3$	$LiTaO_3$	440		5 × 5		[186]
	$LiTaO_3$		180 min			[188]
Li_2O and Ni-Zr alloy	nanocompositenickeloxide	200		3.8 × 2.1		[172]
Ni and $NiV_{0.08}$	$Ni_{1-x}V_xO_y$ and NiO_y	200				[184]
Ni	Ni oxide	338				[173]
	NiOOH	100				[190]
	Porous Ni-oxide	500		5 × 5		[157]
ZnO/In_2O_3	IZO	200~300				[162]
In_2O_3:ZnO (87:13wt%)	IZO	100~200	30 min			[148]
Ir and Ta	IrTaOx	180	90~150 min			[189]
	Ir oxide					[166]
Al	ZnO:Al(ZAO)		10/25/40 min	2 × 2		[185]
CdS, CdTe, $CdCl_2$	CdS, CdTe, $CdCl_2$	70/200/2500				[149]
Si and Co	$Co_xSi_yO_z$					[182]
Nb_2O_5:MoO_3 (90:10)	Nb_2O_5:MoO_3 (90:10)	1120/1090/1080	30 min			[167]
Nb_2O_5	Nb_2O_5				Annealing 400~700℃ for 6 hr	[168]

Chapter 2. ECD fabrication using NPDS

2.1 Overview

Electrochromism is a reversible change in the optical transmittance, absorbance, and/or reflectance of a material in response to an applied voltage [196-198]. The phenomenon was discovered 40 years ago [199], and the electrochromic (EC) effect occurs in many transition metal oxide materials, as well as in some organic molecules and polymers. Electrochromism in metal oxide materials is based on reversible modulation of the transmittance, which occurs by electrically controlling the oxidation state. Metal oxide EC materials that exhibit color changes following electron injection and charge-balancing ion insertion (cathodic coloration) include WO_3, MoO_3, TiO_2, Ta_2O_5, and Nb_2O_5. These oxides become highly transparent upon ion extraction.

EC films are currently being developed for applications in 'smart' window technologies, which represent part of the emerging energy-efficiency advances in buildings and automobile technologies [31, 200-202]. The transmittance of these smart windows can be controlled using a small applied voltage, allowing us to control the amount of daylight, solar heat gain, and internal heat loss through the windows of buildings and vehicles. Tungsten oxide (WO_3) is the most widely studied inorganic EC material, and has also had the greatest commercial uptake. WO_3 is non-toxic and has favorable electrochemical and optical properties [203-208]. Nevertheless, the deposition of WO_3 thin films remains expensive. Techniques used to deposit WO_3 films depend on the application, and include chemical vapor deposition (CVD) [209], radio frequency (RF) sputtering [210], cathodic electrodeposition [211], the sol-gel process [212], and spray pyrolysis [213]. CVD

consumes large quantities of energy, due to the high temperatures involved; it also requires sophisticated condition management and post-processing treatments. RF sputtering requires large quantities of energy because of the high-vacuum conditions. Cathodic electrodeposition, the sol-gel process, and spray pyrolysis methods provide only limited control over the process conditions.

In 2006, Ahn *et al*. reported a room-temperature deposition system based on low-vacuum air-spray, the nano-particle deposition system (NPDS), which they used to deposit nano/micro particles on a substrate [192, 194]. The NPDS technique enables the deposition of metal and ceramic particles with sizes from 100 nm to 100 μm on substrates including ceramics, metals, polymers, and paper, without requiring a precursor. It is relatively simple and low-cost, and is suitable for the mass-production of thin films suitable with potential applications in energy-saving technologies, such as EC windows, which have received much recent research attention [1]. Here, we demonstrate the fabrication of WO_3 films for EC device applications using NPDS.

2.2 Experiments

Figure 2.1 shows a schematic diagram of the NPDS system, which consisted of an air compressor (S30-120-3, Seowon Compressor Co., Ltd), a fluidized-bed aerosol generator (3400A, TSI Incorporated), a subsonic slit nozzle, a vacuum chamber, a vacuum pump (WOVP-0200N, Woosung Vacuum), and an X-Y stage system (AM1-0815-3S, MMT). The nozzle and vacuum chamber were custom-built. The NPDS included a number of commercial components, but the system was designed and developed in our laboratory.

The deposition chamber was evacuated to a base pressure of 10 kPa using a rotary pump, and the target particles were supplied using compressed air at 0.3 MPa. The

powder feed rate was 5 mm^3/min, the velocity of the compressed air was 300 m/s, and the stage speed was 50 µm/s. The path length of the stage was 10 mm and the slit length of the nozzle was 10 mm; therefore the total deposition area was 100 mm^2. The standoff distance (i.e., the separation between the nozzle and the substrate) was 3.0 mm. A small chamber (300 × 300 × 300 mm^3) and short stroke (15 mm) stages were used for the fabrication of relatively small (10 × 10 mm^2) EC films; however, it would be possible to fabricate larger-area films if a larger chamber and stage were used. High-temperature and high-vacuum conditions were not required.

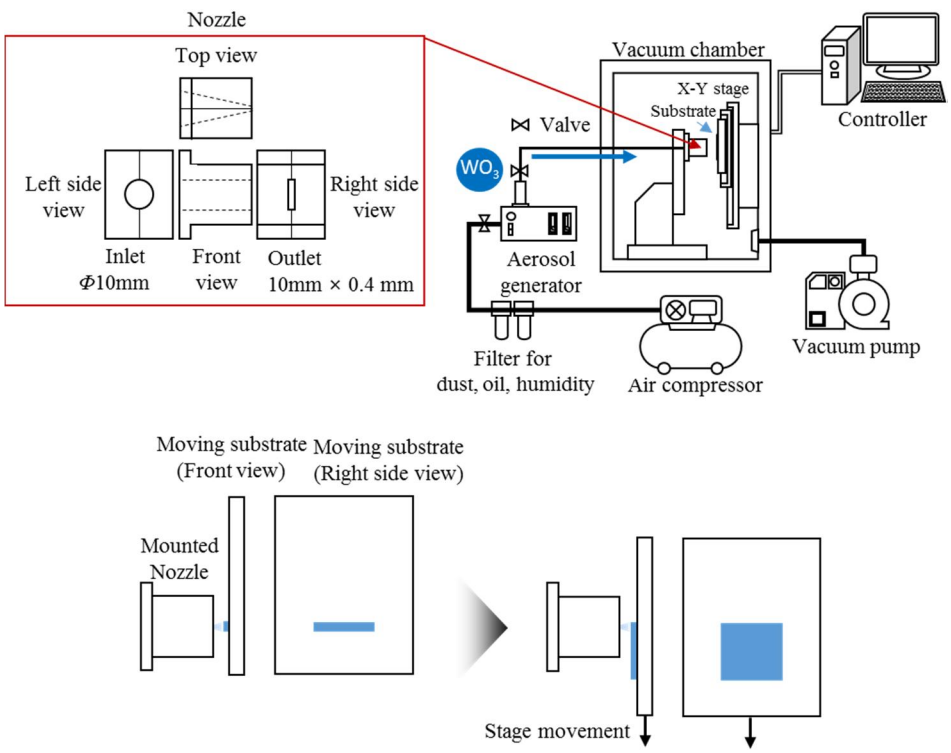

Figure 2.1 A schematic diagram of NPDS nozzle for film deposition

The adhesion of the deposited film was investigated using Scotch tape following the deposition process. The Scotch tape was peeled off manually at ~1 cm/s, and all samples passed this Scotch tape peeling test. In addition, annealing was carried out at 300ºC for 1 hour, and the transmittance was compared before and after annealing.

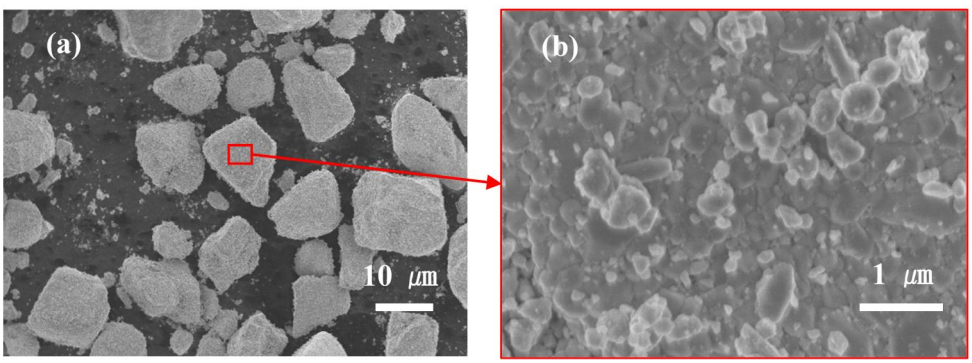

Figure 2.2 SEM image of the WO_3 powder

The WO_3 powder (Sigma–Aldrich) was ≤ 20 μm in diameter, and at least 99% purity (in terms of contamination with trace metals). Figure 2.2 shows SEM images of the surface morphology of the WO_3 powder. During the deposition process, the powder particles underwent fragmentation into smaller particles. The deposition time was 200 s, and a fluidized bed aerosol generator was used to supply the target particles to the chamber, which were then sprayed through the nozzle onto the substrate. The deposition conditions are listed in Table 2.1. A fluorine-doped tin oxide (FTO) glass substrate (Fine Chemicals Industry) was used, which had a sheet resistance of 10 Ω/sq, as well as an indium tin oxide (ITO) glass substrate (Fine Chemicals Industry), which also had a sheet resistance of 10 Ω/sq. The substrates were cleaned using ultra-sonication and then rinsed with acetone, ethanol, and

deionized (DI) water prior to loading into the deposition chamber. The structure of the WO_3 films was analyzed using X-ray diffraction (XRD) with a Cu-Kα radiation source, and the surface morphology and thickness of the films was examined using scanning electron microscopy (SEM) and atomic force microscopy (AFM).

Table 2.1 The NPDS deposition conditions.

Parameter	Value
Stand-off distance* [mm]	3.0
Pressure of compressed air [MPa]	0.3
Chamber vacuum [Torr]	75
Powder feed rate [mm^3/min]	5.0
Compressed air velocity [m/s]	300
Stage speed [μm/s]	50
Carrier gas	Compressed air
Target material	WO_3 powder
Substrate	FTO glass ITO glass

* *Stand-off distance: separation between the nozzle and the substrate*

The electrochemical properties of the WO_3 films were investigated using a three-electrode cell with a Pt counter electrode and an Ag/AgCl reference electrode. A 0.1 M solution of $LiClO_4$ in propylene carbonate (PC) (99.7% anhydrous, Aldrich) was used as the electrolyte. An electrochemical analyzer (CHI 660D, CH instruments) was used to measure the chronocoulometry and cyclic voltammetry of the WO_3 films. Optical transmittance spectra of the films were examined at wavelengths in the range

300–800 nm using an ultraviolet/visible/near-infrared (UV/VIS/NIR) spectrophotometer (V-570, JASCO, Easton, MD).

2.3 Results and discussion

2.3.1 Optical transmittance

Table 2.2 lists the transmittance of specimens in the transparent state, including annealed and non-annealed samples. FTO and ITO glass substrates with no deposited layer were used as a reference. The ITO glass substrate exhibited approximately 2% larger transmittance than the FTO glass substrate. The transmittance of the substrates with the WO_3 EC films was lower than that of the substrates with no EC layer (the difference in transmission with the FTO glass substrate was 15%, and was 12–13% with the ITO glass substrate). The effects of annealing were not significant on the optical transmittance for either substrate.

Table 2.2 Transmittance of transparent specimen comparing annealed and non-annealed treatment.

Transmittance (@ 800 nm)	**FTO glass**	**ITO glass**
$T_{non\text{-}deposited}$	72 %	74 %
$T_{EC\text{-}film,\ non\text{-}annealing}$	57 %	61 %
$T_{EC\text{-}film,\ non\text{-}annealing} - T_{non\text{-}deposited}$	-15 %	-13 %
$T_{EC\text{-}film,\ annealing}$	57 %	62 %
$T_{EC\text{-}film,\ annealing} - T_{non\text{-}deposited}$	-15 %	-12 %

Figure 2.3 and Figure 2.4 show transmission spectra of the EC samples based on FTO glass and ITO glass, respectively, and Table 2.3 lists changes in the transmittance. The contrast in transmittance, ΔT, is a critical metric for electrochromic materials, and is defined as $\Delta T = T_{max} - T_{min}$; i.e., the difference in transmission between the transparent and colored states at a fixed wavelength.

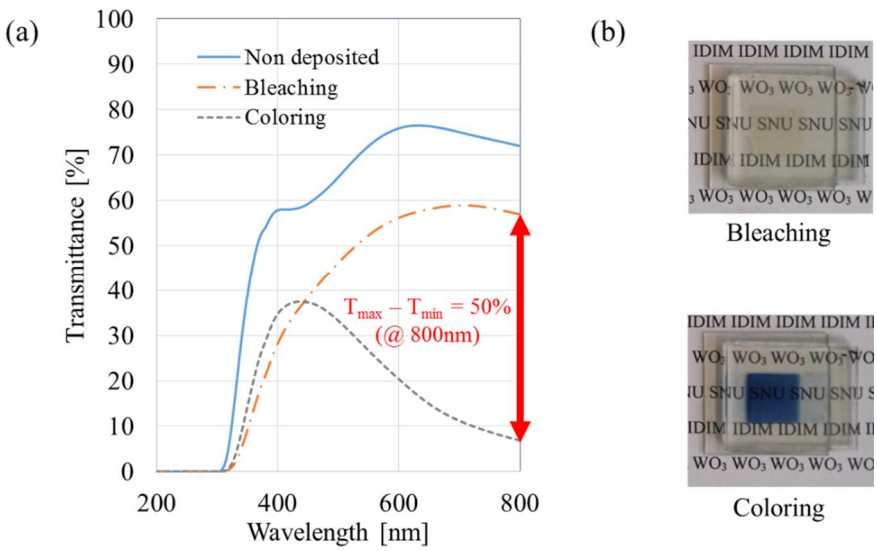

Figure 2.3 (a) Transmittance spectra of the WO_3 film deposited on the FTO glass substrate and (b) photographs of the bleaching (top) and coloring (bottom) states.

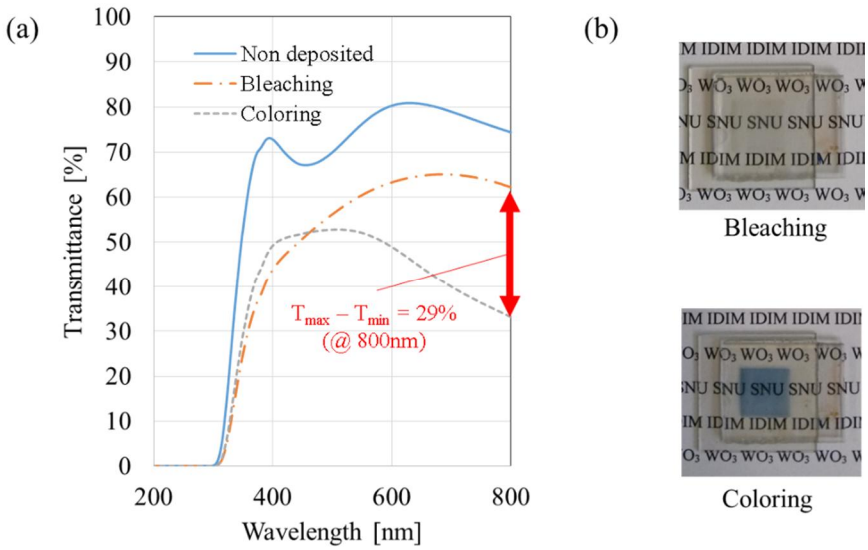

Figure 2.4 (a) Transmittance spectra of the WO_3 film deposited on the ITO glass substrate and (b) photographs of the bleaching (top) and coloring (bottom) states.

Table 2.3 Transmittance of colored specimen comparing annealed and non-annealed treatment.

Transmittance (@ 800 nm)	FTO glass		ITO glass	
	Non-annealing	Annealing	Non-annealing	Annealing
$T_{max,}$	57 %	57 %	61 %	62 %
T_{min}	10 %	7 %	33 %	33 %
ΔT ($T_{max} - T_{min}$)	47 %	50 %	28 %	29 %

With the FTO glass based EC cell, T_{max} was 4–5% smaller than for the ITO glass based cell at 800 nm, but with the FTO glass based EC cell, T_{min} was 23–26% larger

than with the ITO glass based cell (also at 800 nm). As a result, the contrast of the FTO glass based cell was 19–21% larger than that of the ITO glass based cell. Annealing resulted in a variation of only 1–3% in transmittance, which is not significant for EC applications. Table 2.4 lists the contrast between colored and transparent states at several wavelengths.

Table 2.4 Contrast of colored specimen according to wavelength.

Wavelength (nm)	FTO glass		ITO glass	
	Non-annealing	Annealing	Non-annealing	Annealing
300	0 %	0 %	0 %	0 %
400	-3 %	-6 %	-2 %	-5 %
500	16 %	13 %	5 %	4 %
600	37 %	36 %	16 %	14 %
700	46 %	48 %	24 %	25 %
800	47 %	50 %	28 %	29 %

The WO_3 film on the FTO glass substrate exhibited the largest optical contrast of 50% at 800 nm (see also Figure 2.3(a)). At wavelengths in the range 300–450 nm, the transmittance of colored state was larger than that of the transparent state, as shown in Figure 2.3(a) and Figure 2.4(a). Figure 2.3(b) and Figure 2.4(b) show photographs of the transparent and colored states of the WO_3 film on the FTO glass and ITO glass substrates, respectively; the samples appeared dark blue in the colored state and appeared slightly yellow in the transparent state.

2.3.2 X-ray diffraction analysis

Figure 2.5 shows XRD patterns of the deposited WO_3 films on the FTO glass substrate, as well as spectra of the FTO glass and the WO_3 powder in isolation. Figure 2.6 shows XRD patterns of the deposited WO_3 films on the ITO glass substrate, as well as the ITO glass and the WO_3 powder in isolation. Three Bragg reflection peaks were observed at 23.1º, 23.6º, and 24.4° for the WO_3 powder, as well as the WO_3 film on the FTO glass and ITO glass substrates. It follows that the WO_3 had a monoclinic structure, which was retained following deposition on both the FTO and ITO glass substrates.

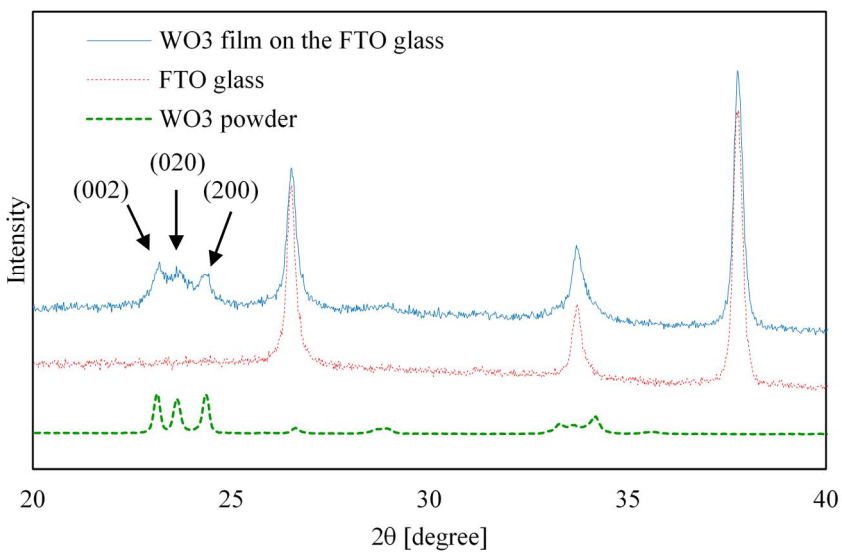

Figure 2.5 XRD patterns of the deposited WO_3 film on the FTO glass, FTO glass only, and the WO_3 powder.

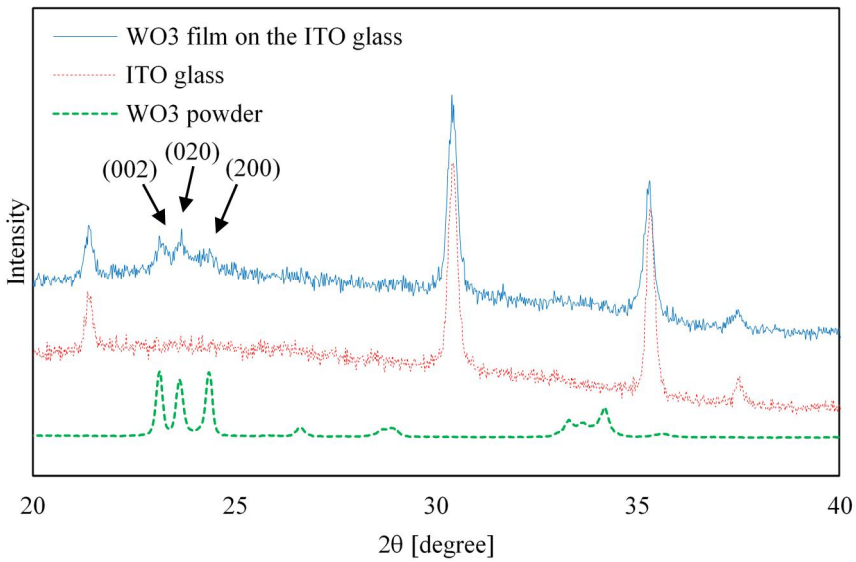

Figure 2.6 XRD patterns of the deposited WO_3 film on the ITO glass, ITO glass only, and the WO_3 powder.

2.3.3 Surface morphology and film thickness

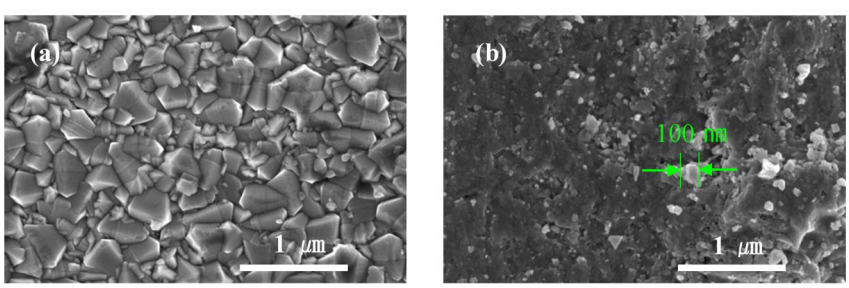

Figure 2.7 SEM images of (a) an FTO glass substrate and (b) a WO_3 film deposited on an FTO glass substrate.

Figure 2.7(a) shows SEM images of the surface of the FTO glass substrate before

deposition, and Figure 2.7(b) shows the surface of the WO_3 film deposited on the FTO glass substrate. Figure 2.8(a) shows SEM images of the surface of the ITO glass substrate before deposition, and Figure 2.8(b) shows the surface of WO_3 film deposited on this substrate.

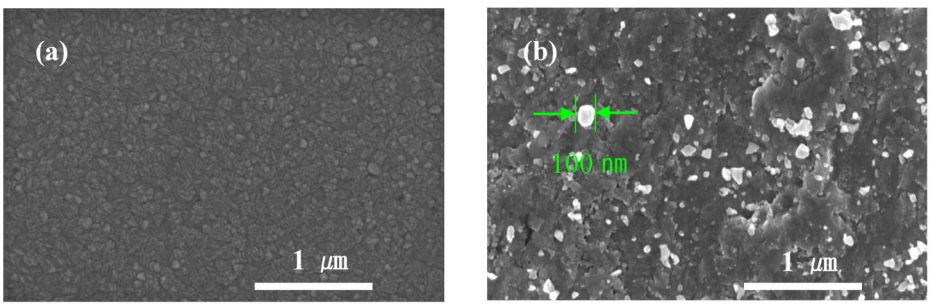

Figure 2.8 SEM images of (a) an ITO glass substrate and (b) a WO_3 film deposited on an ITO glass substrate.

The ITO layer on the glass consisted of crystals sized ~50 μm, whereas the FTO layer on the glass consisted of crystals with a size of up to 500 μm. Therefore, we may expect that the FTO layer on the glass will crack more easily than that the ITO layer on the glass following mild shock. For this reason, an FTO based substrate require a thicker basis substrate than an ITO based substrate. (Here we used 1.1-mm-thick ITO glass substrates and 2.2-mm-thick FTO glass substrates.)

During NPDS process, the bonding mechanism of the WO_3 powders onto the substrate is as follows. First, several particles (with diameters of tens of micrometers) hit the substrate and fragment. These fractured submicron particles stick together due to relatively weak van der Waals forces. Subsequently, further particles hit the accumulated layer submicron particles, and shock compaction of these submicron

particles occurs. Figure 2.9 shows an AFM image of a WO_3 film on an FTO glass substrate.

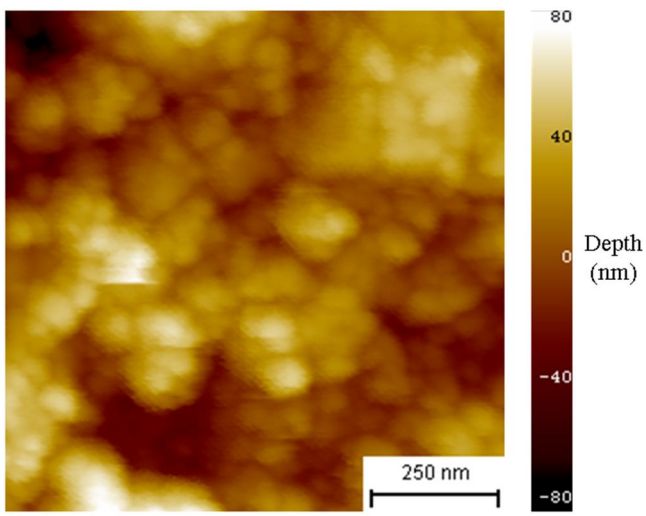

Figure 2.9 AFM image of the WO_3 film deposited on FTO glass.

The average roughness was S_a = 19.0 nm, the root mean squared roughness was S_q = 23.8 nm, and the maximum height difference was S_y = 169 nm. The film was composed of small particles with diameters in the range 50–130 nm. Figure 2.10 shows a cross-sectional SEM image of the WO_3 film deposited on the FTO glass substrate.

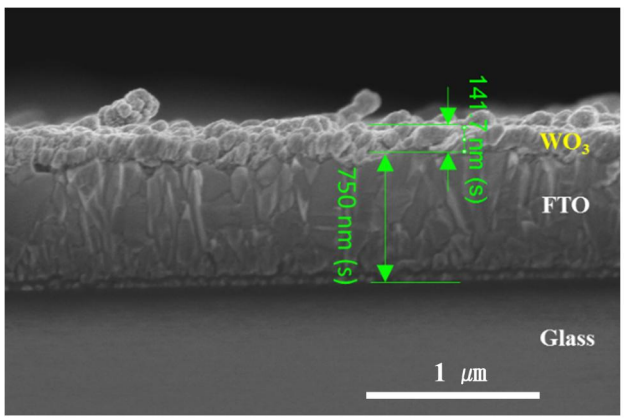

Figure 2.10 Cross-sectional SEM image of the WO_3 film deposited on the FTO glass.

The WO_3 film was approximately 140 nm thick, and the FTO layer was approximately 750 nm thick. Based on the peak-to-valley roughness of 169 nm and the average thickness of 140 nm, the WO_3 film appeared to have a quasi-monolayer structure.

2.3.4 Electrochemical properties

Cyclic voltammetry (CV) was used to investigate Li^+ insertion/extraction processes on the WO_3 film, as shown in Figure 2.11. CV was carried out at room temperature using a 0.1-M solution of $LiClO_4$ in propylene carbonate. The WO_3 films exhibited electrochemically active regions between 3 V and –2.5 V, which was highly reversible. The cathodic peak was 4.4 mA at –2.5 V, corresponding to Li^+ intercalation, and the WO_3 film became dark blue. The anodic peak was –2.0 mA at 0.3 V, which is associated with Li^+ extraction, and the film became transparent yellow.

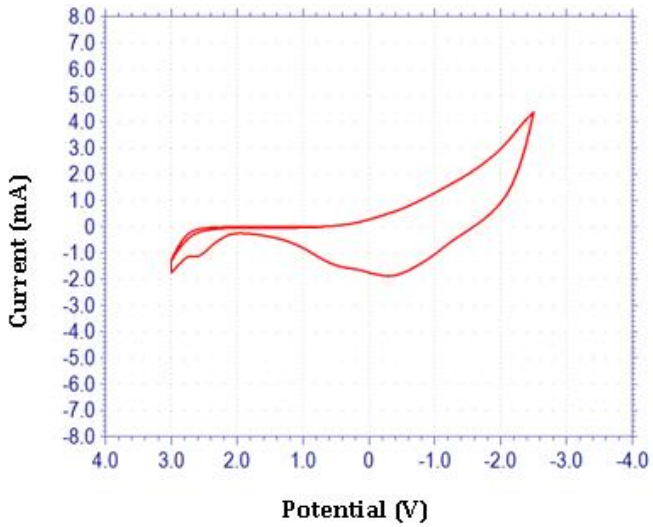

Figure 2.11 Cyclic voltammogram of the WO_3 film (10×10 mm^2) in a 0.1 M $LiClO_4$/propylene carbonate electrolyte.

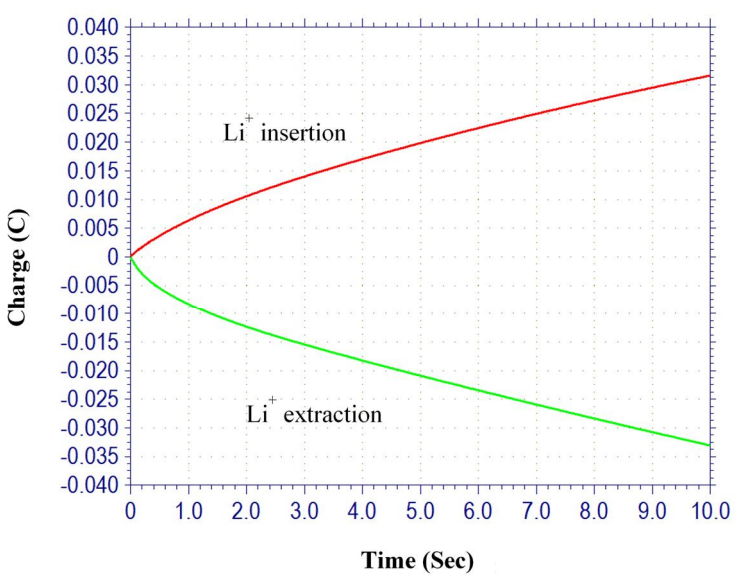

Figure 2.12 Chronocoulometry of the WO_3 film (10×10 mm^2) in a 0.1 M $LiClO_4$/propylene carbonate electrolyte at applied voltages in the range -2.5 V to 3 V.

Only a small change in the applied voltage was required for color switching. The capacitance of the WO_3 film was symmetric, and increased or decreased corresponding to the reduction and oxidation of the film, as shown in Figure 2.12. This also corresponds to reversible color switching.

2.4 Summary of ECDs fabricated using NPDS

WO_3 thin films were deposited on FTO and ITO glass substrates using NPDS at room temperature under low-vacuum conditions. The WO_3 films on the FTO glass substrate exhibited a large EC contrast of 50% at 800 nm, with T_{min} = 7% and T_{max} = 57%. XRD data revealed that the WO_3 thin films formed monoclinic structures. Symmetrical charging processes corresponding to reduction and oxidation of the WO_3 film were observed via chronocoulometry. Cyclic voltammetry measurements revealed that a small applied bias was required for color switching. The color of the WO_3 films changed from transparent yellow to dark blue in response to a change in the applied bias, demonstrating electrochromism. We may therefore conclude the NPDS is a suitable low-cost method for fabricating inorganic electrochromic windows.

Chapter 3. Large-area ECWs and response time model

3.1 Overview

Electrochromic phenomena were discovered in the 1960s [199]. Since then, many researchers have searched for materials with electrochromic properties or ways to improve the performance of ECDs [131, 214-216]. However, most previous ECD studies focused on small-size ECDs with active areas of a few square centimeters. There have been few investigations into large-scale ECDs. In particular, an electrochemical model of the coloration response time has been developed in [217]; however, the error in the estimate provided by this model increases significantly as the active area increases. Current research into ECDs includes studies into electrochromic windows (ECWs) [200, 218]. These dynamic windows darken or lighten electronically in response to the application of small voltages. This enables users to control daylight, solar heat gain, and internal heat loss through the windows of buildings and vehicles. The key issues facing researchers developing ECWs are the deposition of the intended electrochromic film over large areas and the predicted operation time of the ECDs.

In this chapter, we describe a process that can deposit a square meter of electrochromic film for practical applications in ECWs. We also propose a new coloration response time model, which is suitable for large-area ECDs.

3.2 NPDS enlargement for large area applications

NPDS can be used to deposit various oxide particles onto a substrate without any precursors. They can be operated at room temperature under low vacuum conditions. In more detail, nanoparticles are accelerated to high speeds by the vacuum and

compressed air. These particles are then consolidated on the substrate at high heat energy and pressure. Thus, this method can be used to mass produce thin films at relatively low cost. We designed a square-meter NPDS by taking hydrodynamic considerations into account. Our goal was to increase the capacity of the stage, nozzle, vacuum pump, air compressor, vacuum chamber, and aerosol generator for large-area deposition manufacturing applications. The NPDS prototype was then used to prepare WO_3 thin films for use as the cathode in electrochromic window applications.

Figure 3.1 shows a schematic diagram of the large-area NPDS, consisting of an air compressor (PA-BACT3, Powerair Co., Ltd), powder disperser (RBG 1000, PALAS), subsonic slit nozzle, vacuum chamber, vacuum pump (MVP-144, Woosung Vacuum) and an X-Y-Z stage system (CEM-Clipper Plus, Delta Tau). The nozzle and vacuum chamber were custom-designed. The entire system was designed and constructed in our laboratory. And Figure 3.2 shows a real pictures of the large-area NPDS and 3D model.

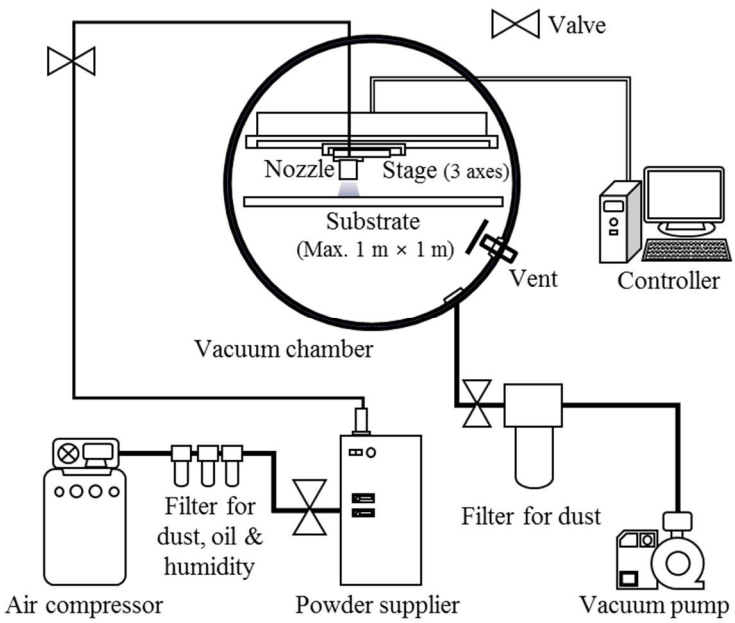

Figure 3.1 Schematic diagram of the large-area nanoparticle deposition system (NPDS)

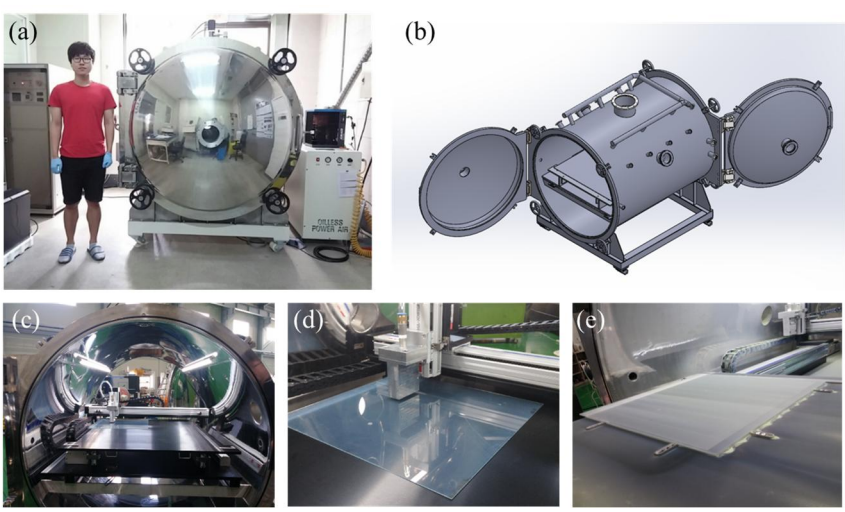

Figure 3.2 Real pictures and 3D model of the large-area nanoparticle deposition system (NPDS): (a) exterior of equipment, (b) 3D model,
(c) interior of equipment, (d) deposition process, (e) deposited substrate

3.3 Fabrication of large area electrochromic windows (ECWs)

The deposition chamber was evacuated to a base vacuum pressure of 75 Torr using a rotary pump, and the target particles were supplied using compressed air (0.3 MPa). The powder feed rate was 25 mm^3/min and the compressed air velocity was 300 m/s. The stage speed was 500 μm/s and the slit length and width of the nozzle were 50 mm and 0.4 mm, respectively. The stand-off distance (SoD; the distance between the nozzle and the substrate) was 3.0 mm. We used a large cylindrical chamber (Φ1.40 m × 1.84 m) and a long stroke (*x*: 1.005 m, *y*: 1.005 m, *z*: 0.050 m) stage to fabricate electrochromic films with a variety of sizes. Five sizes of samples were prepared: 10 × 10 mm^2, 50 × 50 mm^2, 300 × 300 mm^2, 500 × 500 mm^2, and 1 × 1 m^2.

The diameters of the WO_3 nanoparticles (Sigma–Aldrich) were ≤ 20 μm. In terms of contamination by trace metals, the purity of the nanoparticles was at least 99%. The powder particles fragmented into smaller particles during the deposition process, which was carried out at room temperature. The target particles were supplied to the chamber using a powder disperser. They were then sprayed through the nozzle onto the substrate. The deposition conditions are listed in the Table 3.1.

Table 3.1 Large-area NPDS conditions.

Parameter	Value
Stand-off distance* [mm]	3.0
Pressure of compressed air [MPa]	0.3
Chamber vacuum [Torr]	75
Powder feed rate [mm^3/min]	25
Compressed air velocity [m/s]	300
Stage speed [μm/s]	500
Nozzle slit [mm × mm]	50 × 0.4
Carrier gas	Compressed air
Target material	WO_3 powder
Substrate	FTO glass

* *Stand-off distance: separation between the nozzle and the substrate*

We used a fluorine-doped tin oxide (FTO) glass substrate with a sheet resistance (R_{sq}) of 12 Ω/sq. We fabricated electrochromic window samples from the WO_3 films. A 1.0-M solution of $LiClO_4$ in propylene carbonate (PC) (99.7% anhydrous, Aldrich) was used as the electrolyte. For the coloration test, we used a power source and current meter (2450 SourceMeter®, Keithley). The optical transmittance of the ECW samples was measured at a wavelength of 785 nm using a fiber-type laser (Stradus® 785-80, Vortran Laser Technology) and an integrating sphere detector (819D-SL-2-CAL2, Newport Corporation). Figure 3.3 is a real picture of 1 × 1 m^2 class electrochromic window fabricated using large-area NPDS. The uniformity of the 1 × 1 m^2 class electrochromic window was measured.

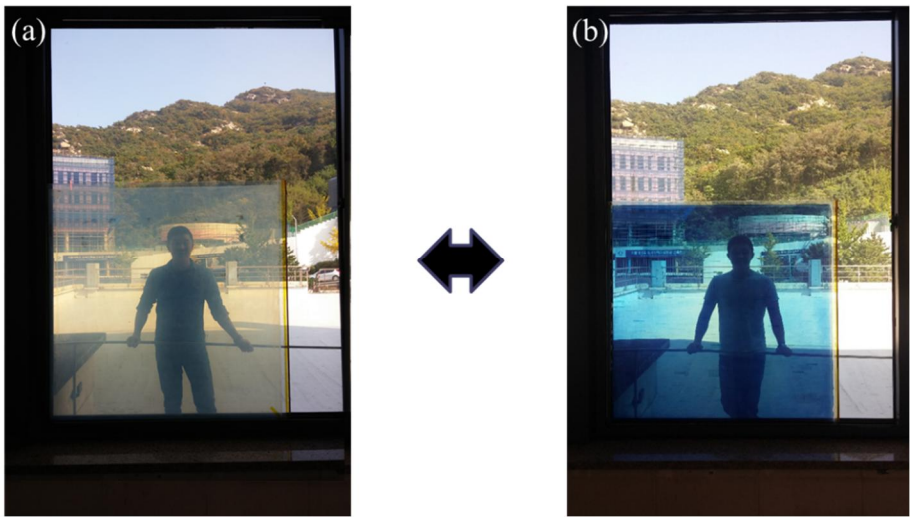

Figure 3.3 An 1 × 1 m^2 class electrochromic window fabricated using large-area NPDS: (a) bleaching state (b) coloring state

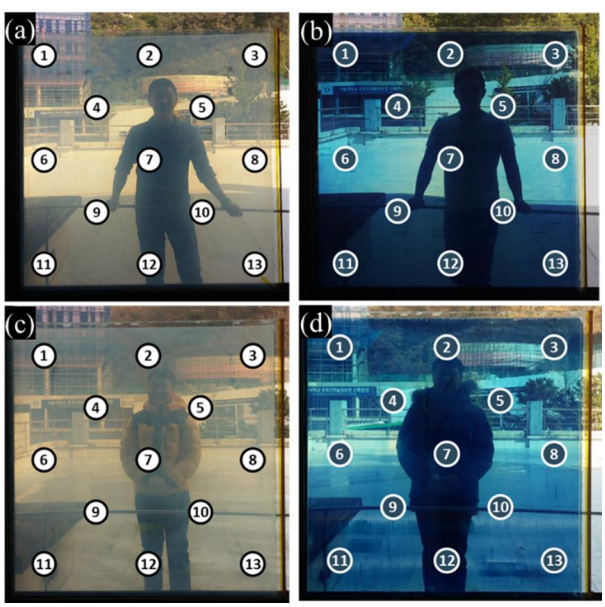

Figure 3.4 The 13 points for measuring transmittance uniformity: (a) bleaching state of sample #1, (b) coloring state of sample #1, (c) bleaching state of sample #2, (d) coloring state of sample #2

Figure 3.4 shows the 13 points for measuring transmittance uniformity of two samples and Table 3.2 shows the transmittance in the bleaching / coloring state at each point. The average transmittance of the sample #1 in the bleaching state and coloring state were 57.8% and 2.3%, respectively, and the uniformity was 1.14% and 1.17%, respectively. The average transmittance of the sample #2 in the bleaching state and the coloring state were 4.8% and 2.4%, respectively, and the uniformity was 1.17% and 1.15%, respectively. The contrasts of Sample #1 and Sample #2 were 55.4% and 52.4%, respectively, and the uniformity were 1.76% and 1.82%, respectively. The uniformity between samples was within 3.0%.

Table 3.2 The transmittance in the bleaching / coloring state at each point.

Sample #1				Sample #2			
Location	T_b [%]	T_c [%]	ΔT [%]	Location	T_b [%]	T_c [%]	ΔT [%]
1	59.2	0.7	58.5	1	54.3	3.5	50.8
2	58.5	1.7	56.8	2	53	1	52
3	59	1.4	57.6	3	56.1	2	54.1
4	57.4	1.7	55.7	4	55.4	1.7	53.7
5	55.5	2.1	53.4	5	54.9	5.3	49.6
6	58.7	1.8	56.9	6	55.9	1.8	54.1
7	59.2	4	55.2	7	56.1	1.2	54.9
8	57.5	2.1	55.4	8	55	2.7	52.3
9	56.4	3.6	52.8	9	56	1.4	54.6
10	58	2.7	55.3	10	52.9	2.4	50.5
11	56.7	1.3	55.4	11	53.1	3.3	49.8
12	57.5	4.8	52.7	12	54.6	2.5	52.1
13	57.5	2.6	54.9	13	55.3	2.4	52.9
Avg.	57.8	2.3	55.4	Avg.	54.8	2.4	52.4
Std.	1.14	1.17	1.76	Std.	1.18	1.15	1.82

3.4 Response model

It is not easy to compare the response times for ECDs as stated in most current research because the definition of the response time is not clearly defined and the sizes of the ECDs vary. Viennet *et al.* proposed an electrochemical model to estimate the coloration response time of ECDs, which they called the diffusion-controlled injection reaction model [217]. In this model, an ECD consists of a series resistance R and diffusional impedance Z_w. When $\alpha = D\left(\frac{zFs}{V_m E_y}\right)^2, t_0 = \alpha R^2, I_0 = \frac{V_0}{R}, Q_0 = I_0 t_0 = \alpha V_0 R,$ where Q is the charge, t is the time, *erfc(x)* is the complementary error function, D is the chemical diffusion coefficient, z is the charge of the transferred ion, F is the Faraday constant, s is the area, V_m is the molar volume, E_y is the slope of the coulometric titration curve, I_0 is the initial current, and V_0 is the initial voltage. The main formula of the model is as follows:

$$\left(\frac{Q}{Q_0}\right) = \boldsymbol{H}\left(\frac{t}{t_0}\right) = e^{\left(\frac{t}{t_0}\right)} \cdot erfc\left(\left(\frac{t}{t_0}\right)^{\frac{1}{2}}\right) + \left(\frac{4t}{\pi t_0}\right)^{\frac{1}{2}} - 1. \quad (3.1)$$

When $R_c = \frac{Q}{V_0 \alpha}, t_d = \frac{\pi Q^2}{4\alpha {V_0}^2},$ equation 3.1 can be reformulated as

$$\mathrm{t} = \frac{4t_d}{\pi} \cdot \left(\frac{R}{R_c}\right)^2 \cdot \boldsymbol{H}^{-1}\left(\frac{R_c}{R}\right). \quad (3.2)$$

The response times calculated using this model agree well with the measured response times when the active areas are small ($\leq 4\ cm^2$). However, if the model is applied to larger active areas ($> 100\ cm^2$), the error between the calculated and

experimental response times becomes significant. When the active area is 100 cm^2, the experimentally measured response time is about four times longer than the estimated response time. Due to this limitation, we propose a new model for electrochromic devices.

Figure 3.5 shows the basic scheme of the new model. The ECW is represented by a resistor–capacitor direct current (RC-DC) circuit. We focused on the transient response of the circuit. First, the current, *I*, is a function of time, *t*:

$$I(t) = \frac{V}{R} e^{-\frac{t}{RC}} . \quad (3.3)$$

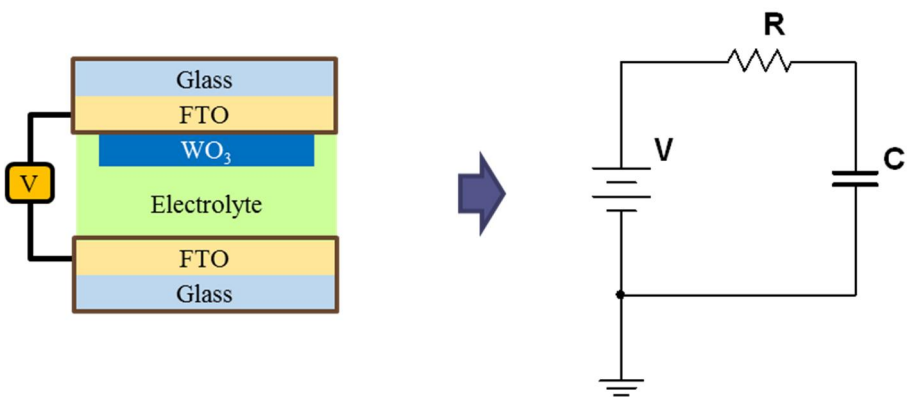

Figure 3.5 Schematic diagram of the electrochromic cell used in the response time model.

The charge, *Q*, is obtained by integrating the current, *I*. The maximum charge, Q_{max}, is the product of the electrochromic capacitance of the ECW and the applied voltage.

$$Q(t) = \int_0^t I(t)dt = \int_0^t \frac{V}{R} e^{-\frac{t}{RC}} dt = CV\left(1 - e^{-\frac{t}{RC}}\right) \quad (3.4)$$

$$Q_{max} = CV \quad (3.5)$$

We assume that the transmittance T is proportional to $Q_{max} - Q$.

$$T(t) \propto (Q_{max} - Q(t)) \quad (3.6)$$

Then, T is represented by a first order polynomial of $Q_{max} - Q$.

$$T(t) = a(Q_{max} - Q(t)) + b = \text{a}\left(CV - CV\left(1 - e^{-\frac{t}{RC}}\right)\right) + b \quad (3.7)$$

$$T(t) = aCVe^{-\frac{t}{RC}} + b \quad (3.8)$$

$$T(t_i = 0) = T_i,\ T(t_n) = T_n \quad (3.9)$$

Where t_i is the initial time, "zero", T_i is the transmittance at that time, t_n is an arbitrary time during the coloration process, and T_n is the transmittance at that time.

Then, equation 3.8 is replaced by Equation 3.10. The transmittance *T(t)* and the response time function *t(T)* can now be written as a function of t_n, T_i, T_n, R and C, as given below:

$$T(t) = \frac{T_i - T_n}{1 - e^{-\frac{t_n}{RC}}} e^{-\frac{t}{RC}} - \frac{T_i - T_n}{1 - e^{-\frac{t_n}{RC}}} + T_i \quad (3.10)$$

$$t(T) = -RC \ln\left(1 - \frac{T_i - T}{T_i - T_n}\left(1 - e^{-\frac{t_n}{RC}}\right)\right) \quad (3.11)$$

In reality, the resistance *R* and capacitance *C* consist of several components.

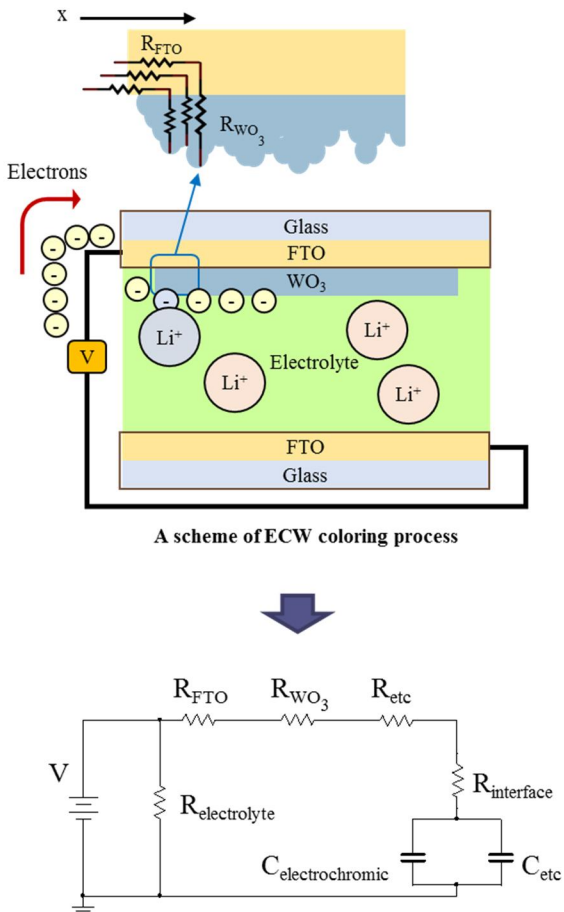

Figure 3.6 Expanding scheme of the resistor–capacitor (RC) direct current (DC) circuit

Figure 3.6 shows the expansion scheme for the RC-DC circuit. *R* is the sum of the

resistances of the FTO, WO_3, and interface. C is the sum of the electrochromic capacitance. Each resistance can be represented as a specific resistance, width, thickness, and length. c is the electrochromic capacitance per unit area. As $R = \rho\frac{l}{A} = \rho\frac{x}{w \cdot t} = R_s \cdot \frac{x}{w}$ (ρ *is the specific resistance,* l *or* x *is the length,* A *is the cross section area,* w *is the width,* t *is the thickness, and* R_s *is the sheet resistance*), as follows:

$$R = R_{FTO} + R_{WO_3} + R_{interface} + R_{etc} \tag{3.12}$$

$$R_{FTO} = \rho_{FTO} \cdot \frac{x}{w \cdot t_{FTO}} = R_{s,\,FTO} \cdot \frac{x}{w} \tag{3.13}$$

$$R_{WO_3} = \rho_{WO_3} \cdot \frac{t_{WO_3}}{x \cdot w} \tag{3.14}$$

$$C = C_{electrochromic} + C_{etc} \tag{3.15}$$

$$C_{electrochromic} = c_{electrochromic} \cdot x \cdot w \tag{3.16}$$

The expanded formula for RC is proportional to x^2, which is the square of the length of one side of the active area of the ECW.

$$RC = (R_{FTO} + R_{WO_3} + R_{interface} + R_{etc}\ )(\ C_{electrochromic} + C_{etc}\ ) = \rho_{FTO} \cdot \frac{x}{w \cdot t_{FTO}} \cdot c_{electrochromic} \cdot x \cdot w + \rho_{WO_3} \cdot \frac{t_{WO_3}}{x \cdot w} \cdot c_{electrochromic} \cdot x \cdot w + (R_{interface} + R_{etc}) \cdot c_{electrochromic} \cdot x \cdot w + (R_{FTO} + R_{WO_3} + R_{interface} + R_{etc}\ ) \cdot C_{etc} = c_{electrochromic} \cdot (R_{s,\,FTO} \cdot x^2 + \rho_{WO_3} \cdot t_{WO_3} + (R_{interface} + R_{etc}) \cdot x \cdot w) + (R_{FTO} + R_{WO_3} + R_{interface} + R_{etc}) \cdot C_{etc} \quad (3.17)$$

$$x = w\ (in\ the\ case\ of\ square),\ \ \rho_{WO_3} \cdot t_{WO_3} \approx 0\ \ and\ \ if\ \ R_{etc},\ C_{etc} \approx 0, \quad (3.18)$$

$$RC = c_{electrochromic} \cdot (R_{s,\,FTO} + R_{interface}) \cdot x^2 = \gamma \cdot x^2 \quad (3.19)$$

Finally, we obtain a function for the response time based on the expanded formula for the RC.

$$t(x) = -\gamma \cdot x^2 \cdot \ln\left(1 - \frac{T_i - T}{T_i - T_n}\left(1 - e^{-\frac{t_n}{\gamma \cdot x^2}}\right)\right) \quad (3.20)$$

3.5 Comparison between calculated and measured response time

3.5.1 Electrochromic current

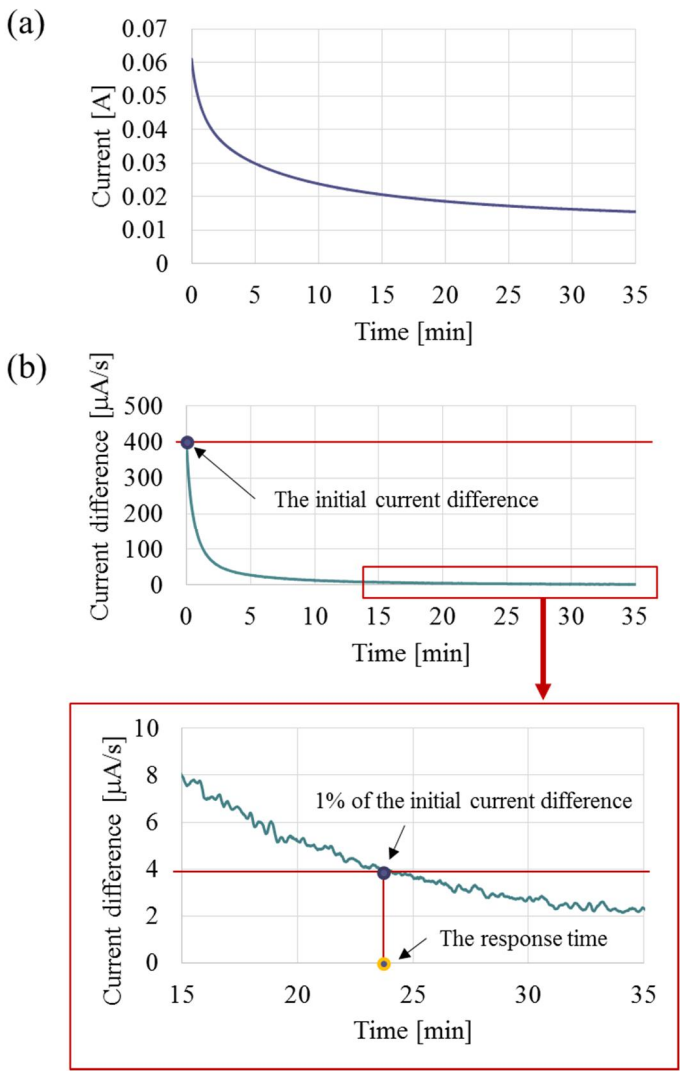

Figure 3.7 Measured current data from the 500 × 500 mm^2 electrochromic window (ECW) as a function of time: (a) current and (b) current difference

Figure 3.7(a) shows the measured current data from a 500 × 500 mm^2 ECW as a function of time. The response time was defined as the time it takes for the current difference to reach 1% of its initial value. In the case of Figure 3.7(b), the initial current difference was 395 mA/s, corresponding to a response time of 24.0 min, as this was the time that it took for the current difference to reach 3.95 mA/s. At the response time, the current is considered to be zero.

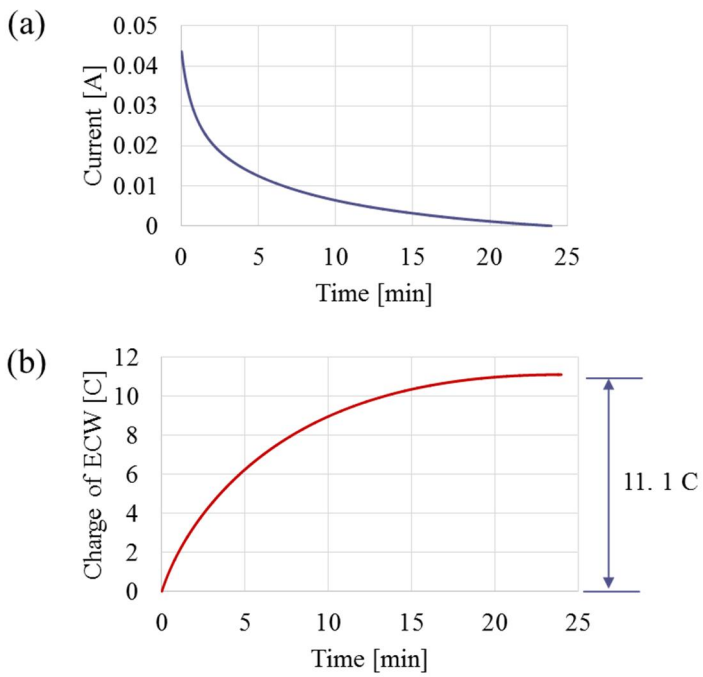

Figure 3.8 Converting current data from the 500 × 500 mm^2 ECW as a function of time: (a) modified current and (b) ECW charge

We then integrated the current to calculate the electrochromic charge of the ECW (Figure 3.8) and divided Q_{max} by the voltage to obtain the capacitance, which was 3.7

F in this case. The capacitance per unit area was 14.8 F/m^2.

3.5.2 Optical transmittance

Figure 3.9 shows the measured transmittance data from the 500 × 500 mm^2 ECW as a function of time at a wavelength of 785 nm. We compared these data to the estimates from the new response time model. Table 3.3 shows the transmittance in 3-min increments.

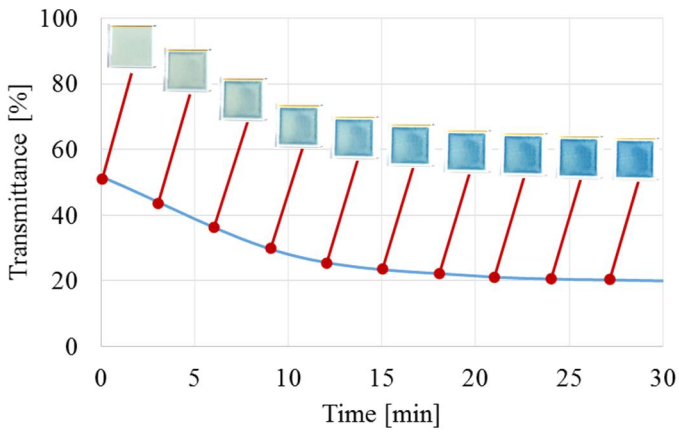

Figure 3.9 Transmittance variation of the 500 × 500 mm^2 ECW as a function of time at wavelength 785 nm

Table 3.3 Transmittance of the 500 × 500 mm^2 ECW at 785 nm.

Time [min]	Measured value (A) [%]	Calculated value (B) [%]	Difference (A-B) [%]
0	51.8	51.8	0.0
3	44.0	38.8	5.2
6	36.1	31.4	4.7
9	29.9	26.0	3.9
12	25.7	23.5	2.2
15	23.6	21.7	1.9
18	22.4	20.7	1.7
21	21.0	20.2	0.8
24	19.9	19.9	0.0

3.5.3 Evaluation of the response time model

Figure 3.10 shows a comparison between the measured transmittance values over time and the values calculated using equation 3.10.

$$T(t) = \frac{T_i - T_n}{1 - e^{-\frac{t_n}{RC}}} e^{-\frac{t}{RC}} - \frac{T_i - T_n}{1 - e^{-\frac{t_n}{RC}}} + T_i \qquad (3.10)$$

We used transmittance data measured at the initial time and 24 min later. The resistance and capacitance of the ECW were, respectively, 90 Ω and 3.7 F. In this case, the maximum difference between the calculated transmittance and the measured transmittance was 6.3%, after 4.6 min.

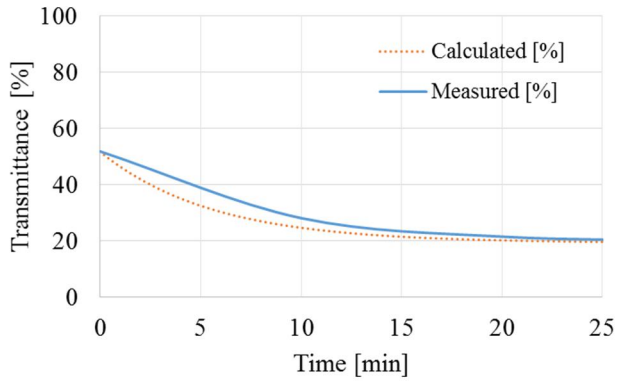

Figure 3.10 Comparison between the calculated and measured transmittance of the ECW.

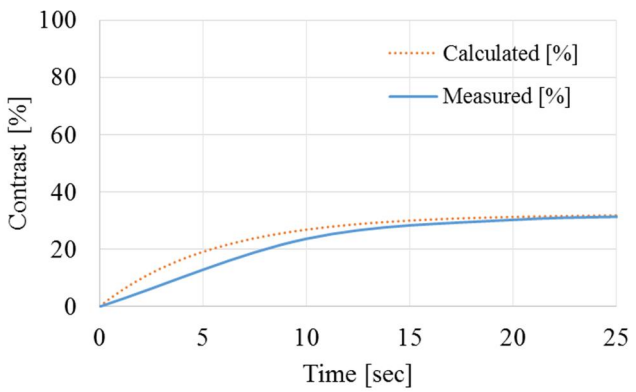

Figure 3.11 Comparison between the calculated and measured contrast of the ECW.

More simply, a difference of transmittance between before and after coloration, shortly contrast "ΔT" is just proportional to "Q". ΔT can be expressed as a function of t_n, T_i, T_n, R and C:

$$\Delta T(t) = \frac{1-e^{-\frac{t}{RC}}}{1-e^{-\frac{t_n}{RC}}} \cdot (T_i - T_n) \tag{3.21}$$

Figure 3.11 shows a graph of the calculated transmittance and the measured transmittance. The conclusions drawn from this figure are similar to those drawn from Figure 3.10.

$$t(x) = -\gamma \cdot x^2 \cdot \ln\left(1 - \frac{T_i - T_n}{T_i - T_{n+\alpha}}\left(1 - e^{-\frac{t_{n+\alpha}}{\gamma \cdot x^2}}\right)\right) \tag{3.22}$$

We also evaluated equation 3.22, which expresses the response time as a function of the size of the ECW, by comparing its results to the coloring response time data from 10 × 10 mm^2, 50 × 50 mm^2, 300 × 300 mm^2, 500 × 500 mm^2 and 1 × 1 m^2 ECWs. The results are summarized in Table 3.4.

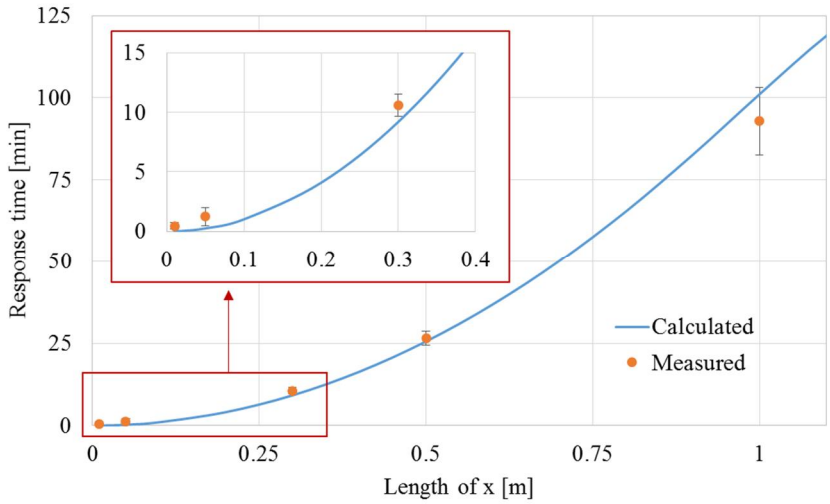

Figure 3.12 Comparison between the calculated and measured response time of the ECW as a function of size

Table 3.4 Comparison between the measured and calculated response times.

Length of ECW [m]	Active area of ECW [m^2]	Measured value (A) [min]	Calculated value (B) [min]	Difference (A-B) [min]
0.01	0.0001	0.46	0.01	0.45
0.05	0.0025	1.25	0.26	0.99
0.30	0.09	10.6	9.2	1.38
0.50	0.25	26.4	25.6	0.87
1.00	1.00	92.8	101.1	-8.23

We used 11.1 F/m^2, 12 Ω/sq, and 78 Ω as the capacitance per unit area, sheet resistance of the FTO, and interface resistance, respectively. Essentially, the

transmittance changes continuously with time. $T_{n+\alpha}$ represents the transmittance after a sufficiently long period of time ($t_{n+\alpha}$= 10,000 s), and $\frac{T_i - T_n}{T_i - T_{n+\alpha}} = 0.99$ indicates that the transmittance at the defined response time represents 99% of the transmittance after sufficient time. Figure 3.12 shows that, in the case of large-scale ECWs, the response time estimates obtained using our model are in good agreement with the measured data.

3.6 Summary of response time model for large-area ECWs

We developed a large-area NPDS and used it to deposit WO_3 particles onto FTO glass. As it uses non-toxic particles with no precursors, NPDS is a low-cost, ecofriendly process. We used our NPDS prototype to fabricate ECWs with dimensions 10 × 10 mm^2, 50 × 50 mm^2, 300 × 300 mm^2, 500 × 500 mm^2, and 1 × 1 m^2. We then developed an RC-DC transient-based ECW response time model for estimating the coloring time of large-area ECWs. This model allows the variations in transmittance to be estimated as a function of time for specific ECWs. We also calculated the response time for the target transmittance. We confirmed that our model can be used to estimate the coloring response time as a function of the size of the ECW by comparing the measured values to the resulting estimates.

Chapter 4. Plasma-assisted NPDS

4.1 Overview

As mentioned in Chapter 1, electrochromic devices can be fabricated in a variety of ways. In addition, the performance of electrochromic devices has been improved through various attempts at each process. Among the various performance evaluation indexes of the electrochromic device, a contrast is considered to be the most important one. The contrast is the light transmittance difference between bleaching state and coloring state of ECDs. In the case of electrochromic devices fabricated using NPDS, the maximum contrast known to the academic community up to now is 50% at 800 nm wavelength. Despite the various advantages of NPDS, it is still lower value compared to other processes relatively (Figure 4.1). An attempt was made to introduce a plasma treatment to improve the contrast of an electrochromic device made of NPDS.

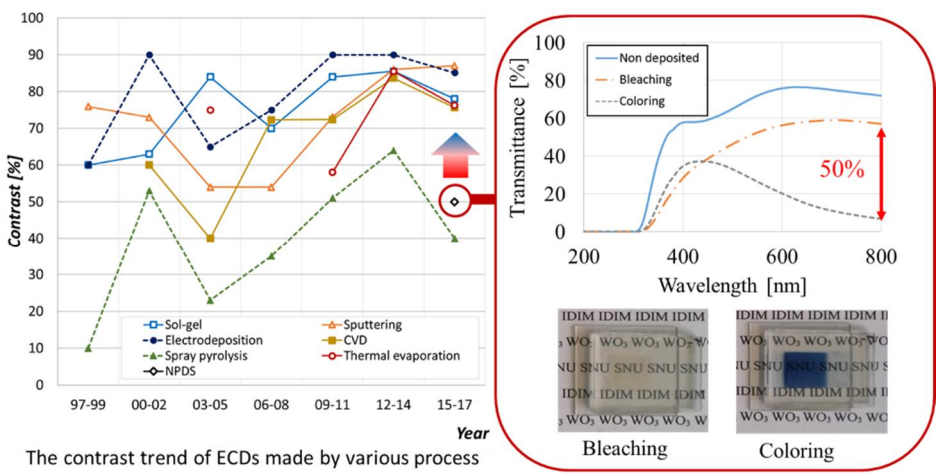

Figure 4.1 The contrast trend of ECDs made by each process according to time.

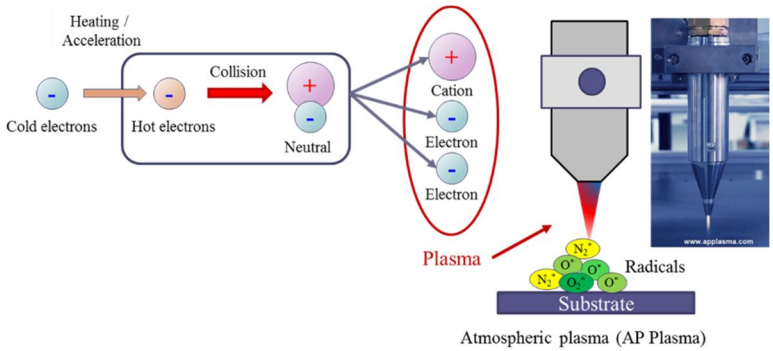

Figure 4.2 The principle of plasma generation and a schematic diagram of atmospheric plasma torch

Plasma is a fourth state of matter, not a solid, a liquid, or a gas, which is a general state of matter. Plasma is represented by an ionized gas, as in figure 4.2. Therefore, it has electrical conductivity and is electrically and chemically unstable. Such a plasma has a high activation energy, so that the surface of an object substance can be easily modified even at a low temperature. In particular, it is used for removal of static electricity, removal of organic layer, removal of moisture, surface activation, etc., and plasma treated surface increases adhesion.

4.2 System design and configuration

As shown in figure 4.3, plasma was introduced into NPDS to improve the deposition adhesion of WO_3. The plasma generated by the plasma power supply is injected like a flame through the plasma torch. WO_3 powder sprayed in aerosol form from the powder feeder is plasma treated in the plasma-aerosol block. The plasma-treated WO_3 is injected through a nozzle in a vacuum chamber and deposited on a substrate. At this time, the deposition adhesion is improved by increasing the adhesion between the substrate and the powder. Moreover the adhesion between the

following powder and the existing deposited particles is also increased. As a result, the deposition adhesion is further improved.

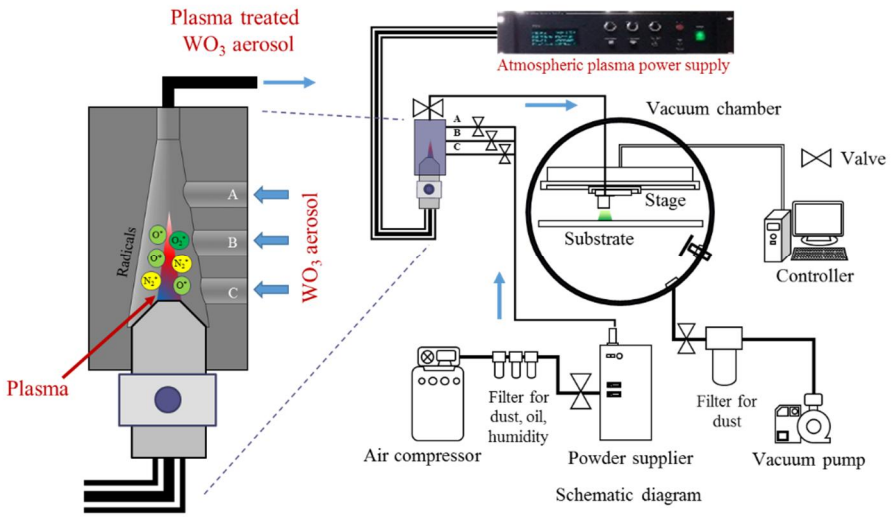

Figure 4.3 A schematic diagram of plasma-aerosol block and plasma-assisted NPDS

Figure 4.4 shows the plasma block applied to the actual NDPS. WO_3 aerosol input ports are A, B, and C, so that the level of plasma treatment can be controlled. When the port A is used, the plasma treatment is the least, and when the port C is used, the plasma treatment becomes the strongest.

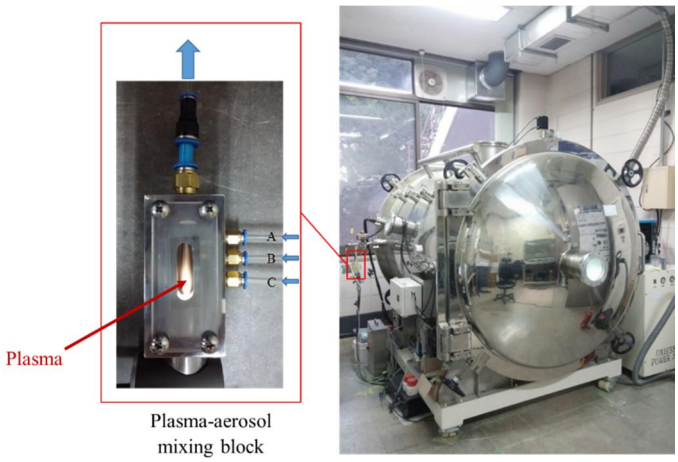

Figure 4.4 A real pictures of plasma-aerosol block and plasma-assisted NPDS

4.3 Evaluation

To evaluate the effect of plasma assisted NPDS, WO_3 deposition was performed. In this chapter, two kinds of stage speeds were applied. Table 4.1 shows the deposition parameters of NPDS, and Table 4.2 summarizes the parameters of the plasma generator.

Table 4.1 NPDS deposition parameters

Parameters	Value
Chamber vacuum [Torr]	75
Deposition pressure [MPa]	0.3
Stand-off distance (SoD) [mm]	3
Stage speed [μm/s]	50, 500

Table 4.2 AP plasma parameters

Parameters	Value
Voltage [V]	400
Duty [%]	24
Frequency [kHz]	23
Power [W]	400

4.3.1 Results of WO_3 powder deposition

WO_3 powder was a product of HKK Solution CO., LTD. and had a specification of D50 dimension 300 nm, and 3N%(Min) purity. Figure 4.5 shows the WO_3 powder taken by SEM and the fine shape of the particles making up the powder. The powder has a diameter of about 5 to 15 micrometers, and each powder is porously packed in a plate-like particle of about 200 nm, so that the density is considered to be low.

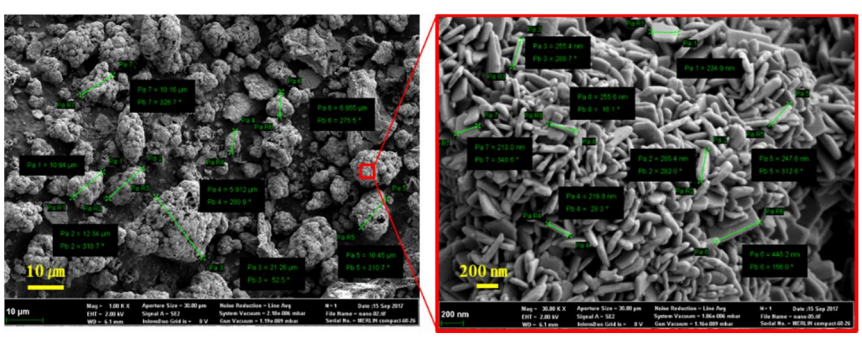

Figure 4.5 A SEM images of WO_3 powder

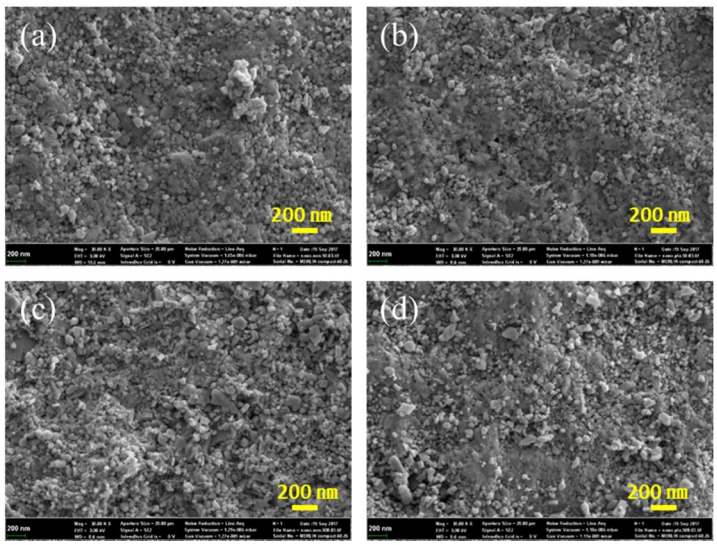

Figure 4.6 SEM images of WO_3 deposited surface under various conditions: (a) Stage speed 50 μm/s, non-treatment, (b) 50 μm/s, plasma-treatment, (c) 500 μm/s, non-treatment, (d) 500 μm/s, plasma-treatment

Figure 4.6 shows SEM images of WO_3 deposited surface under various conditions. The change of the deposited surface shape due to the difference of the stage speed seems to be insignificant.

However, changes in surface properties were confirmed through contact angles and crystal structure studies. Figure 4.7 shows the contact angle at each condition. After the plasma treatment, the contact angle decreased. When the contact angle is reduced, the active surface area where the electrolyte and the electrochromic layer contact each other is increased, thereby increasing the difference in transmittance (Figure 4.8).

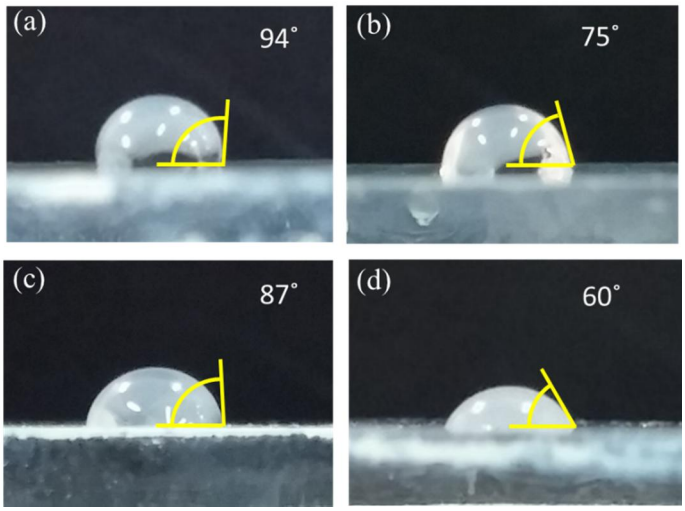

Figure 4.7 Contact angles of WO_3 deposited surface under various conditions: (a) Stage speed 50 μm/s, non-treatment, (b) 50 μm/s, plasma-treatment, (c) 500 μm/s, non-treatment, (d) 500 μm/s, plasma-treatment

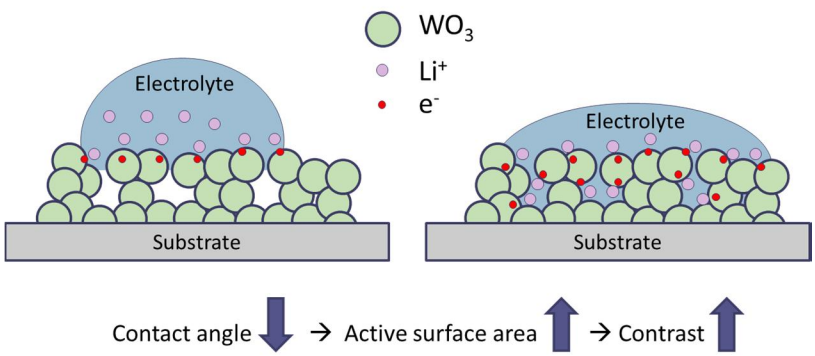

Figure 4.8 Effect of contact angle on electrochromic performance

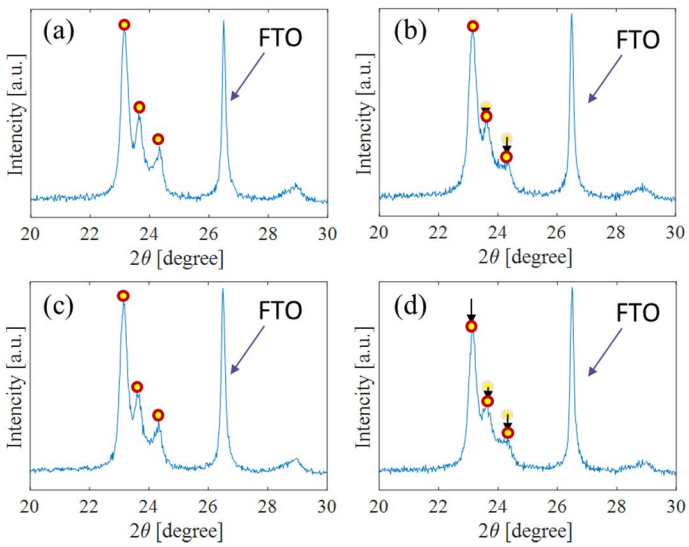

Figure 4.9 XRD analysis results of WO_3 deposited surface under various conditions: (a) Stage speed 50 μm/s, non-treatment, (b) 50 μm/s, plasma-treatment, (c) 500 μm/s, non-treatment, (d) 500 μm/s, plasma-treatment

Figure 4.9 shows the XRD analysis results under each condition. After the plasma treatment, it is observed that the peak of tungsten oxide is decreasing. This means that the crystal structure is further amorphized. The electrochromism phenomenon is widely known to exhibit good performance when the electrochromic material is amorphous as compared with the crystalline material [219].

4.3.2 Results of electrochromic performance

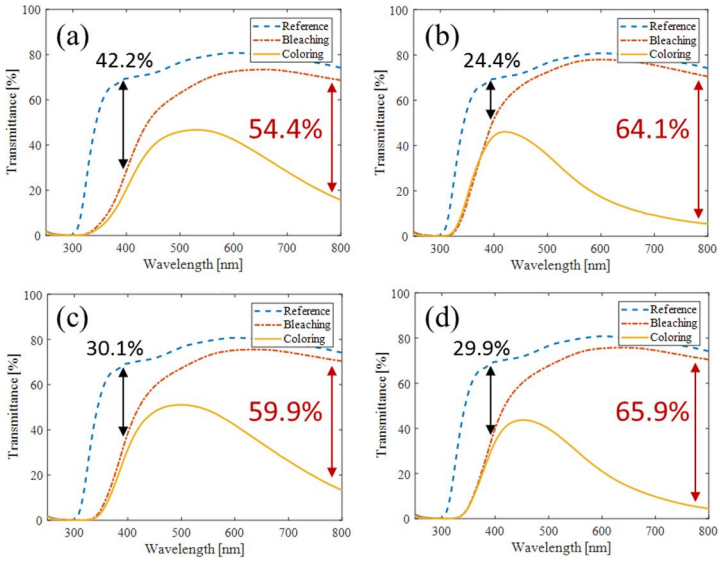

Figure 4.10 Transmittance of ECDs based on WO_3 deposited under various conditions: (a) Stage speed 50 μm/s, non-treatment, (b) 50 μm/s, plasma-treatment, (c) 500 μm/s, non-treatment, (d) 500 μm/s, plasma-treatment

Figure 4.10 shows the transmittance in each case. The difference in transmittance significantly increases through the plasma treatment. Meanwhile, the faster the stage speed, the higher the transmittance at bleaching state, and the higher the difference in transmittance.

4.4 Summary of plasma-assisted NPDS effects

Table 4.3 summarizes the effects of the plasma treatment. The respective deposition conditions were compared based on the difference in transmittance at a specific wavelength (800 nm). It was found that the performance was significantly improved after the plasma treatment and the performance was increased when the stage speed was fast. The optimum process conditions were obtained by plasma treatment of WO_3 powder and using stage speed of 500 μm/s. The contrast at that time was 65.9%, which was about 16% higher than that of the conventional 50%.

Table 4.3 Contrast comparison of ECDs fabricated by various conditions

Parameter		Contact Angle (degree)	Crystal Structure (XRD)	Contrast (%) (@ 800 nm Wavelength)	
Stage speed (μm/s)	Plasma			Average of samples	STDEV
50	Non treatment	94	Amorphous	54.4	4.0
	Plasma treatment	75	More amorphous	64.1	3.0
500	Non treatment	87	Amorphous	59.9	4.1
	Plasma treatment	60	More amorphous	65.9	0.1

Chapter 5. Conclusion

Recent technological advances have resulted in the development of various ECDs. Herein, processes to fabricate ECDs are introduced and discussed relative to electrochromic materials. In contrast to semiconductors that require crystallinity and very high surface quality, ECD can use an amorphous structure with a porous surface; this requires new processes to be developed. Seven representative ECD fabrication processes are summarized and discussed in this paper. The most important factors in determining the cost of the process are those of the process temperature and vacuum conditions. Most electrodeposition and sol-gel processes are conducted under atmospheric pressure, regardless of the process temperature. CVD can be performed under many conditions and the maximum process temperature can reach over 1,000°C. Sputtering is usually conducted at room temperature but some processes require high vacuum and high temperatures. The NPDS, which is newly introduced in this paper, is a direct deposition method that can be used at room temperature under low-vacuum conditions.

WO_3 thin films were deposited on FTO and ITO glass substrates using NPDS at room temperature under low-vacuum conditions. The WO_3 films on the FTO glass substrate exhibited a large EC contrast of 50% at 800 nm, with T_{min} = 7% and T_{max} = 57%. XRD data revealed that the WO_3 thin films formed monoclinic structures. Symmetrical charging processes corresponding to reduction and oxidation of the WO_3 film were observed via chronocoulometry. Cyclic voltammetry measurements revealed that a small, applied bias was required for color switching. The color of the WO_3 films changed from transparent yellow to dark blue in response to a change in the applied bias, demonstrating electrochromism.

Based on these results, a large-area NPDS was developed and used to deposit WO_3 particles onto FTO glass. Large-area NPDS is a low-cost, ecofriendly process that uses non-toxic particles with no precursors. We used our NPDS prototype to fabricate ECWs with the dimensions 10×10 mm^2, 50×50 mm^2, 300×300 mm^2, 500×500 mm^2 and 1×1 m^2. We then developed an RC–DC transient-based ECW response-time model to estimate the coloring time of large-area ECWs. This model allowed the variations in transmittance to be estimated as a function of time for specific ECWs. We also calculated the response time for the target transmittance. Comparing measured with predicted values confirmed that our model can be used to estimate the coloring response time as a function of the size of the ECW.

Finally, plasma treatment was introduced to the NPDS to improve the optical transmittance difference performance of electrochromic devices. As a result, the difference in transmittance increased from 50% to 65.9%, indicating a significant performance improvement.

Commercialization is a major concern and drives the development of new deposition processes that are environmentally friendly, low-cost and provide enhanced deposition options. Our NPDS is just such a method for the fabrication of inorganic ECWs.

Bibliography

1. Ahn, S.-H., *An evaluation of green manufacturing technologies based on research databases.* International Journal of Precision Engineering and Manufacturing-Green Technology, 2014. 1(1): p. 5-9.
2. Department, E.E.R.E., *DoE U.Buildings energy databook*. 2011.
3. Schirmer, O.F., *PLENARY SESSIONSmall polaron aspects of defects in oxide materials.* J. Phys. Colloques, 1980. 41: p. 479-484.
4. Gerlach, E., *Carrier scattering and transport in semiconductors treated by the energy-loss method.* Journal of Physics C: Solid State Physics, 1986. 19(24): p. 4585.
5. Cogan, S.F., et al., *Free-electron electrochromic modulation in crystalline Lix WO_3.* Journal of Applied Physics, 1986. 60(8): p. 2735-2738.
6. Arntz, F.O., et al., *Near-infrared reflectance modulation with electrochromic crystalline WO_3 films deposited on ambient temperature glass substrates by an oxygen ion-assisted technique.* Journal of Applied Physics, 1990. 67(6): p. 3177-3179.
7. Lee, S.-H., et al., *Effect of crystallinity on electrochromic mechanism of Lix WO_3 thin films.* Solid State Ionics, 2003. 156(3–4): p. 447-452.
8. Lupu, N., *Electrodeposited Nanowires and Their Applications*. 2010: Sciyo. com.
9. Liu, G., et al., *Vertically cross-linking silver nanoplate arrays with controllable density based on seed-assisted electrochemical growth and their structurally enhanced SERS activity.* Journal of Materials Chemistry, 2010. 20(4): p. 767-772.
10. Tsuboi, A., K. Nakamura, and N. Kobayashi, *Multicolor Electrochromism Showing Three Primary Color States (Cyan–Magenta–Yellow) Based on Size-and Shape-Controlled Silver Nanoparticles.* Chemistry of Materials, 2014. 26(22): p. 6477-6485.
11. Deng, J., M. Gu, and J. Di, *Electrochromic properties of WO_3 thin film onto gold nanoparticles modified indium tin oxide electrodes.* Applied Surface Science, 2011. 257(13): p. 5903-5907.
12. Xia, X., et al., *Cobalt oxide ordered bowl-like array films prepared by electrodeposition through monolayer polystyrene sphere template and electrochromic properties.* ACS Applied Materials & Interfaces, 2009. 2(1): p. 186-192.
13. Yuan, Y., et al., *Electrochromism in mesoporous nanowall cobalt oxide thin films prepared via lyotropic liquid crystal media with electrodeposition.* Journal of Membrane Science, 2010. 364(1): p. 298-303.
14. Wang, L., X.C. Song, and Y.F. Zheng, *Electrochromic properties of nanoporous Co_3O_4 thin films prepared by electrodeposition method.* Micro & Nano Letters, IET, 2012. 7(10): p. 1026-1029.
15. Di Yao, D., et al., *Electrochromic properties of TiO_2 nanotubes coated with*

electrodeposited MoO_3. Nanoscale, 2013. 5(21): p. 10353-10359.
16. Liao, C.-C., *Lithium-driven electrochromic properties of electrodeposited nickel hydroxide electrodes.* Solar Energy Materials and Solar Cells, 2012. 99: p. 26-30.
17. Sonavane, A., et al., *Efficient electrochromic nickel oxide thin films by electrodeposition.* Journal of Alloys and Compounds, 2010. 489(2): p. 667-673.
18. Yuan, Y., et al., *Enhanced electrochromic properties of ordered porous nickel oxide thin film prepared by self-assembled colloidal crystal template-assisted electrodeposition.* Electrochimica Acta, 2011. 56(3): p. 1208-1212.
19. Zhao, L., et al., *Optical and electrochemical properties of Cu-doped NiO films prepared by electrochemical deposition.* Applied Surface Science, 2011. 257(9): p. 3974-3979.
20. Dalavi, D.S., et al., *Efficient maximization of coloration by modification in morphology of electrodeposited NiO thin films prepared with different surfactants.* Journal of Solid State Electrochemistry, 2012. 16(1): p. 253-263.
21. Su, G., et al., *Electrodeposition in organic system and properties of NiO electrochromic films.* Science China Technological Sciences, 2012. 55(6): p. 1545-1550.
22. Cai, G., et al., *Ultra fast electrochromic switching of nanostructured NiO films electrodeposited from choline chloride-based ionic liquid.* Electrochimica Acta, 2013. 87: p. 341-347.
23. Cai, G.-f., et al., *One-step fabrication of nanostructured NiO films from deep eutectic solvent with enhanced electrochromic performance.* Journal of Materials Chemistry A, 2013. 1(13): p. 4286-4292.
24. Bodurov, G., et al., *Investigation of electrodeposited NiO films as electrochromic material for counter electrodes in "Smart Windows".* Materials Letters, 2014. 117: p. 270-272.
25. Sonavane, A., et al., *Simple and rapid synthesis of NiO/PPy thin films with improved electrochromic performance.* Electrochimica Acta, 2010. 55(7): p. 2344-2351.
26. Chen, W.-K., et al., *A study on the electrochromic properties of polyaniline/silica composite films with an enhanced optical contrast.* Electrochimica Acta, 2009. 54(18): p. 4408-4415.
27. Yang, P., et al., *Large-Scale Fabrication of Pseudocapacitive Glass Windows that Combine Electrochromism and Energy Storage.* Angewandte Chemie International Edition, 2014. 53(44): p. 11935-11939.
28. Mello, H.J.N.P.D. and M. Mulato, *Optochemical sensors using electrodeposited polyaniline films: Electrical bias enhancement of reflectance response.* Sensors and Actuators B: Chemical, 2015. 213: p. 195-201.
29. Wang, S.-M., et al., *High performance visible and near-infrared region electrochromic smart windows based on the different structures of polyoxometalates.* Electrochimica Acta, 2013. 113: p. 240-247.
30. Kraft, A. and M. Rottmann, *Properties, performance and current status of the*

laminated electrochromic glass of Gesimat. Solar Energy Materials and Solar Cells, 2009. 93(12): p. 2088-2092.

31. Rong, Y., et al., *New effective process to fabricate fast switching and high contrast electrochromic device based on viologen and Prussian blue/antimony tin oxide nano-composites with dark colored state.* Electrochimica Acta, 2011. 56(17): p. 6230-6236.
32. Seelandt, B. and M. Wark, *Electrodeposited Prussian Blue in mesoporous TiO_2 as electrochromic hybrid material.* Microporous and Mesoporous Materials, 2012. 164: p. 67-70.
33. Wang, M.-J., et al., *Characterization of TiO_2 thin films prepared by electrolytic deposition for lithium ion battery anodes.* Thin Solid Films, 2012. 520(22): p. 6744-6751.
34. Kim, S., M. Taya, and C. Xu, *Contrast, switching speed, and durability of V_2O_5–TiO_2 film-based electrochromic windows.* Journal of The Electrochemical Society, 2009. 156(2): p. E40-E45.
35. Jin, A., et al., *Multi-electrochromism behavior and electrochromic mechanism of electrodeposited molybdenum doped vanadium pentoxide films.* Electrochimica Acta, 2010. 55(22): p. 6408-6414.
36. Wei, Y., et al., *Structural characterization and electrical and optical properties of V_2O_5 films prepared via ultrasonic spraying.* Thin Solid Films, 2013. 534: p. 446-451.
37. Liu, Y., et al., *Electrochemical and electrochromic properties of novel nanoporous NiO/V_2O_5 hybrid film.* Solar Energy Materials and Solar Cells, 2015. 132: p. 467-475.
38. Giannouli, M. and G. Leftheriotis, *The effect of precursor aging on the morphology and electrochromic performance of electrodeposited tungsten oxide films.* Solar Energy Materials and Solar Cells, 2011. 95(7): p. 1932-1939.
39. Dinh, N.N., et al., *Mixed nanostructured Ti-W oxides films for efficient electrochromic windows.* Journal of Nanomaterials, 2012. 2012: p. 4.
40. Song, X.C., et al., *Electrochromic Properties of WO_3-MoO_3 Nanocomposite Films Prepared by Electrodeposition Method.* Current Nanoscience, 2013. 9(3): p. 330-334.
41. Zhang, J., et al., *Enhanced electrochromic performance of highly ordered, macroporous WO_3 arrays electrodeposited using polystyrene colloidal crystals as template.* Electrochimica Acta, 2013. 99: p. 1-8.
42. Cai, G., et al., *Efficient electrochromic materials based on TiO_2@WO_3 core/shell nanorod arrays.* Solar Energy Materials and Solar Cells, 2013. 117: p. 231-238.
43. Cheng, C.-P., et al., *Operation mechanism investigation of electrochromic display devices using tungsten oxides based on solid-state metal–oxide–metal capacitor structures.* Solid-State Electronics, 2014. 99: p. 16-20.
44. Evecan, D., O. Gurcuoglu, and E.O. Zayim, *Electrochromic device application of tungsten oxide film with polymer electrolytes.* Microelectronic Engineering, 2014. 128: p. 42-47.

45. More, A., et al., *Electrodeposition of nano-granular tungsten oxide thin films for smart window application.* Materials Letters, 2014. 134: p. 298-301.
46. Pang, Y., et al., *Size-controlled Ag nanoparticle modified WO_3 composite films for adjustment of electrochromic properties.* Thin Solid Films, 2010. 518(8): p. 1920-1924.
47. Ling, H., et al., *One-pot sequential electrochemical deposition of multilayer poly (3, 4-ethylenedioxythiophene): poly (4-styrenesulfonic acid)/tungsten trioxide hybrid films and their enhanced electrochromic properties.* Journal of Materials Chemistry A, 2014. 2(8): p. 2708-2717.
48. Dulgerbaki, C., et al., *PEDOT/WO3 Hybrid Nanofiber Architectures for High Performance Electrochromic Devices.* Electroanalysis, 2016: p. n/a-n/a.
49. Najafi-Ashtiani, H., A. Bahari, and S. Ghasemi, *A dual electrochromic film based on nanocomposite of copolymer and WO_3 nanoparticles: Enhanced electrochromic coloration efficiency and switching response.* Journal of Electroanalytical Chemistry, 2016. 774: p. 14-21.
50. Gaikwad, D.K., et al., *Influence of disordered morphology on electrochromic stability of WO_3/PPy.* Journal of Alloys and Compounds, 2016. 669: p. 240-245.
51. Rayón, E., J. Cembrero, and B. Marí, *Electrochromic switching of electrodeposited ZnO+ $Zn_5(OH)_8Cl_2$ films.* Materials Letters, 2011. 65(23): p. 3424-3426.
52. Ma, L., et al., *Fabricating red–blue-switching dual polymer electrochromic devices using room temperature ionic liquid.* Solar Energy Materials and Solar Cells, 2009. 93(5): p. 564-570.
53. Wei, H.-Y., et al., *Dual-color electrochromic films incorporating a periodic polymer nanostructure.* RSC Advances, 2012. 2(11): p. 4746-4753.
54. Ramírez, C.L. and A.R. Parise, *Solvent resistant electrochromic polymer based on methylene-bridged arylamines.* Organic Electronics, 2009. 10(5): p. 747-752.
55. Granqvist, C.G., *Handbook of inorganic electrochromic materials*. 1995: Elsevier.
56. Scherer, G.W. and C.J. Brinker, *Sol-gel science: The physics and chemistry of sol-gel processing.* Academic: New York, 1990.
57. Aegerter, M.A., *Sol-gel chromogenic materials and devices*. 1996: Springer.
58. Pierre, A.C., *Introduction to sol-gel processing*. Vol. 1. 2013: Springer Science & Business Media.
59. Egger, P., G.D. Soraru, and S. Diré, *Sol-gel synthesis of polymer-YSZ hybrid materials for SOFC technology.* Journal of the European Ceramic Society, 2004. 24(6): p. 1371-1374.
60. Gaudon, M., et al., *Thick YSZ films prepared via a modified sol–gel route: Thickness control (8–80μm).* Journal of the European Ceramic Society, 2006. 26(15): p. 3153-3160.
61. Lenormand, P., et al., *Potentialities of the sol–gel route to develop cathode and electrolyte thick layers: Application to SOFC systems.* Surface and Coatings Technology, 2008. 203(5): p. 901-904.

62. Vo, N.X.P., et al., *Fabrication of an anode-supported Sofc with a sol-gel coating method for a mixed-gas fuel cell*, in *Key Engineering Materials*. 2005. p. 455-461.
63. Aparicio, M., A. Jitianu, and L.C. Klein, *Sol-gel processing for conventional and alternative energy*. 2012: Springer Science & Business Media.
64. Judeinstein, P., et al., *An "all gel" electrochromic device.* Solid State Ionics, 1988. 28: p. 1722-1725.
65. Ozer, N., F. Tepehan, and N. Bozkurt, *An "all-gel" electrochromic device.* Thin Solid Films, 1992. 219(1): p. 193-198.
66. Macêdo, M.A. and M.A. Aegerter, *Sol-gel electrochromic device.* Journal of Sol-Gel Science and Technology, 1994. 2(1): p. 667-671.
67. Avellaneda, C.O., et al., *Characterization of an all Sol-Gel Electrochromic Device WO_3/Ormolyte/CeO_2-TiO_2.* Journal of Sol-Gel Science and Technology, 2000. 19(1): p. 447-451.
68. Bell, J.M., I.L. Skryabin, and A.J. Koplick, *Large area electrochromic films – preparation and performance.* Solar Energy Materials and Solar Cells, 2001. 68(3–4): p. 239-247.
69. Leftheriotis, G., S. Papaefthimiou, and P. Yianoulis, *The effect of water on the electrochromic properties of WO_3 films prepared by vacuum and chemical methods.* Solar Energy Materials and Solar Cells, 2004. 83(1): p. 115-124.
70. Šurca, A., et al., *Electrochromic and Structural Studies of Nanocrystalline Fe/V (1:2) Oxide and Crystalline $Fe_2V_4O_{13}$ Films.* Journal of The Electrochemical Society, 2000. 147(6): p. 2358-2370.
71. Orel, B., et al., *Comparative studies of "all sol–gel" electrochromic devices with optically passive counter-electrode films, ormolyte Li^+ ion-conductor and WO_3 or Nb_2O_5 electrochromic films.* Solar Energy Materials and Solar Cells, 1999. 56(3–4): p. 343-373.
72. Livage, J. and D. Ganguli, *Sol–gel electrochromic coatings and devices: a review.* Solar Energy Materials and Solar Cells, 2001. 68(3): p. 365-381.
73. Bradley, D.C., R.C. Mehrotra, and D. Gaur, *Metal alkoxides.* 1978.
74. Pope, M., *Heteropoly and isopoly oxometalates: inorganic chemistry concepts (Inorganic Chemistry Concepts, vol 8).* 1983, Springer, Hamburg.
75. Sakka, S., *Preparation and properties of sol-gel coating films.* Journal of Sol-Gel Science and Technology, 1994. 2(1): p. 451-455.
76. Yamamoto, Y., K.-i. Kamiya, and S. Sakka, *Study on the Properties of Coating Films Prepared from Metal Alkoxides.* Journal of the Ceramic Association, Japan, 1982. 90(1042): p. 328-333.
77. Yamashita, H., T. Yoko, and S. Sakka, *Preparation of $Li_2B_4O_7$ Films with Preferential Orientation by Sol–Gel Method.* Journal of the American Ceramic Society, 1991. 74(7): p. 1668-1674.
78. Judeinstein, P., et al., *Investigation of ion-conducting ormolytes: structure-property relationships.* Chemistry of Materials, 1994. 6(2): p. 127-134.

79. Judeinstein, P. and J. Livage, *Sol–gel synthesis of WO_3 thin films.* J. Mater. Chem., 1991. 1(4): p. 621-627.
80. Vroon, Z.A.E.P. and C.I.M.A. Spee, *Sol—gel coatings on large area glass sheets for electrochromic devices.* Journal of Non-Crystalline Solids, 1997. 218: p. 189-195.
81. Pyper, O., et al., *Nanocrystalline structure of WO_3 thin films prepared by the sol-gel technique.* Materials research bulletin, 1998. 33(7): p. 1095-1101.
82. Moser, F.H. and N.R. Lyman, *US Patent 4855161.* 1989.
83. Wang, B., et al., Huadong Huagong Xueynan XueBao, 1992.
84. Mendez-Vivar, J., et al., *The sol-gel route to molybdenum oxides.* Journal of Non-Crystalline Solids, 1990. 121(1): p. 26-30.
85. Charbouillot, Y., et al., *Aminosils: new solid state protonic materials by the sol-gel process.* Journal of non-crystalline solids, 1988. 103(2): p. 325-330.
86. Tepehan, F.Z., et al., *Optical properties of sol–gel dip-coated Ta_2O_5 films for electrochromic applications.* Solar energy materials and solar cells, 1999. 59(3): p. 265-275.
87. Kamimori, T., J. Nagai, and M. Mizuhashi, *Electrochromic devices for transmissive and reflective light control.* Solar energy materials, 1987. 16(1): p. 27-38.
88. Orel, B., et al., *All Sol-Gel electrochromic devices with Li^+ ionic conductor, WO_3 electrochromic films and SnO2 counter-electrode films.* Journal of sol-gel science and technology, 1998. 11(1): p. 87-104.
89. Patil, C., et al., *Synthesis of electrochromic vanadium oxide by pulsed spray pyrolysis technique and its properties.* Journal of Physics D: Applied Physics, 2009. 42(2): p. 025404.
90. Patil, C., et al., *Electrochromic performance of the mixed V_2O_5–WO_3 thin films synthesized by pulsed spray pyrolysis technique.* Current Applied Physics, 2014. 14(3): p. 389-395.
91. Mujawar, S., et al., *Electrochromism in composite WO_3–Nb_2O_5 thin films synthesized by spray pyrolysis technique.* Journal of Applied Electrochemistry, 2011. 41(4): p. 397-403.
92. Bhosale, A., et al., *Synthesis and characterization of highly stable optically passive CeO_2–ZrO_2 counter electrode.* Electrochimica Acta, 2010. 55(6): p. 1900-1906.
93. Bertus, L., A. Enesca, and A. Duta, *Influence of spray pyrolysis deposition parameters on the optoelectronic properties of WO 3 thin films.* Thin Solid Films, 2012. 520(13): p. 4282-4290.
94. Mousavi, M., et al., *The effect of solution concentration on the physical and electrochemical properties of vanadium oxide films deposited by spray pyrolysis.* Journal of Semiconductors, 2013. 34(10): p. 103001.
95. Denayer, J., et al., *Surfactant-assisted ultrasonic spray pyrolysis of nickel oxide and lithium-doped nickel oxide thin films, toward electrochromic applications.* Applied Surface Science, 2014. 321: p. 61-69.
96. Mahajan, S., et al., *Structural, morphological, optical and electrochromic properties*

of Ti-doped MoO_3 thin films. Solar Energy Materials and Solar Cells, 2009. 93(2): p. 183-187.

97. Mukherjee, R. and P.P. Sahay, *Improved electrochromic performance in sprayed WO_3 thin films upon Sb doping.* Journal of Alloys and Compounds, 2016. 660: p. 336-341.
98. Desai, J., et al., *Spray pyrolytic synthesis of large area NiO_x thin films from aqueous nickel acetate solutions.* Applied Surface Science, 2006. 253(4): p. 1781-1786.
99. Kholmanov, I.N., et al., *Improved electrical conductivity of graphene films integrated with metal nanowires.* Nano letters, 2012. 12(11): p. 5679-5683.
100. Li, X., et al., *Large-area synthesis of high-quality and uniform graphene films on copper foils.* Science, 2009. 324(5932): p. 1312-1314.
101. Bae, S., et al., *Roll-to-roll production of 30-inch graphene films for transparent electrodes.* Nature nanotechnology, 2010. 5(8): p. 574-578.
102. White, C.M., et al., *Flexible electrochromic devices based on crystalline WO_3 nanostructures produced with hot-wire chemical vapor deposition.* Thin Solid Films, 2009. 517(12): p. 3596-3599.
103. Mahan, A., et al., *Hot-wire chemical vapor deposition of crystalline tungsten oxide nanoparticles at high density.* Chemical physics letters, 2005. 413(1): p. 88-94.
104. Li, C.-P., et al., *Electrochromic films produced by ultrasonic spray deposition of tungsten oxide nanoparticles.* Solar Energy Materials and Solar Cells, 2012. 99: p. 50-55.
105. Lee, S.H., et al., *Crystalline WO_3 nanoparticles for highly improved electrochromic applications.* Advanced Materials, 2006. 18(6): p. 763-766.
106. Lin, Y.-S., H.-T. Chen, and J.-Y. Lai, *Electrochromic performance of PECVD-synthesized WO_xC_y thin films on flexible PET/ITO substrates for flexible electrochromic devices.* Thin Solid Films, 2009. 518(5): p. 1377-1381.
107. Lin, Y.S., Y.L. Chiang, and J.Y. Lai, *Effects of oxygen addition to the electrochromic properties of WO_{3-z} thin films sputtered on flexible PET/ITO substrates.* Solid State Ionics, 2009. 180(1): p. 99-105.
108. Hou, X. and K.L. Choy, *Processing and Applications of Aerosol-Assisted Chemical Vapor Deposition.* Chemical Vapor Deposition, 2006. 12(10): p. 583-596.
109. Choy, K., *Chemical vapour deposition of coatings.* Progress in materials science, 2003. 48(2): p. 57-170.
110. Tahir, A.A., et al., *Photoelectrochemical and photoresponsive properties of Bi2S3 nanotube and nanoparticle thin films.* Chemistry of Materials, 2010. 22(17): p. 5084-5092.
111. Dharmadasa, R., A.A. Tahir, and K. Wijayantha, *Single step growth and characterization of zinc oxide, tin oxide, and composite ($Zn_xSn_l- xO_y$) nanoplate and nanocolumn electrodes.* Journal of the American Ceramic Society, 2011. 94(10): p. 3540-3546.
112. Tahir, A.A. and K.U. Wijayantha, *Photoelectrochemical water splitting at*

nanostructured $ZnFe_2O_4$ electrodes. Journal of Photochemistry and Photobiology A: Chemistry, 2010. 216(2): p. 119-125.

113. Bloor, L.G., et al., *Tantalum and titanium doped In2O3 thin films by aerosol-assisted chemical vapor deposition and their gas sensing properties.* Chemistry of Materials, 2012. 24(15): p. 2864-2871.
114. Sialvi, M.Z., et al., *Electrochromic and colorimetric properties of Nickel (II) oxide Thin films prepared by aerosol-assisted chemical vapor deposition.* ACS applied materials & interfaces, 2013. 5(12): p. 5675-5682.
115. Trunec, D., et al., *Deposition of hard thin films from HMDSO in atmospheric pressure dielectric barrier discharge.* Journal of Physics D: Applied Physics, 2010. 43(22): p. 225403.
116. Lommatzsch, U. and J. Ihde, *Plasma Polymerization of HMDSO with an Atmospheric Pressure Plasma Jet for Corrosion Protection of Aluminum and Low-Adhesion Surfaces.* Plasma Processes and Polymers, 2009. 6(10): p. 642-648.
117. Kakiuchi, H., et al., *Investigation of deposition characteristics and properties of high-rate deposited silicon nitride films prepared by atmospheric pressure plasma chemical vapor deposition.* Thin Solid Films, 2005. 479(1): p. 17-23.
118. Hodgkinson, J.L., H.M. Yates, and D.W. Sheel, *Low temperature growth of photoactive titania by atmospheric pressure plasma.* Plasma Processes and Polymers, 2009. 6(9): p. 575-582.
119. Sheel, D.W. and J.L. Hodgkinson, *Atmospheric-Pressure Glow Discharge CVD of Composite Metallic Aluminium Thin Films.* Plasma Processes and Polymers, 2007. 4(5): p. 537-547.
120. Hodgkinson, J.L., et al., *Atmospheric pressure glow discharge CVD of Al_2O_3 thin films.* Plasma Processes and Polymers, 2006. 3(8): p. 597-605.
121. Barankin, M., et al., *Plasma-enhanced chemical vapor deposition of zinc oxide at atmospheric pressure and low temperature.* Solar energy materials and solar cells, 2007. 91(10): p. 924-930.
122. Korotkov, R., et al., *Atmospheric plasma discharge chemical vapor deposition of SnO_x thin films using various tin precursors.* Thin Solid Films, 2008. 516(15): p. 4720-4727.
123. Čada, M., et al., *Investigation of the low temperature atmospheric deposition of TCO thin films on polymer substrates.* Surface and Coatings Technology, 2004. 177: p. 699-704.
124. Suzuki, T. and H. Kodama, *Diamond-like carbon films synthesized under atmospheric pressure synthesized on PET substrates.* Diamond and Related Materials, 2009. 18(5): p. 990-994.
125. Fanelli, F., R. d'Agostino, and F. Fracassi, *Atmospheric Pressure PE-CVD of Fluorocarbon Thin Films by Means of Glow Dielectric Barrier Discharges.* Plasma Processes and Polymers, 2007. 4(9): p. 797-805.
126. Merche, D., et al., *Synthesis of polystyrene thin films by means of an atmospheric-*

pressure plasma torch and a dielectric barrier discharge. Plasma Science, IEEE Transactions on, 2009. 37(6): p. 951-960.

127. Lin, Y.S., S.S. Wu, and T.H. Tsai, *High-Rate Deposition of Electrochromic Organotungsten Oxide Thin Films for Flexible Electrochromic Devices by Atmospheric Pressure Plasma Jet: The Effect of Substrate Distance.* Plasma Processes and Polymers, 2011. 8(8): p. 728-739.
128. Lin, Y.-S., et al., *Lithium electrochromism of atmospheric pressure plasma jet-synthesized NiO_xC_y thin films.* Journal of Solid State Electrochemistry, 2012. 16(8): p. 2581-2590.
129. Lin, Y.-S., et al., *Enhanced lithium electrochromism of atmospheric pressure plasma jet-synthesized tungsten/molybdenum oxide films for flexible electrochromic devices.* Journal of Solid State Electrochemistry, 2013. 17(4): p. 1077-1088.
130. Lin, Y.-S., T.-H. Tsai, and W.-H. Lu, *Lithium Electrochemical and Electrochromic Properties of Atmospheric Pressure Plasma Jet-Synthesized Tungsten/Molybdenum Mixed Oxide Films for Flexible Electrochromic Devices.* Plasma Science, IEEE Transactions on, 2014. 42(12): p. 3772-3785.
131. Lin, Y.-S., Y.-C. Chen, and S.-W. Tien, *Effects of oxygen addition on enhancing electrochromic performance of flexible tungsten/tantalum oxide films using an atmospheric pressure plasma jet.* Surface and Coatings Technology, 2013. 221: p. 173-181.
132. Khalifa, Z., H. Lin, and S.I. Shah, *Structural and electrochromic properties of TiO_2 thin films prepared by metallorganic chemical vapor deposition.* Thin Solid Films, 2010. 518(19): p. 5457-5462.
133. Jahan Biglari, M., et al., *Chemical vapor deposition of poly (3-alkylthiophene) nanoparticles on fabric: Chemical and electrochemical characterization.* Journal of Applied Polymer Science, 2014. 131(17).
134. Nejati, S. and K.K. Lau, *Chemical Vapor Deposition Synthesis of Tunable Unsubstituted Polythiophene.* Langmuir, 2011. 27(24): p. 15223-15229.
135. Chelawat, H., S. Vaddiraju, and K. Gleason, *Conformal, conducting poly (3, 4-ethylenedioxythiophene) thin films deposited using bromine as the oxidant in a completely dry oxidative chemical vapor deposition process.* Chemistry of Materials, 2010. 22(9): p. 2864-2868.
136. Im, S.G., et al., *Grafted conducting polymer films for nano-patterning onto various organic and inorganic substrates by oxidative chemical vapor deposition.* Advanced Materials, 2007. 19(19): p. 2863.
137. Bhattacharyya, D. and K.K. Gleason, *Single-step oxidative chemical vapor deposition of −COOH functional conducting copolymer and immobilization of biomolecule for sensor application.* Chemistry of Materials, 2011. 23(10): p. 2600-2605.
138. Pereira, S., et al., *Electrochromic behavior of NiO thin films deposited by e-beam evaporation at room temperature.* Solar Energy Materials and Solar Cells, 2014. 120:

p. 109-115.
139. Sivakumar, R., et al., *Molybdenum oxide (MoO_3) thin film based electrochromic cell characterisation in 0.1M $LiClO_4$. PC electrolyte.* Surface Engineering, 2009. 25(7): p. 548-554.
140. Wang, C.M., et al., *Effect of deposition temperature on the electrochromic properties of electron beam-evaporated WO_3 thin films.* Integrated Ferroelectrics, 2014. 158(1): p. 62-68.
141. Chiu, P.K., et al., *Investigation of the Microstructure, Porosity, Adhesion, and Optical Properties of a WO_3 Film Fabricated Using an E-Beam System With Ion Beam-Assisted Deposition.* IEEE Transactions on Magnetics, 2014. 50(7).
142. Kubo, T., et al., *Electrochromic Properties of Li_xNi_yO Films Deposited by RF Magnetron Sputtering.* Journal of The Electrochemical Society, 2009. 156(8): p. H629-H633.
143. Tajima, K., et al., *Accelerated degradation studies on electrochromic switchable mirror glass based on magnesium–nickel thin film in simulated environment.* Solar Energy Materials and Solar Cells, 2010. 94(10): p. 1716-1722.
144. Tajima, K., et al., *Fabrication study of proton injection layer suitable for electrochromic switchable mirror glass.* Thin Solid Films, 2010. 519(2): p. 934-937.
145. Tajima, K., et al., *Fabrication of solid electrolyte Ta_2O_5 thin film by reactive dc magnetron sputtering suitable for electrochromic all-solid-state switchable mirror glass.* Nippon Seramikkusu Kyokai Gakujutsu Ronbunshi/Journal of the Ceramic Society of Japan, 2011. 119(1385): p. 76-80.
146. Chu, C.H., H.W. Wu, and J.L. Huang, *Novel WO_3 Based Electrochromic Device for High Optical Modulation and Infrared Suppression.* IEEE Electron Device Letters, 2015. 36(3): p. 256-258.
147. Wang, C.-K., et al., *Characterization of electrochromic tungsten oxide film from electrochemical anodized RF-sputtered tungsten films.* Ceramics International, 2013. 39(4): p. 4293-4298.
148. Gomes, L., et al., *IZO deposition by RF and DC sputtering on paper and application on flexible electrochromic devices.* Displays, 2013. 34(4): p. 326-333.
149. Park, Y., et al., *Sputtered CdTe thin film solar cells with Cu2Te/Au back contact.* Thin Solid Films, 2013. 546: p. 337-341.
150. Lim, J.W., et al., *High electrochromic performance of co-sputtered vanadium–titanium oxide as a counter electrode.* Solar Energy Materials and Solar Cells, 2009. 93(12): p. 2069-2074.
151. Noguchi, D., et al., *Formation of WO_3 Reduction Coloring Thin Film Using a Combination Sputtering Method Featuring Radio-Frequency Oxygen Plasma Irradiation.* Shinku, 2011. 54(5): p. 317-321.
152. Nah, Y.-C., *Effects of Sputter Parameters on Electrochromic Properties of Tungsten Oxide Thin Films Grown by RF Sputtering.* Korean journal of materials research, 2011. 21(12): p. 703-707.

153. Inamdar, A.I., et al., *Effects of oxygen stoichiometry on electrochromic properties in amorphous tungsten oxide films.* Thin Solid Films, 2012. 520(16): p. 5367-5371.
154. Kalagi, S.S., et al., *Transmission attenuation and chromic contrast characterization of R.F. sputtered WO_3 thin films for electrochromic device applications.* Electrochimica Acta, 2012. 85: p. 501-508.
155. Oka, N., et al., *Reactive-gas-flow sputter deposition of amorphous WO_3 films for electrochromic devices.* Thin Solid Films, 2013. 532: p. 1-6.
156. Madhavi, V., et al., *Effect of molybdenum doping on the electrochromic properties of tungsten oxide thin films by RF magnetron sputtering.* Ionics, 2014. 20(12): p. 1737-1745.
157. Wen, R.-T., G.A. Niklasson, and C.G. Granqvist, *Electrochromic nickel oxide films and their compatibility with potassium hydroxide and lithium perchlorate in propylene carbonate: Optical, electrochemical and stress-related properties.* Thin Solid Films, 2014. 565: p. 128-135.
158. Kang, S.H., et al., *Photo and Electrochemical Characteristics Dependent on the Phase Ratio of Nanocolumnar Structured TiO_2 Films by RF Magnetron Sputtering Technique.* Chemistry of Materials, 2009. 21(13): p. 2777-2788.
159. Lansåker, P.C., et al., *TiO_2/Au/TiO_2 multilayer thin films: Novel metal-based transparent conductors for electrochromic devices.* Thin Solid Films, 2009. 518(4): p. 1225-1229.
160. Gillaspie, D., et al., *Nanocomposite counter electrode materials for electrochromic windows.* Journal of the Electrochemical Society, 2010. 157(3): p. H328-H331.
161. Green, S.V., C.G. Granqvist, and G.A. Niklasson, *Structure and optical properties of electrochromic tungsten-containing nickel oxide films.* Solar Energy Materials and Solar Cells, 2014. 126: p. 248-259.
162. Rodrigues, L.C., et al., *Application of hybrid materials in solid-state electrochromic devices.* Optical Materials, 2009. 31(10): p. 1467-1471.
163. Jee, S.H., et al., *Characteristics of Li–P–W–O–N electrolyte for all solid state electrochromic devices.* Electrochimica Acta, 2011. 56(27): p. 9741-9745.
164. Chen, H., et al., *Fabrication and ionic conductivity of amorphous Li–Al–Ti–P–O thin film.* Journal of Non-Crystalline Solids, 2011. 357(16–17): p. 3267-3271.
165. Tajima, K., et al., *Optical switching properties of all-solid-state switchable mirror glass based on magnesium–nickel thin film for environmental temperature.* Solar Energy Materials and Solar Cells, 2010. 94(2): p. 227-231.
166. Ito, S., et al., *Electrochromic properties of iridium oxide thin films prepared by reactive sputtering in O_2 or H_2O atmosphere.* Journal of Vacuum Science & Technology B, 2015. 33(4): p. 041204.
167. Usha, N., et al., *Effect of substrate temperature on the properties of Nb_2O_5:MoO_3 (90:10) thin films prepared by rf magnetron sputtering technique.* Journal of Alloys and Compounds, 2015. 649: p. 112-121.
168. Coşkun, Ö.D., S. Demirel, and G. Atak, *The effects of heat treatment on optical,*

structural, electrochromic and bonding properties of Nb_2O_5 thin films. Journal of Alloys and Compounds, 2015. 648: p. 994-1004.

169. Kelly, P.J. and J.W. Bradley, *Pulsed magnetron sputtering - process overview and applications.* Journal of Optoelectronics and Advanced Materials, 2009. 11(9): p. 1101-1107.
170. Hsi-Chao, C., J. Der-Jun, and C. Chien-Han, *Investigation of Optical and Electrochromic Properties of Tungsten Oxide Deposited with Horizontal.* Japanese Journal of Applied Physics, 2012. 51(4R): p. 045503.
171. Chen, H.-C., et al., *Bond and electrochromic properties of WO_3 films deposited with horizontal DC, pulsed DC, and RF sputtering.* Electrochimica Acta, 2013. 93: p. 307-313.
172. Gil-Rostra, J., et al., *Tuning the transmittance and the electrochromic behavior of $Co_xSi_yO_z$ thin films prepared by magnetron sputtering at glancing angle.* Solar Energy Materials and Solar Cells, 2014. 123: p. 130-138.
173. Valyukh, I., et al., *Spectroscopic ellipsometry characterization of electrochromic tungsten oxide and nickel oxide thin films made by sputter deposition.* Solar Energy Materials and Solar Cells, 2010. 94(5): p. 724-732.
174. Sun, X., Z. Liu, and H. Cao, *Electrochromic properties of N-doped tungsten oxide thin films prepared by reactive DC-pulsed sputtering.* Thin Solid Films, 2011. 519(10): p. 3032-3036.
175. Tajima, K., et al., *Electrochromic switchable mirror foil with tantalum oxide thin film prepared by reactive DC magnetron sputtering in hydrogen-containing gas.* Surface and Coatings Technology, 2011. 205(15): p. 3956-3960.
176. Karuppasamy, A., *Electrochromism in surface modified crystalline WO_3 thin films grown by reactive DC magnetron sputtering.* Applied Surface Science, 2013. 282: p. 77-83.
177. Arvizu, M.A., et al., *Electrochromism in sputter-deposited W–Ti oxide films: Durability enhancement due to Ti.* Solar Energy Materials and Solar Cells, 2014. 125: p. 184-189.
178. Garcia-Garcia, F.J., et al., *In operando X-ray absorption spectroscopy analysis of structural changes during electrochemical cycling of WO_3 and $W_xSi_yO_z$ amorphous electrochromic thin film cathodes.* Journal of Physical Chemistry C, 2015. 119(1): p. 644-652.
179. Kumar, K.U., S.M. Dhanya, and A. Subrahmanyam, *Flexible electrochromics: magnetron sputtered tungsten oxide (WO_{3-x}) thin films on Lexan (optically transparent polycarbonate) substrates.* Journal of Physics D: Applied Physics, 2015. 48(25): p. 255101.
180. Li, C., et al., *The deposition and microstructure of amorphous tungsten oxide films by sputtering.* Vacuum, 2015. 118: p. 125-132.
181. Tajima, K., et al., *Electrochemical evaluation of Ta_2O_5 thin film for all-solid-state switchable mirror glass.* Solid State Ionics, 2009. 180(6-8): p. 654-658.

182. Madhavi, V., et al., *Structural, optical and electrochromic properties of RF magnetron sputtered WO_3 thin films.* Physica B: Condensed Matter, 2014. 454: p. 141-147.
183. Avendaño, E., et al., *Coloration Mechanism in Proton-Intercalated Electrochromic Hydrated NiO y and $Ni_{1-x}V_xO_y$ Thin Films.* Journal of The Electrochemical Society, 2009. 156(8): p. P132-P138.
184. Wang, T., X. Diao, and P. Ding, *Orthogonal optimization for room temperature magnetron sputtering of ZnO:Al films for all-solid electrochromic devices.* Applied Surface Science, 2011. 257(8): p. 3748-3752.
185. Song, X., et al., *Properties of NiOx and its influence upon all-thin-film ITO/NiO_x/$LiTaO_3$/WO_3/ITO electrochromic devices prepared by magnetron sputtering.* Vacuum, 2015. 111: p. 48-54.
186. Choi, D.S., et al., *Electrochromic characterization of amorphous tungsten oxide films deposited on indium tin oxide and CVD-graphene electrodes by RF magnetron sputtering.* Journal of Ceramic Processing Research, 2014. 15(4): p. 273-276.
187. Liu, Q., et al., *An all-thin-film inorganic electrochromic device monolithically fabricated on flexible PET/ITO substrate by magnetron sputtering.* Materials Letters, 2015. 142: p. 232-234.
188. Yun, S.U., et al., *Enhanced Electrochromic Properties of Ir–Ta Oxide Grown Using a Cosputtering System.* Journal of The Electrochemical Society, 2010. 157(7): p. J256-J260.
189. Yoshio, A., et al., *Effects of Sputtering Gas Pressure on Electrochromic Properties of Ni Oxyhydroxide Thin Films Prepared by Reactive Sputtering in H_2O Atmosphere.* Japanese Journal of Applied Physics, 2010. 49(11R): p. 115802.
190. Sun, X., Z. Liu, and H. Cao, *Effects of film density on electrochromic tungsten oxide thin films deposited by reactive dc-pulsed magnetron sputtering.* Journal of Alloys and Compounds, 2010. 504, Supplement 1: p. S418-S421.
191. Gil-Rostra, J., et al., *Electrochromic Behavior of WxSiyOz Thin Films Prepared by Reactive Magnetron Sputtering at Normal and Glancing Angles.* ACS Applied Materials & Interfaces, 2012. 4(2): p. 628-638.
192. Chun, D.M., et al., *TiO_2 coating on metal and polymer substrates by nano-particle deposition system (NPDS).* CIRP Annals - Manufacturing Technology, 2008. 57(1): p. 551-554.
193. Chun, D.-M., et al., *Nano-particle deposition system (NPDS): Low energy solvent-free dry spray process for direct patterning of metals and ceramics at room temperature.* International Journal of Precision Engineering and Manufacturing, 2012. 13(7): p. 1107-1112.
194. Kim, M.-S., et al., *Room temperature deposition of TiO_2 using nano particle deposition system (NPDS): Application to dye-sensitized solar cell (DSSC).* International Journal of Precision Engineering and Manufacturing, 2011. 12(4): p. 749-752.

195. Park, S.-I., et al., *Low-cost fabrication of WO_3 films using a room temperature and low-vacuum air-spray based deposition system for inorganic electrochromic device applications.* Thin Solid Films, 2015. 589: p. 412-418.
196. Granqvist, C.G., *Introduction*, in *Handbook of Inorganic Electrochromic Materials*. 1995, Elsevier Science B.V.: Amsterdam. p. 1-15.
197. Deb, S.K., *Reminiscences on the discovery of electrochromic phenomena in transition metal oxides.* Solar Energy Materials and Solar Cells, 1995. 39(2): p. 191-201.
198. Deb, S.K., *Opportunities and challenges in science and technology of WO_3 for electrochromic and related applications.* Solar Energy Materials and Solar Cells, 2008. 92(2): p. 245-258.
199. Deb, S.K., *A Novel Electrophotographic System.* Applied Optics, 1969. 8(S1): p. 192-195.
200. Lampert, C.M., *Large-area smart glass and integrated photovoltaics.* Solar Energy Materials and Solar Cells, 2003. 76(4): p. 489-499.
201. Kim, S. and M. Taya, *Electropolymerization kinetic study of 3,3-dimethyl-3,4-dihydro-2H-thieno[3,4-b][1,4]dioxepine and its optical optimization for electrochromic window applications.* Electrochimica Acta, 2010. 55(19): p. 5307-5311.
202. Kim, S. and M. Taya, *Electrochromic windows based on V_2O_5–TiO_2 and poly (3,3-dimethyl-3,4-dihydro-2H-thieno[3,4-b][1,4]dioxepine) coatings.* Solar Energy Materials and Solar Cells, 2012. 107: p. 225-229.
203. LAMPERT, C.M., *ELECTROCHROMICS- HISTORY, TECHNOLOGY, AND THE FUTURE*, in *Solid State Ionics*. 2011, WORLD SCIENTIFIC. p. 411-422.
204. Lee, S.-H., et al., *Electrochromic coloration efficiency of a-WO_{3-y} thin films as a function of oxygen deficiency.* Applied Physics Letters, 1999. 75(11): p. 1541-1543.
205. Reichman, B. and A.J. Bard, *The Electrochromic Process at WO_3 Electrodes Prepared by Vacuum Evaporation and Anodic Oxidation of W.* Journal of The Electrochemical Society, 1979. 126(4): p. 583-591.
206. Masetti, E., et al., *Analysis of the influence of the gas pressure during the deposition of electrochromic WO_3 films by reactive RF sputtering of W and WO_3 target.* Solar Energy Materials and Solar Cells, 1999. 56(3): p. 259-269.
207. Wang, X.G., et al., *Structure–property relationships in electrochromic WO_3 films deposited by reactive sputtering.* Solar Energy Materials and Solar Cells, 2000. 63(2): p. 197-205.
208. Park, S.-S. and J.D. Mackenzie, *Sol-gel-derived tin oxide thin films.* Thin Solid Films, 1995. 258(1): p. 268-273.
209. Gordon, R.G., et al., *Atmospheric pressure chemical vapor deposition of electrochromic tungsten oxide films.* Thin Solid Films, 2001. 392(2): p. 231-235.
210. Stowell, M., et al., *RF-superimposed DC and pulsed DC sputtering for deposition of transparent conductive oxides.* Thin Solid Films, 2007. 515(19): p. 7654-7657.

211. Gurcuoglu, O., D. Evecan, and E. Ozkan Zayim, *Synthesis and characterization of tungsten oxide films by electrodeposition with various precursors and electrochromic device application.* Journal of Solid State Electrochemistry, 2015. 19(2): p. 403-413.
212. Bessière, A., et al., *Sol–gel deposition of electrochromic WO_3 thin film on flexible ITO/PET substrate.* Electrochimica Acta, 2001. 46(13): p. 2251-2256.
213. de León, J.M.O.R., et al., *Improving electrochromic behavior of spray pyrolised WO_3 thin solid films by Mo doping.* Electrochimica Acta, 2011. 56(5): p. 2599-2605.
214. Gesheva, K.A., T.M. Ivanova, and G. Bodurov, *Transition metal oxide films: Technology and "Smart Windows" electrochromic device performance.* Progress in Organic Coatings, 2012. 74(4): p. 635-639.
215. Punitha, K., R. Sivakumar, and C. Sanjeeviraja, *Enhanced Colouration Efficiency of Pulsed DC Magnetron Sputtered WO3 Films Cycled in H_2SO_4 Electrolyte Solution.* Smart Materials Research, 2014. 2014: p. 9.
216. Cheng, C.-P., et al., *Performance improvement of electrochromic display devices employing micro-size precipitates of tungsten oxide.* Applied Physics A, 2014. 116(4): p. 1553-1559.
217. Viennet, R., J.P. Randin, and I.D. Raistrick, *Effect of Active Surface Area on the Response Time of Electrochromic and Electrolytic Displays.* Journal of The Electrochemical Society, 1982. 129(11): p. 2451-2453.
218. Korgel, B.A., *Materials science: Composite for smarter windows.* Nature, 2013. 500(7462): p. 278-279.
219. El-Nahass, M.M., et al., *Electrochromic properties of amorphous and crystalline WO_3 thin films prepared by thermal evaporation technique.* Materials Science in Semiconductor Processing, 2015. 29(Supplement C): p. 201-205.

초 록

전기변색은 외부에서 인가된 전압 하에서 색의 변화를 수반하는 현상이다. 오늘날 그 중요성이 커지면서 다양한 제조 공정이 전기변색 소자 (Electrochromic device, ECD) 를 제조하는 데 사용되고 있다. 먼저 각 주요 공정을 소개하고 각 공정 변수들을 비교하였다. 이 논문에서 논의된 여섯 가지 대표적인 제조 공정은 전착, 졸-겔, 분무 열분해, 화학 기상 증착 (CVD), 열 증착 및 스퍼터링이다.

전기변색소자의 상용화를 위해서는 환경 문제, 비용, 성능 및 제작가능 크기 등을 고려하는 것이 필요한데, 본 연구에서는 저가 친환경 공정인 나노입자 적층시스템 (Nano-particle deposition system, NPDS) 을 새롭게 도입하여 전기변색소자를 제작하는 데에 성공하였고, 또한 이를 대형화하여 상용화의 가능성을 보였다.

나노입자 적층시스템은 저진공 챔버 안에서 입자 에어로졸을 분사하는 것을 기반으로 하는 상온 적층 시스템으로써, 이를 사용하여 투명전극기판인 불소 첨가 산화주석 (FTO) 및 인듐 첨가 산화주석 (ITO) 기판에 전기변색물질인 산화텅스텐 (WO_3) 박막을 적층하였다. WO_3 필름의 성분구성은 X 선 회절 (XRD) 을 사용하여 확인하였으며, 표면형상은 주사 전자 현미경 (SEM) 및 원자간력 현미경 (AFM) 을 사용하여 관찰하였다. 필름의 전기 화학적 성질은 순환 전압 전류법 (Cyclic voltammetry) 및 크로노쿨론법 (Chronocoulometry) 를 사용하여 조사하였다. 적층된 WO_3 필름과 상대전극, 전해질을 이용하여, 전기변색소자를 완성하였으며, 소정의 적용 전압(3 V)을 인가하였을 때, WO_3 필름의 색은 투명한 황색에서 진한 파란색으로 변화하여 전기변색현상을 나타냈다. 이 WO_3 필름 기반의 전기변색소자는 800 nm 파장에서 50%의 광투과도 차이를 나타내었다.

나노입자 적층시스템의 전기변색소자 제작 가능성을 확인한 후, 대면적 나노입자 적층시스템 (Large-area NPDS) 를 구축하였고, 이를 이용하여 WO_3 을 기반으로 하는 대면적 전기변색 유리창 (Electrochromic windows, ECW)을 제작하였다. 작동면적이 증가될수록 기존의 전기변색시간 모델은 실제값과 차이를 많이 보였고, 이를 보완하기 위해, 저항-커패시터 (RC) 직류 회로의 과도 응답을 기반으로 하는 전기변색시간 모델을 새롭게 개발하였다. 이 모델은 전기변색 유리창의 작동면적의 크기에 따른 전기변색시간을 예측할 수 있도록 개발되었다. 10 × 10 mm^2, 50 × 50 mm^2, 300 × 300 mm^2, 500 × 500 mm^2, 1 × 1 m^2 의 작동면적을 가지는 총 5 종류의 샘플을 제작하여 모델과 비교하였다. 각 샘플이 변색될 때의 전류 및 투과율 변화를 측정하였으며, 전기변색시간은 전류의 변화량을 이용하여 정의하였다. 이 모델에 따르면 RC 값은 작동면적 한 변의 길이의 제곱에 비례하였다. 제안된 전기변색시간 모델을 사용하여 도출된 변색시간은 상대적으로 큰 작동면적을 가지는 전기변색 유리창의 실측치와 잘 일치하였다.

전기변색소자의 광투과도 차이값 향상을 위해 기존 나노입자 적층시스템에 플라즈마 공정을 도입하는 시도를 하였다. 플라즈마는 기체분자가 이온화되어 있는 제 4의 물질상태이다. 전기변색 물질인 WO_3 입자에 플라즈마 처리를 함으로써, WO_3 입자 적층 표면의 접촉각이 감소하였는데, 이는 WO_3 적층 표면과 전해질이 더욱 밀착되어 반응면적이 증가됨을 의미하며, WO_3 표면 결정구조는 더욱 비정질화된 것으로 확인되었다. 결과적으로 광투과도 차이가 기존 50%에서 65.9%로 향상되었다.

주요어: 전기변색소자, 나노입자 적층시스템, 대면적 전기변색 유리창, 전기변색시간 모델, 플라즈마 처리

학 번: 2013-30196